MARTIN MARIETTA ENERGY SYSTEMS LIBRARIES

3 4456 0273987 4

ORNL-6463

ornl

OAK RIDGE NATIONAL LABORATORY

MARTIN MARIETTA

SCINFUL: A Monte Carlo Based Computer Program to Determine a Scintillator Full Energy Response to Neutron Detection for E_n Between 0.1 and 80 MeV: Program Development and Comparisons of Program Predictions with Experimental Data

J. K. Dickens

OAK RIDGE NATIONAL LABORATORY
CENTRAL RESEARCH LIBRARY
CIRCULATION SECTION
4500N ROOM 175
LIBRARY LOAN COPY
DO NOT TRANSFER TO ANOTHER PERSON
If you wish someone else to see this report, send in name with report and the library will arrange a loan.
UCN-7969 3 9 77

OPERATED BY
MARTIN MARIETTA ENERGY SYSTEMS, INC.
FOR THE UNITED STATES
DEPARTMENT OF ENERGY

Printed in the United States of America. Available from
National Technical Information Service
U.S. Department of Commerce
5285 Port Royal Road, Springfield, Virginia 22161
NTIS price codes—Printed Copy: A07; Microfiche A01

This report was prepared as an account of work sponsored by an agency of the United States Government. Neither the United States Government nor any agency thereof, nor any of their employees, makes any warranty, express or implied, or assumes any legal liability or responsibility for the accuracy, completeness, or usefulness of any information, apparatus, product, or process disclosed, or represents that its use would not infringe privately owned rights. Reference herein to any specific commercial product, process, or service by trade name, trademark, manufacturer, or otherwise, does not necessarily constitute or imply its endorsement, recommendation, or favoring by the United States Government or any agency thereof. The views and opinions of authors expressed herein do not necessarily state or reflect those of the United States Government or any agency thereof.

ORNL-6463

Engineering Physics and Mathematics Division

SCINFUL: A Monte Carlo Based Computer Program to Determine a Scintillator Full Energy Response to Neutron Detection for E_n Between 0.1 and 80 MeV: Program Development and Comparisons of Program Predictions with Experimental Data

J. K. Dickens

DATE PUBLISHED — April 1988

Prepared for the
Office of Energy Research
Nuclear Physics

NOTICE: This document contains information of a preliminary nature. It is subject to revision or correction and therefore does not represent a final report.

Prepared by the
OAK RIDGE NATIONAL LABORATORY
Oak Ridge, Tennessee 37831
operated by
MARTIN MARIETTA ENERGY SYSTEMS, INC.
for the
U.S. DEPARTMENT OF ENERGY
under contract DE-AC05-84OR21400

MARTIN MARIETTA ENERGY SYSTEMS LIBRARIES

3 4456 0273987 4

CONTENTS

ACKNOWLEDGMENTS v
ABSTRACT vii
1. INTRODUCTION 1
2. PHYSICS OVERVIEW 2
3. REACTION KINEMATICS AND ENERGETICS IN SCINFUL . . . 8
4. DISCUSSION OF CROSS SECTIONS 15
5. ANGULAR DISTRIBUTIONS 20
6. FLUORESCENT LIGHT CONSIDERATIONS 22
7. OTHER FEATURES IN SCINFUL 28
8. COMPARISONS WITH EXPERIMENTAL DATA AND OTHER PROGRAM CALCULATIONS 29
9. IMPROVEMENTS AND POTENTIAL EXTENSIONS 101
REFERENCES 103
APPENDIX A 108
APPENDIX B 112
APPENDIX C 114

ACKNOWLEDGMENTS

The author extends his thanks to Dr. J. L. Romero for providing the angle-integrated data presented in Figures 10 to 23. Thanks are also extended to Dr. E. J. Axton for helpful comments on $n + {}^{12}C$ cross sections. Appreciation of a telephone discussion with Dr. J. Hale concerning the new $n + H$ evaluation and oral transmission of cross-section values for E_n to 30 MeV is extended. Thanks are also due to Dr. R. W. Finlay and to Dr. N. Ollson for illuminating correspondence. I express my appreciation to Dr. R. W. Peelle and to Dr. R. R. Spencer for careful readings of the draft manuscript and very pertinent remarks in their respective reviews. Dr. Spencer also provided the programming for choosing a neutron energy from a Maxwellian distribution. I also extend my thanks to Dr. D. C. Larson for many "blackboard" sessions which helped clarify and solve many problems as they arise. Finally, I express my great appreciation to Mrs. S. R. Damewood for her careful and patient work needed to prepare this report.

ABSTRACT

This document provides a discussion of the development of the FORTRAN Monte Carlo program SCINFUL (for scintillator full response), a program designed to provide a calculated full response anticipated for either an NE-213 (liquid) scintillator or an NE-110 (solid) scintillator. The program may also be used to compute angle-integrated spectra of charged particles (p, d, t, ^{3}He, and α) following neutron interactions with ^{12}C. Extensive comparisons with a variety of experimental data are given. There is generally overall good agreement (<10% differences) of results from SCINFUL calculations with measured detector efficiencies for the incident design neutron energy range of 0.1 to 80 MeV. Calculations of detector responses, i.e., $N(E_r)$ vs E_r where E_r is the response pulse height, reproduce measured detector responses with an accuracy which, at least partly, depends upon how well the experimental configuration is known. For $E_n < 16$ MeV and for $E_r > 15\%$ of the maximum pulse height response, calculated spectra are within $\pm 5\%$ of experiment on the average. For E_n up to 50 MeV similar good agreement is obtained with experiment for $E_r > 30\%$ of maximum response. For E_n up to 75 MeV the calculated shape of the response agrees with measurements, but the calculation underpredicts the measured response by up to 30%.

1. INTRODUCTION

The purpose of the computer program SCINFUL is to compute by Monte Carlo methods the complete response of a scintillator detector to incident neutrons. There are a number of existing computer programs[1–12] designed to predict, if not complete responses, at least the efficiencies of such detectors for a few selected thresholds, where efficiency is defined as the number of detected events (having pulse heights $\geq$ threshold) per number of neutrons incident upon some surface of the detector. A well used, and copied, program is the 20-year-old ORNL program O5S.[1] As originally written, O5S was an adaptation of an earlier general-purpose neutron-transport code O5R;[13] indeed, O5S incorporated many of the features of the parent code. O5S was used primarily for the liquid scintillator NE-213 (made by Nuclear Enterprises, Ltd.), later extended to the solid scintillator NE-110 (also made by Nuclear Enterprises, Ltd.) when it was determined experimentally[14] that proton pulse height in "light" units for NE-110 was essentially equal to proton pulse height for NE-213. The program O5S was not particularly designed for $E_n > 17$ MeV, and demanding that the program provide adequate computed responses for $E_n > 20$ MeV required new programming additions (for example, substituting relativistic for non-relativistic transformations). Consequently, although perhaps 10% of the programming of the "parent" O5S was kept, the present program is sufficiently new to warrant a new name: SCINFUL, for <u>scin</u>tillator <u>full</u> response to neutron detection.

2. PHYSICS OVERVIEW

SCINFUL is written for a scintillator of NE-213 or NE-110 in the shape of a right circular cylinder; the cartesian coordinate axes, as shown in Figure 1, have their origin in the center of the front face of the detector. A user's manual and a complete listing of Version.1 of the program are given in a separate report.[15] Some physics aspects, construction of the program, and comparisons with measurements and other computer code predictions, are discussed in the present report.

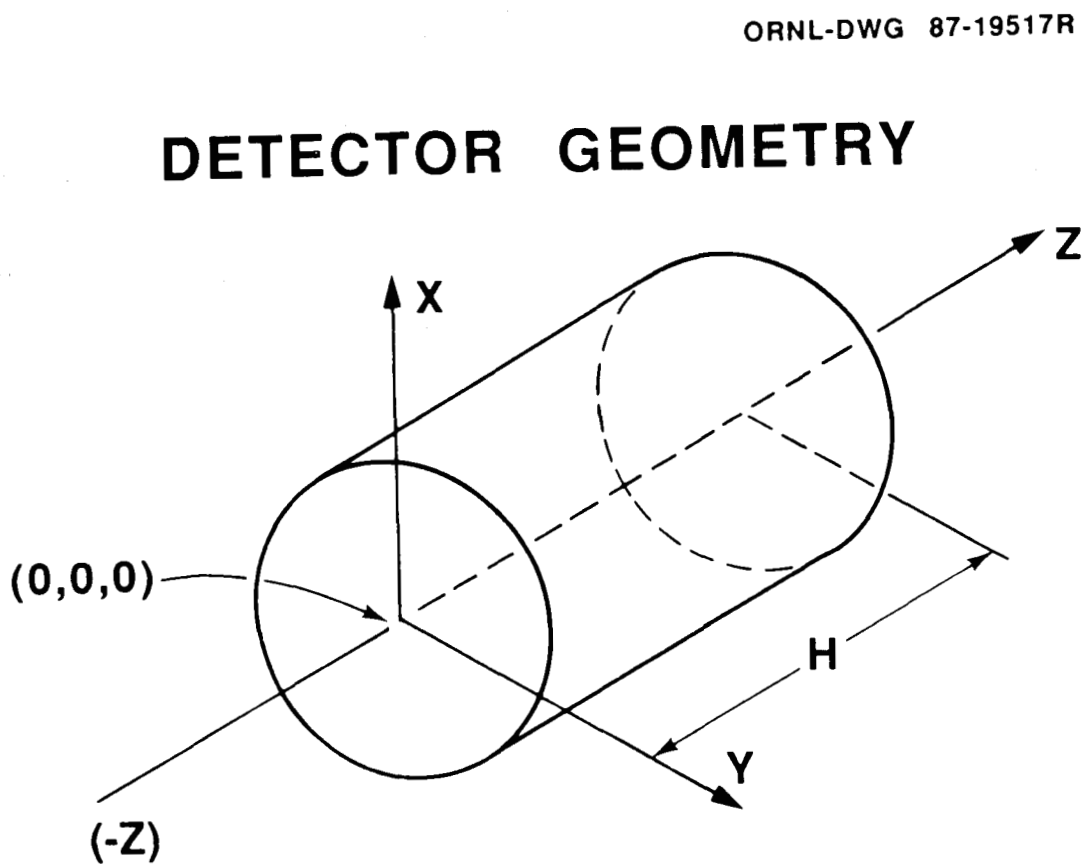

Fig. 1. Three-dimensional view of the detector geometry used in SCINFUL. The Cartesian coordinate axes are centered on the front face of the detector. The photomultiplier tube (or light pipe) is coupled to the detector at $Z = +H$eight. For most applications the neutron source will be placed along the $-Z$ axis; however, the source may be positioned at any location with respect to the detector, even inside.

Before delving into the program it may be useful to review some basic concepts of neutron detection using a scintillation detector. For neutrons of energies $< \sim 10$ MeV, detection relies primarily on neutron scattering from hydrogen and subsequent interaction of the recoil proton with a scintillation material producing photons which are then converted to electrons at the photocathode of a photomultiplier tube, as exhibited schematically in the top of Figure 2. The output of the photomultiplier tube is a pulse which is a monotonic function of the energy of the recoil proton; the functional dependence, however, is not necessarily linear.

The schematic in the center of Figure 2 shows another method of detecting neutrons, in which the neutron undergoes a nuclear reaction resulting in one or more charged ions, and these charged ions interact with the scintillation material to produce photons, etc. Interpretation of the output pulse from the photomultiplier depends upon the types and energies of the charged ions intercepted by the scintillator.

The organic scintillation detector schematically represented by the bottom drawing of Figure 2 combines the "hydrogenous radiator" and "carbon target" with the "scintillator" into a single unit, such that a neutron interaction in the detector should result in fluorescent photons emanating from the detector to the photocathode of the photomultiplier tube. The output pulse from the photomultiplier tube, however, is not a monotonic function of the incident neutron's energy nor even of the amount of energy lost by the neutron in the detector (in the case that a scattered neutron subsequently escapes the detector). Indeed, for a series of separate interactions in the detector by a number of incident similar neutrons, the photomultiplier output pulses will range in amplitude from very nearly zero up to some maximal amount (which amount is monotonically, but not linearly, dependent upon incident neutron energy); the purpose of the program SCINFUL is to determine, as a computer "experiment," the expected pulse height distribution of these photomultiplier output pulses.

For detection of low-energy neutrons, the detector does not have to be very big to contain (i.e., slow down and stop) the recoil protons, and for a small detector most of the neutrons will scatter only once, or at most twice, in the detector. However, as the neutron energy extends above about 20 MeV, ranges of the recoil protons require larger detectors. Not only will multiple scattering of the incident neutron become more likely, but the relative probability of interaction with the carbon with

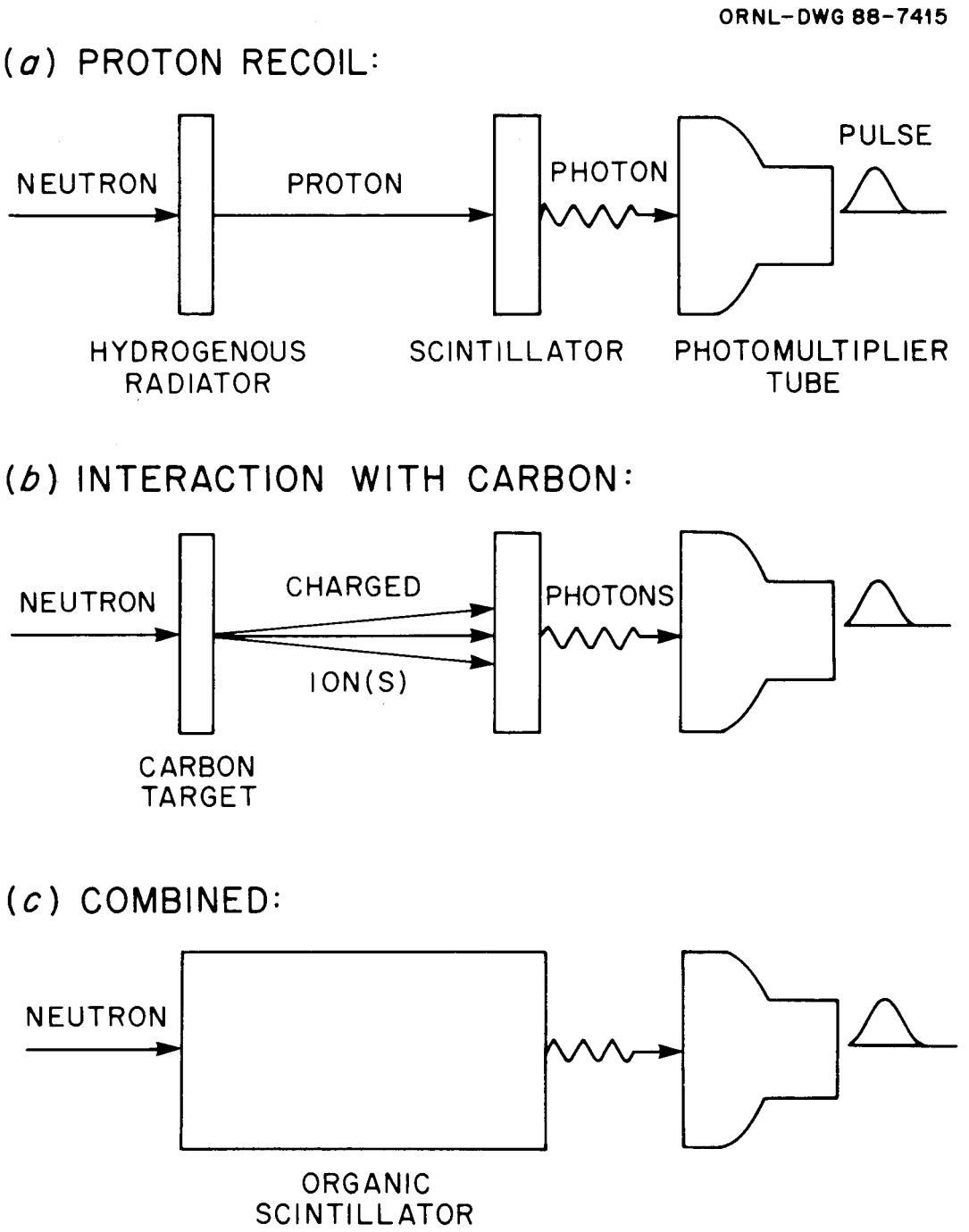

Fig. 2. Schematic illustrations of neutron detection. In all three illustrations the important aspect is that a neutron interaction with material results in at least one charged ion, and the net result is an electronic pulse as output from a photomultiplier tube.

respect to interaction with the hydrogen increases, and so modeling the various $n + {}^{12}\mathrm{C}$ reactions becomes important. As an example, consider a "history" for a high-energy incident neutron as schematically shown in Figure 3. The neutron first has a collision with a hydrogen atom, and the scattered neutron traverses some path before colliding with a carbon atom. In the example, this latter collision is of the type ${}^{12}\mathrm{C}(n, np){}^{11}\mathrm{B}$. The secondary neutron is shown to interact once again, this time with a hydrogen atom, and then the neutron escapes the detector volume, and the "history" of collisions for this incident neutron is complete. Slowing down of each of the four charged particles results in photons being created by fluorescence, and some fraction of the total of the created photons will intercept the photocathode end of the detector.

In following the history exhibited in Figure 3, one may observe several features that must be modeled in the program. The first task is to determine whether or not the first scattering takes place. This task is done by first determining the total probability using total cross-section data for any interaction as a function of path length of the neutron in the detector, then determining the internal path length in the direction given by the neutron's velocity vector from the neutron's point of entry to another surface of the detector, and then choosing by Monte Carlo the length along that path before the neutron interacts. If the Monte Carlo choice places the interaction inside of the detector, then the second task is to determine the type of interaction that took place, a task which requires cross-section data for all of the types of interactions energetically available.

Having gotten this far, the third task is to determine (again by Monte Carlo choice) the energetics and kinematics of the chosen reaction, and once having completed the reaction, to determine (a) the light output for each charged ion and (b) the direction and energy of the scattered neutron (if there is one) in the detector coordinates. Now the process just described is repeated for the scattered neutron, namely (a) determine a new probability for interaction, (b) determine a new path length to the surface of the detector along the scattered path, (c) determine by Monte Carlo if an interaction takes place inside the detector and, if so, what type, (d) do the energetics, kinematics, and fluorescent photon production by the charged ions, and (e) determine the second-scattered (in this example) neutron's energy and direction in the detector.

ORNL-DWG 88-7413

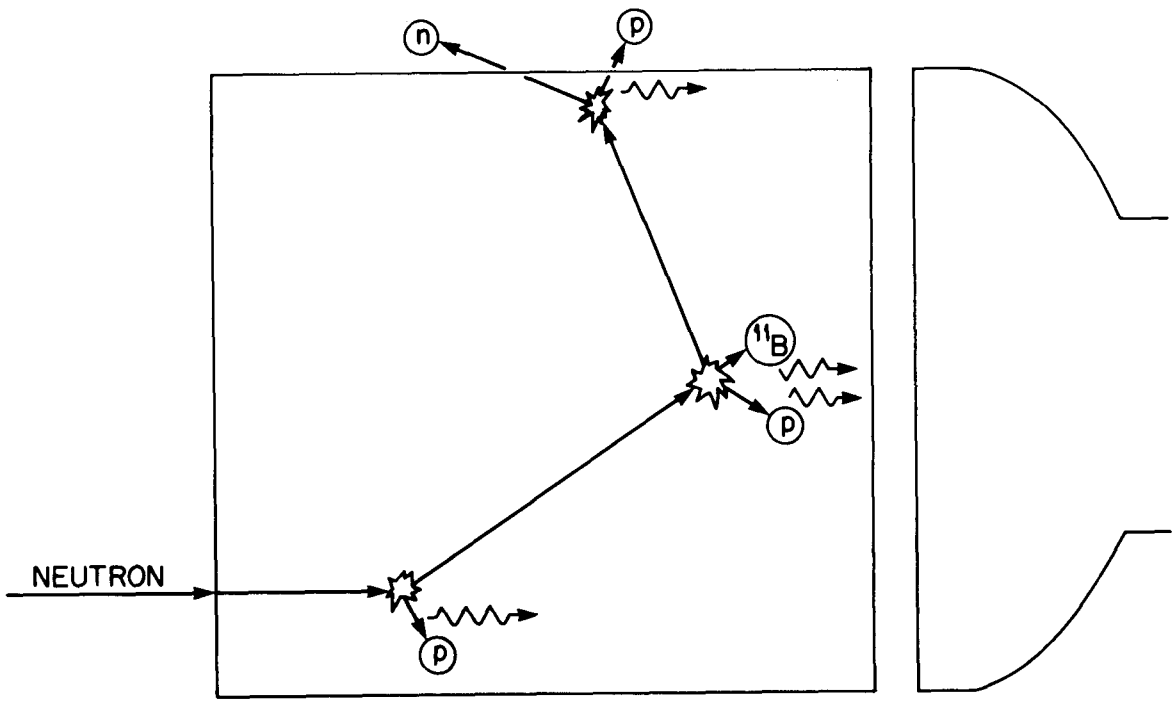

Fig. 3. Schematic illustration of a possible "history" for detection of a neutron in an organic scintillator. In this illustration the incoming neutron first collides with a hydrogen atom, and some of the kinetic energy of the subsequent recoil proton is converted into fluorescent light. The once-scattered neutron then strikes a ^{12}C atom, and the event postulated in this history is a $^{12}C(n,np)^{11}B$ reaction. Again, some of the kinetic energy of the recoiling ^{11}B ion and of the outgoing proton is converted into fluorescent light. The neutron leaving this reaction site is postulated to collide with a hydrogen atom very near the surface of the detector. After this collision both the recoil proton and neutron escape the detector. Only a portion of the proton's initial kinetic energy is absorbed in the detector and so only that portion can interact with the organic molecules to produce fluorescent light. The escape of the neutron signals the end of the "history" of nuclear interactions by the neutron with the scintillation detector. All that remains is to determine the expected photomultiplier output pulse size on the basis of summation of the separate fluorescent yields.

Before leaving Figure 3, there are two other features exhibited that should be noted. The third scattering shows the recoil proton escaping the detector before all of its energy is lost. For high-energy neutrons, escapes of recoil protons are important, and so determining energetics of these processes is modeled in SCINFUL. Another feature shown in this figure is the characteristic that centers of fluorescent photon production will be at various places in the detector. It may be important, and this facet will be discussed later, that fluorescent photon absorption by the

scintillator medium is important, and so one may need to include the capability to attenuate the light produced at the interaction point before it reaches the photocathode. This possible fluorescent photon absorption is approximated by a simple exponential attenuation in SCINFUL.

One may, at this point in the discussion, divide the problem of determining $n + {}^{12}\mathrm{C}$ contributions* to detector response into three rather broad areas: (1) cross sections; (2) reaction kinematics and energetics; and (3) fluorescence photon (or "light units" as termed in the literature) production. The three categories are not completely independent, however, particularly as the incident neutron energy becomes $> \sim$20 MeV when multi-body breakup of the ${}^{12}\mathrm{C}$ becomes energetically possible,[16] and, in fact, likely. Indeed, very little experimental information exists on cross sections for neutron interactions with ${}^{12}\mathrm{C}$ for $E_n > 20$ MeV, and so one must infer such cross sections from available charged-particle yield data and from comparisons of calculated responses with such measured responses as exist in the literature. In the next section the programming of the reaction kinematics and energetics will be presented, and discussions of cross sections and photon production will follow.

* Naturally occurring carbon has an isotopic composition of 98.9% in the isotope ${}^{12}\mathrm{C}$ and 1.1% in the isotope ${}^{13}\mathrm{C}$. The present version of SCINFUL approximates the carbon isotopic composition as being 100% of the ${}^{12}\mathrm{C}$ isotope.

3. REACTION KINEMATICS AND ENERGETICS IN SCINFUL

For $E_n < 15$ MeV the only multi-body breakup reaction energetically available for $n + {}^{12}\mathrm{C}$ is the $n + {}^{12}\mathrm{C} \rightarrow n' + 3\alpha$ reaction, and this reaction warrants a separate section for discussion of computations of energy partitioning among the four outgoing particles[16,17] (see Appendix A). For $E_n > 18$ MeV other tertiary reactions become important. Development of the programming for the $n + {}^{12}\mathrm{C} \rightarrow p + n' + {}^{11}\mathrm{B}$ reaction is prototypical of the programming for all of the other breakup reactions, and so the programming concepts for this reaction will be presented in some detail.

Figure 4 exhibits schematically the energetics involved for, let us suppose, a 40-MeV neutron interaction with ${}^{12}\mathrm{C}$. For purposes of this discussion one may assume that the incident neutron results in excitation of the "compound" nucleus which then decays by emission of a proton. The total available energy for this decay is limited to that determined by the energy needed to result in the creation of the final ${}^{11}\mathrm{B}$ heavy ion, and the total available energy must be shared by the kinetic energies of the outgoing proton and the outgoing ${}^{12}\mathrm{B}$ ion. Calculations using the nuclear reaction mechanism program TNG[18] predict the outgoing proton energy distribution for the reaction $n + {}^{12}\mathrm{C} \rightarrow p + {}^{12}\mathrm{B}$, and the energy distribution predicted for $E_n = 40$ MeV is shown in Figure 5. For SCINFUL the exhibited histogram has been approximated by a simple analytical function,

$$\Phi(E_p) = E_p * EXP(-E_p/Temp) * (1.0 - EXP(-K * E_p/B)) \tag{1}$$

which, for $E_n = 40$ MeV, is shown by the smooth curve in Figure 5 for $K = 1.5$, $B = 2.9$ (both values deduced for the O5S code[1]), and $Temp = Temp(E_n)$, a "temperature." $Temp$ is a parameter deduced empirically such that the function Φ gives a reasonable representation of the proton "continuum" as calculated by the nuclear model code TNG[18] for E_n up to 70 MeV. The formula for $Temp$ used in SCINFUL is given by

$$Temp = E_n * [0.1245 + 0.001 * ABS(E_n - 45.0)] \tag{2}$$

The program chooses by Monte Carlo an outgoing proton energy from the exhibited distribution and computes the corresponding heavy-ion recoil energy. The

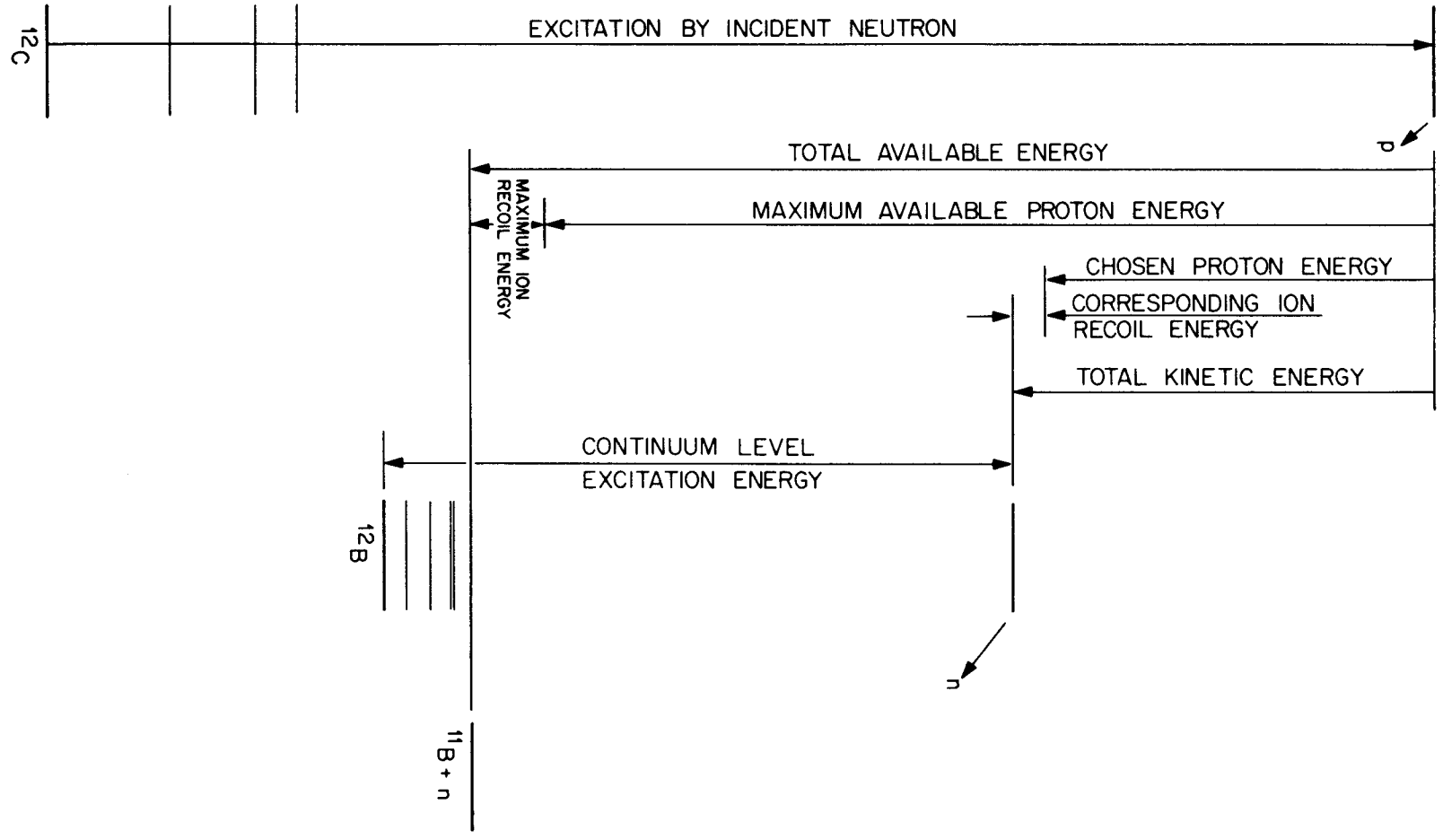

Fig. 4. Energetics associated with a $^{12}C(n,pn)^{11}B$ reaction. In this schematic the process is, first, a $^{12}C(n,p)^{12}B$ reaction leaving the ^{12}B in a very highly excited continuum state, and then, second, the highly excited ^{12}B "fissions" into a neutron plus an ^{11}B ion.

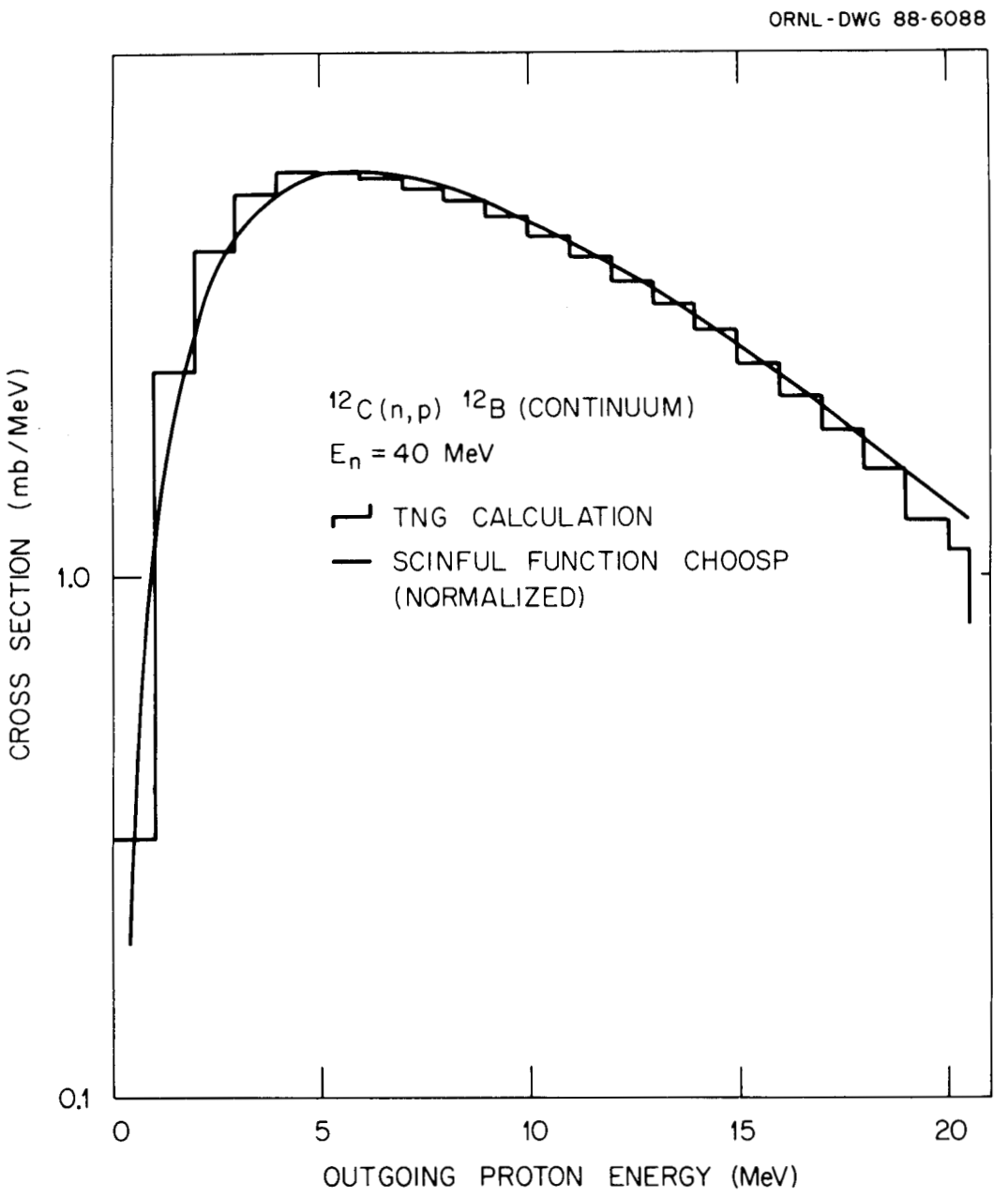

Fig. 5. Distribution of kinetic energies of the outgoing proton in a $^{12}C(n,p)^{12}B$ reaction for $E_n = 40$ MeV. The histogram was computed using TNG (ref. 18). The normalized curve is the analytic function used in SCINFUL from which to choose, by Monte Carlo techniques, a proton kinetic energy. In this case the TOTAL AVAILABLE ENERGY described by Figure 4 is ~20.5 MeV.

program also chooses by Monte Carlo the scattering angles with respect to the incident neutron direction (for this reaction measurements[19,20] indicate a strong forward peaking in the proton angular distribution). The proton's velocity vector must be transformed from the center-of-mass back to laboratory coordinates based on the detector's coordinate system to be able to determine if the proton may escape from the detector, a task which becomes more important with increasing E_n. Energy left over after determining the kinetic energies is assigned as excitation energy to the residual ^{12}B ion, in this example, a sufficient energy to result in subsequent decay of the ^{12}B ion by neutron emission.

The next step is to determine the characteristics of the "fission" of the excited ^{12}B ion into a neutron and an ^{11}B ion. The overall concepts for determining the energetics are essentially the same as the proton emission from the excited ^{13}C "compound nucleus" except that there is less TOTAL AVAILABLE ENERGY and the neutron emission has a different Φ function. Indeed, the appropriate $\Phi(E_n)$ for decay of the ^{12}B ion isn't known; what is used is an approximation representing $\Phi(E_n)$ computed by the TNG code for the neutron continuum following $n + {}^{12}\mathrm{C} \rightarrow n' + {}^{12}\mathrm{C}$. An example of a computed $\Phi(E_n = 40 \text{ MeV})$ is exhibited in Figure 6. The analytic function used to represent this function was taken from the O5S code and is,

$$\Phi(E_n) = EXP(-E_n/Temp) * E_n^{1.5} \tag{3}$$

where, again, the parameter $Temp$ is a function of E_n deduced from TNG[18] calculations at different incident E_n to give a reasonable representation of the Φ function for all E_n up to 70 MeV. As used in SCINFUL,

$$Temp = 0.065 * E_n + 0.001 * E_n^2 \ . \tag{4}$$

This Φ function does not reproduce the TNG results as well as $\Phi(E_p)$ of Figure 5 reproduces TNG results for proton emission, but $\Phi(E_n)$ is reasonably close to TNG calculations over most of the incident and outgoing neutron energy ranges needed for SCINFUL.

Returning to the reaction being studied in Figure 4 one now chooses by Monte Carlo a neutron kinetic energy and then obtains the corresponding ^{11}B ion energy;

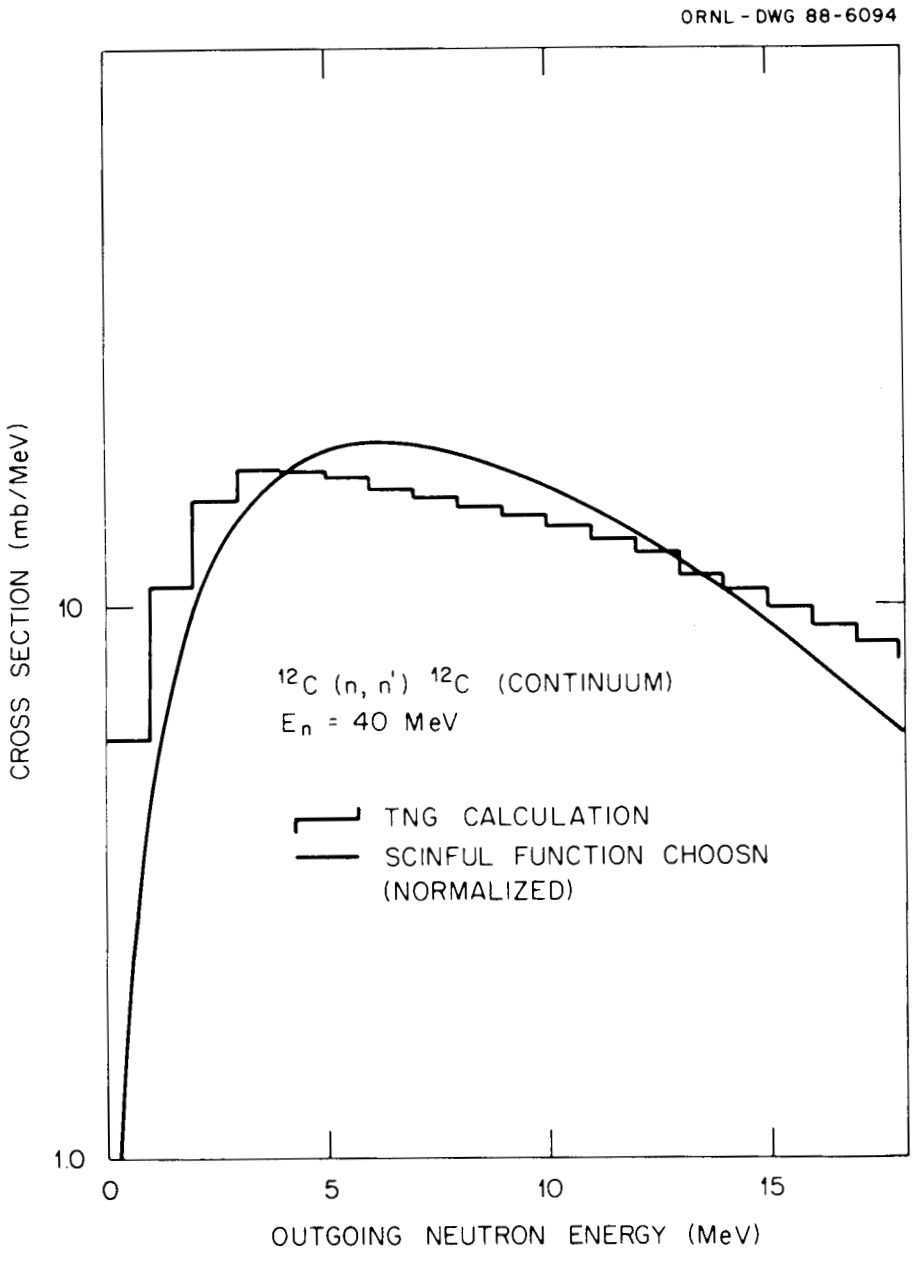

Fig. 6. Distribution of kinetic energies of the outgoing neutron in a $^{12}C(n,n')^{12}C$ reaction for $E_n = 40$ MeV and for the residual ^{12}C in a highly excited continuum state. The histogram was computed using TNG (ref. 18). The normalized curve was taken from the O5S code (ref. 1) and is used in SCINFUL to choose a neutron kinetic energy.

the energy left over corresponds to a "continuum" excitation energy in ^{11}B. Energies of levels in ^{11}B are known[21] up to $E_x \sim 11$ MeV, and SCINFUL checks to see if the "continuum" excitation energy is small enough to be "matched" with a known level in ^{11}B. If so, the "continuum" excitation energy is set equal to the chosen known level energy in ^{11}B, and the outgoing neutron kinetic energy is adjusted from the Monte Carlo choice to agree with that expected for decay to the chosen known level in ^{11}B. The remaining task for the calculation of the decay of the highly-excited ^{12}B ion is to determine the outgoing neutron's direction. The "fission" of the ^{12}B ion is isotropic in the center of mass; then the calculation needs to transform the neutron's velocity vector into the detector laboratory coordinates for further study of this neutron's history.

At this point the important features of kinematics and energetics exhibited in Figure 4 have been discussed. The calculation may not be complete, however, unless the residual ^{11}B ion has been left in its ground state. If the ^{11}B ion is left in a state of excitation, either in one of its known energy levels or in an even more energetic "continuum" level of excitation, SCINFUL continues to follow subsequent decay of the ^{11}B ion. Decay of this ion is modeled from information deduced from Ajzenburg-Selove's compilation;[21] in SCINFUL, for example, a highly excited "continuum" level in ^{11}B decays 56% of the time by alpha emission and 44% of the time by (a second) neutron emission. Bound states of ^{11}B, of course, decay by gamma-ray emission; some of the unbound known levels also decay partially by gamma-ray emission. These gamma-ray decays are modelled into SCINFUL as either one or two gamma rays, and any such gamma rays are traced in SCINFUL for possible interaction in the detector. If the excited ^{11}B ion is determined to decay by alpha emission, the resulting ^{7}Li ion is tested for possible further decay, and if the excited ^{11}B ion is determined to decay by neutron emission, the resulting ^{10}B ion is tested for possible further decay.

In the fashion just described, for a sufficiently energetic incident neutron, the program may determine an overall breakup of the ^{12}C atom into as many as four charged particles (checking two protons and/or deuterons for possible escape) and two neutrons. Reactions programmed into the present version of SCINFUL are given in Appendix B.

It must be evident that something labelled a "cross section" was used to determine the initial type of reaction by the neutron, in the example of Figure 4 being

$n + {}^{12}\mathrm{C} \rightarrow p + ...$ Once the reaction has been initiated the remaining choices for the reaction are governed by random walk through the physics maze made up of outgoing nucleon energy distributions [equations (1) and (3)] and programmed decay modes of excited intermediate "heavy" ions [^{12}C through ^{6}Li]. One needs at least to attempt to deduce yields for multi-body breakup reactions for two reasons: (a) they surely occur when the reaction channel opens up energetically; and (b) the summed fluorescent light output for the several light charged ions $(p, d, ...)$ is larger than the light output for a single heavy charged ion having all of the residual kinetic energy. (Three 5-MeV alphas will together provide approximately the same light output as one 85-MeV carbon ion.) However, for $E_n > 35$ MeV, only at $E_n = 90$ MeV is there published[22] information about experimental measurements of multi-body breakup reactions. The programming in SCINFUL provides a method for estimating yields for multi-body breakup reactions and so, hopefully, provides a more realistic estimate of detector response, at least for E_n up to 80 MeV.

An important point to note is that the calculational procedures just outlined are also used for initial two-body reactions in SCINFUL, for example ${}^{12}\mathrm{C}(n, \alpha){}^{9}\mathrm{Be}$ (ground state) reactions. Put another way, even though the kinematics of this two-body reaction can be described (at least nonrelativistically) by a closed, analytical formulation in the laboratory reference frame, SCINFUL, unlike other response codes, does not utilize specific two-body formulations. Rather, SCINFUL is a very modular program, and the programming philosophy is that of linking subroutines and functions in a series of short statements which follow a standard "outline" for any reaction. The final program may not be efficient in terms of CPU running time*, but it has had the distinct advantage, at least during the program writing period, of being easy to follow, hence, easy to test the individual parts – easy to debug.

* The present version of SCINFUL requires up to twice the O5S execution time on the ORELA VAX 11/785 computer for the same problem.

4. DISCUSSION OF CROSS SECTIONS

Data used for cross sections in SCINFUL are included as part of the programming. For all of the major $n + {}^{12}C$ reaction channels, cross section values are given pointwise in tabular form in DATA statements, and table lookup and interpolation methods are used to obtain cross section values as needed.

The most important cross sections are (1) for $n + H$ scattering and (2) the total cross section for $n + {}^{12}C$ reactions. For the former the Gammel formula[23] is used except for the very lowest neutron energies. (Cross sections obtained using the Gammel formula[23] are compared in Appendix C with a recent evaluation by Dodder and Hale.[24]) The total $n + {}^{12}C$ cross section is not tabulated in SCINFUL (as it is in some other programs) but instead is obtained by summing the partial reaction cross sections that are in the program. Thus, in the development of the cross-section data set used in SCINFUL, careful attention was given to ensure that the total cross sections thus obtained were correct.

It is evident that cross-section data sets developed for earlier response programs were almost as individual as the programs, since particularly for $E_n > \sim 15$ MeV, earlier authors tailored cross sections so that their programs would calculate "correct" efficiencies. In particular, effort was expended on the believed to be large ${}^{12}C(n,p){}^{12}B$ + ${}^{12}C$ $(n,np){}^{11}B$ cross section for $E_n > 20$ MeV,[25] but it appears from the present study (to be discussed in a later section of this report) that the experimental data were not correctly interpreted.

Cross sections for $E_n < 20$ MeV used in SCINFUL were, for the most part, taken from the U. S. ENDF/B-V evaluation[26] (rather than, say, the del Guerra evaluation[27] or the more recent partial evaluation for E_n between 14 and 20 MeV by Brenner et al.[28]) In this energy range, however, the cross sections for the ${}^{12}C(n,n')3\alpha$ breakup reaction have been the subject of some study. Axton[29] has determined that the experimental values reported by Antolkovic et al.[17] are probably too large. Values used in SCINFUL were determined following adjustments to the Antolkovic et al.[17] cross sections as needed to obtain a better representation of measured detector responses.

Cross sections for $E_n > 20$ MeV in SCINFUL were also tailored when necessary for reasons already discussed, namely that cross sections for the multi-body breakup reactions simply aren't known. Such experimental data as exist have been

used to help define cross sections. For example, the excitation function for the $^{12}C(n,2n)^{11}C$ reaction in SCINFUL is shown in Figure 7. It agrees with the recent data of Anders et al.[30] up to 34 MeV, cross section data being somewhat larger than earlier data.[31] For $E_n > 34$ MeV one can only "evaluate" the excitation function by a "best estimate" smooth curve which intersects 22 mb at $E_n = 90$ MeV, i.e., the value quoted (but not measured) by Kellogg.[22] However, for $E_n > 34.5$ MeV threshold energy, SCINFUL is programmed to consider possible further decay of the ^{11}C ion by proton emission. Hence the excitation function shown in Figure 7 exhibits a second threshold effect for E_n between 35 and 40 MeV to account for this extra reaction channel. Insofar as comparisons with the cross sections shown for three other programs,[1,8,12] there are evident differences in cross sections used, but how much such differences might affect total response calculations would be quite difficult to determine.

A second cross section excitation function to be discussed here which is of importance in SCINFUL is shown in Figure 8 and is the cross section used for $n + {}^{12}C \rightarrow d + ...$ reactions. Most of the earlier programs don't include deuteron reactions; however deuteron spectra have been measured at $E_n = 27$, 40 and 61 MeV by Subramanian et al.[20] and at 56 MeV by McNaughton et al.[19] Furthermore, deuteron fluorescent light is different from proton fluorescent light.[32] So since the goal is to provide overall detector response (and not just efficiencies with respect to a few chosen biases) the deuteron channels need to be included, and so must cross section values be included. For $E_n < 20$ MeV, the data shown are from ENDF/B-V,[26] and one must decide how to extrapolate for $E_n > 20$ MeV. The problem is compounded in the first place because some of the deuteron channels may result in 2 deuterons, and these reaction channels are programmed into SCINFUL. Furthermore, also as programmed into SCINFUL, some of the reactions which start out with proton emission as given in Figure 4 may also include a deuteron as one of the final reaction nucleons. The excitation function shown in Figure 8 was obtained by an iterative process such that SCINFUL results reasonably well reproduce the experimental deuteron data[20] just discussed. The major difference between the excitation function in SCINFUL and that in the program of Anghinolfi et al.[9] is for E_n between threshold and 30 MeV. As discussed later the relatively large cross section of ~ 70 mb at $E_n \sim 19$ MeV appears to be supported by some recent detector efficiency measurements.[33]

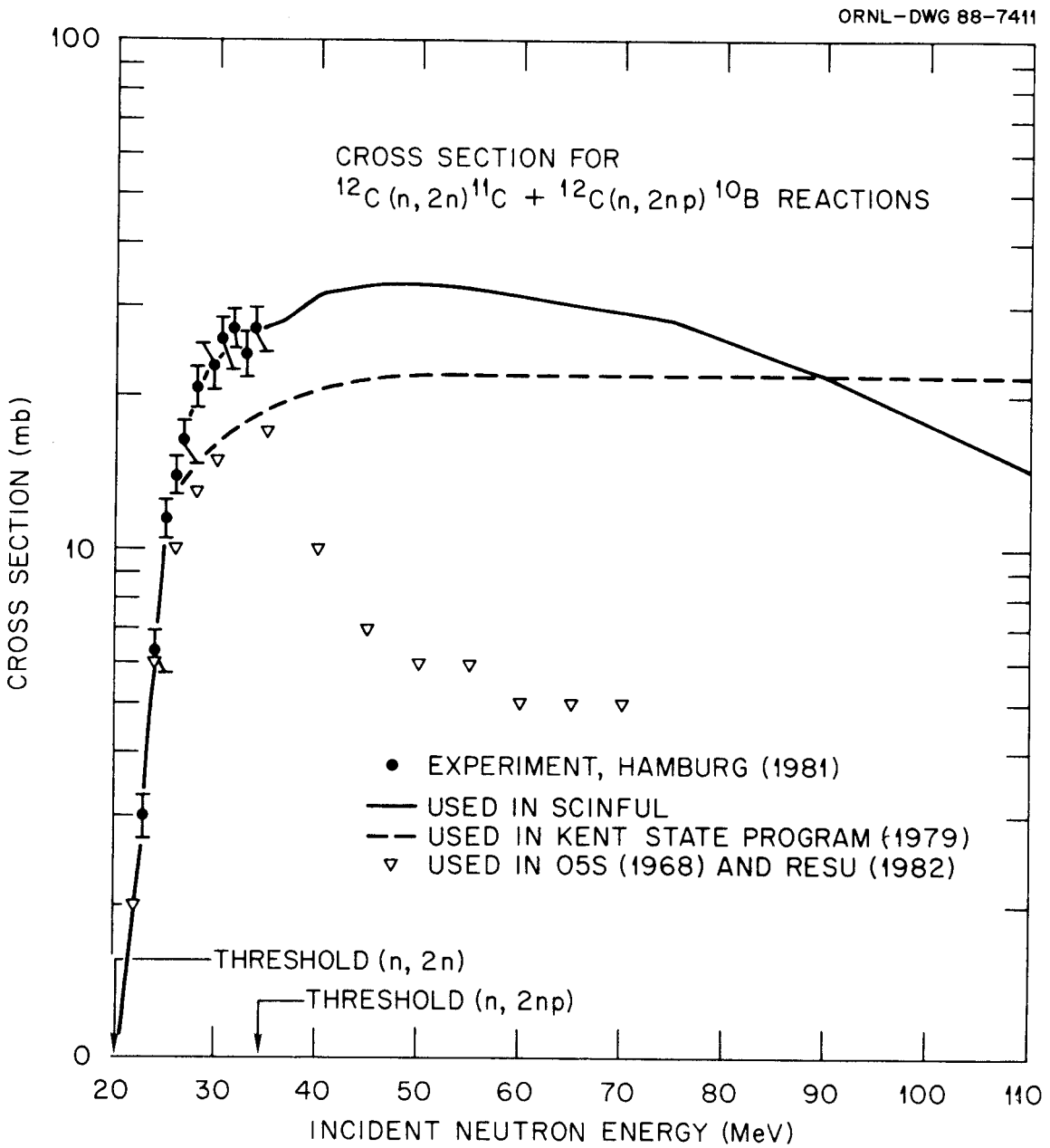

Fig. 7. Cross sections for the primary $^{12}C(n,2n)^{11}C$ reaction. The data are from the experiment of Anders et al. (ref. 30). The solid curve is used in SCINFUL and includes an addition for $E_n > 35$ MeV to account for possible subsequent "fission" of the excited ^{11}C ion into a proton plus ^{10}B ion, that is, in effect a $^{12}C(n,2np)^{10}B$ reaction in addition to the primary reaction. The dashed line represents the cross section for the primary reaction in the code of Cecil et al. (ref. 8), and the open triangles represent cross sections used in O5S (ref. 1) and in RESU (ref. 12).

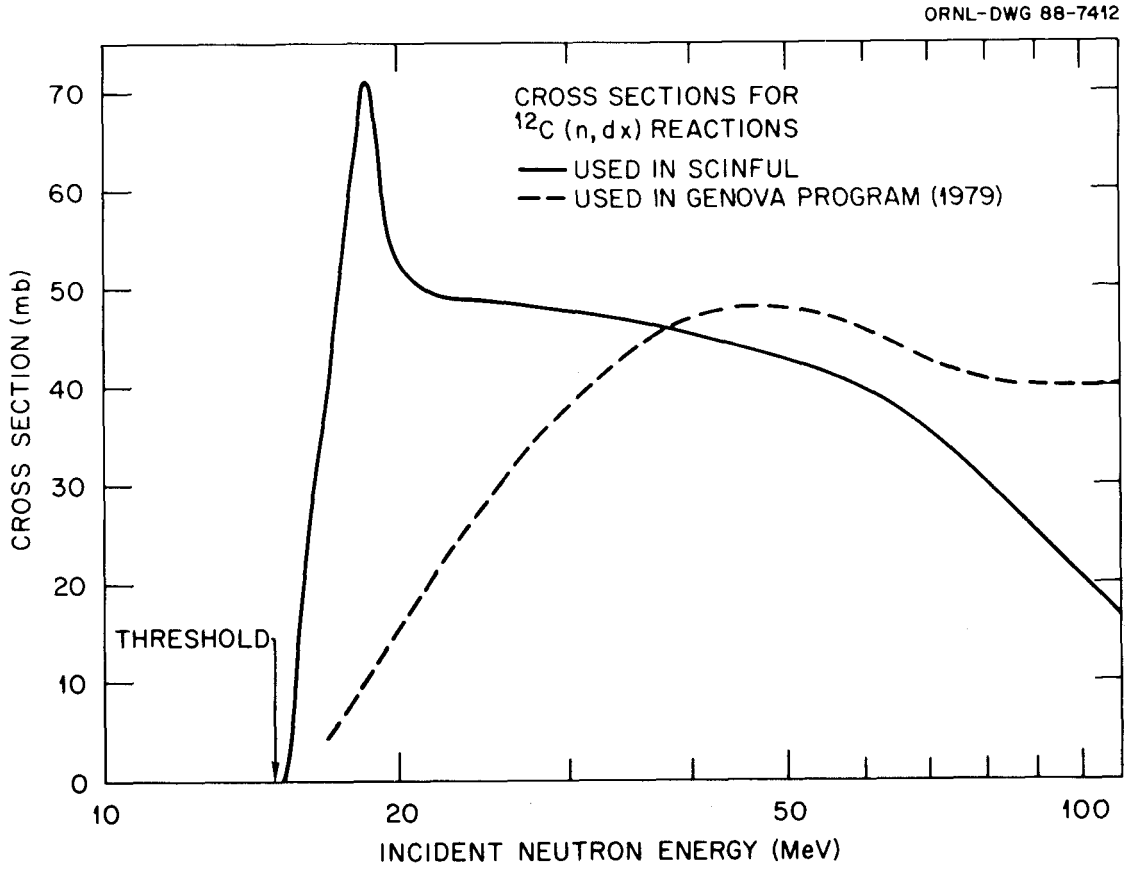

Fig. 8. Cross sections for the primary $^{12}C(n,d)^{11}B$ reaction. The solid curve represents the cross sections used in SCINFUL, and these include all of the reactions following the primary reaction which are obtained following breakup of a highly-excited ^{11}B ion. The dashed curve represents cross sections used in the code of Anghinolfi et al. (ref. 9). The major disagreement is for $E_n < 25$ MeV; the solid curve for $E_n < 20$ MeV is taken from the U.S. ENDF/B-V evaluation (ref. 26).

It must be apparent at this point in the discussion that "cross sections" used in SCINFUL are not meant to be true cross sections for all reactions, except that they are constrained to sum up to the correct total cross section at any E_n. Rather, these values are simply the means by which SCINFUL chooses which major reaction type starts the collision history. For some of the major reaction types, for example $^{12}C(n,n')^{12}C$ [$E_x = 4.43$ MeV], the SCINFUL-tabulated cross section should be a true cross section. And, indeed, one may expect tabulated cross sections to be true cross sections for $E_n < 18$ MeV, since the major reaction types are clearly indepen-

dent of each other. But for $E_n > 35$ MeV, when the same final multi-body breakup reaction can be obtained from different initial major reaction types [for example, $(n, 2np)$ and $(n, p2n)$ reactions] the tabulated cross sections are not as meaningful. In fact, the cross sections would need to be changed if SCINFUL programming were subsequently extended to compute, for example, $(n, 3n...)$ reactions.

Finally, to end this section on cross sections, the difference between SCINFUL and earlier response codes in justification for cross section "adjustments" should be reiterated. Earlier authors adjusted cross sections ad hoc so as to obtain correct detector efficiencies, an engineering justification. The justification for adjustments to arrive at cross sections used in SCINFUL is a more physical one; the cross sections plus the programming attempt to provide computed particle energy spectra for comparisons with measured particle energy spectra[20,34] which, because of some probability of multi-particle emission, cannot by themselves be used to determine cross sections.

5. ANGULAR DISTRIBUTIONS

Most of the angular distributions of $n + {}^{12}\mathrm{C}$ major type reactions are handled in SCINFUL by means of tabulated Legendre polynomial coefficients. For neutron elastic scattering from carbon and for $E_n < 20$ MeV, the tabulation of these coefficients is taken from the ENDF/B-V evaluation.[26] For $E_n = 20.8$, 26 and 40 MeV, polynomial fits were made to data of Meigooni et al.[35] Angular distributions for elastic scattering for $E_n > 40$ MeV use the results of the 40-MeV polynomial fit; very little precision is lost since the angular distribution is so strongly peaked forward.

Angular distributions of inelastically scattered neutrons from the ${}^{12}\mathrm{C}(n, n')^{12}\mathrm{C}$ [$E_x = 4.43$ MeV] are also computed in SCINFUL using Legendre polynomial coefficients although with a much coarser grid than for elastic scattering. For E_n between 9.2 and 13 MeV, data of Glasgow et al.[36] were used, as were data for $E_n = 20.8$ and 26 MeV of Meigonni et al.[35]

Angular distributions of alphas from the ${}^{12}\mathrm{C}(n, \alpha)^9\mathrm{Be}$ [ground state] reaction are very important to include in the response programming.[37] Fits to obtain polynomial coefficients were made to three data sets[37–39] covering the incident neutron energy range between 8.0 and 15.6 MeV. For $E_n > 15.6$ MeV the polynomial coefficients obtained for the 15.6-MeV data are used; however, the cross section for the ground-state alpha reaction is decreasing rapidly, and so using a possibly incorrect set of coefficients for $E_n > 15.6$ MeV will have only a very small effect on the computed response.

For $n + {}^{12}\mathrm{C} \rightarrow p + \ldots$ reactions and $n + {}^{12}\mathrm{C} \rightarrow d + \ldots$ reactions, McNaughton et al.[19] report substantial forward peaking of the outgoing protons and deuterons for $E_n = 56$ MeV. For use in SCINFUL, these data are included as a table of probability vs scattering angle, one table for protons and one table for deuterons, and these tables are used for $E_n \geq 56$ MeV. For E_n between threshold and 56 MeV, proton and deuteron angular distributions are moderated toward isotropy from the 56-MeV data.

For $n + {}^{12}\mathrm{C} \rightarrow t + \ldots$ reactions and $n + {}^{12}\mathrm{C} \rightarrow {}^3\mathrm{He} + \ldots$ reactions, the data of Subramanian et al.[20] at $E_n = 27.4$, 39.7, and 60.7 MeV were used to determine Legendre polynomial coefficients to represent the angular distributions.

For other inelastic scattering from carbon or alpha output reactions, the angular distributions are assumed to be isotropic. In fact some inelastic scattering data for higher E_n have been reported,[35] and the angular distributions are not isotropic, but the amount of anisotropy is not very great, and the approximation of isotropy should have very little effect upon computed detector responses.

Turning now to neutron scattering from hydrogen, for $E_n < 13.7$ MeV the angular distribution is assumed to be isotropic in the center of mass. For $E_n >$ 13.7 MeV, the angular distribution of the neutron's scattering is represented by Legendre polynomial coefficients, tabulated for 16 values of incident neutron energy between 13.7 and 100 MeV. Tabulated values used in SCINFUL were those deduced by Verbinski and Textor and used in O5S[1] (see Appendix C for a discussion of comparisons with the recent Dodder and Hale evaluation[24]).

6. FLUORESCENT LIGHT CONSIDERATIONS

The third part of the neutron detection process illustrated in Figure 2 is the absorption of the energy of the charged ion and the concomitant creation of light by excitation of the molecules of the scintillator. Although experimental work was performed in the early years of scintillation spectrometry to determine the fundamental physics of this phenomenon,[40] the fact is that it remains today the least understood part of the neutron detection process. Indeed, for modern users of scintillation detectors the important aspect is not the absolute quantification of fluorescent light that is created (in lumens, for example) but rather the quantification of the electronic output pulse of the photomultiplier tube. And although the quantification of the electronic output pulse can be made on an absolute basis in some electronic unit (say, volts), that unit is by itself not very useful since it depends upon the specific hardware of the measurement system. What is desired is a nuclear physics unit related to energy absorption by the detector which should be independent of the specific hardware; what has evolved is a hybrid labelled a "light" unit, which is not light (i.e., photons) but which does depend, on an absolute scale, upon the material that makes up the scintillator as well as the characteristics of the photomultiplier tube. In an early definition, one "light" unit was the (essentially maximum) pulse height observed following detection of ^{60}Co gamma rays by the detector. More modern usage defines the "light" unit in terms of the electronic pulse height that would be observed upon detection of a monoenergetic 1-MeV electron by the scintillator. For detector calibrations purposes, however, one uses gamma-ray sources for calibrations and takes the forward-scattered Compton electrons to be responsible for the largest electronic pulse heights observed from the photomultiplier tube. A rather complete discussion of a standard pulse-height calibration is given in ref. 41.

One difficulty with the above-discussed calibration method is that it hides one aspect of the total neutron detection process, an aspect that was not specifically mentioned during the discussion of Figure 2, but was mentioned in passing during the discussion of Figure 3, and that aspect has to do with the efficiency by which the system converts the energy of the fluorescent photons into electrons at the photocathode of the photomultiplier tube. A few experiments have been reported[42–45] which show that the efficiency for events which take place in the detector some distance from the photocathode is less than the efficiency for events which take place

in the detector close to the photocathode. The usual calibration procedure results in a spread in sizes of output pulses which is then interpreted as a "resolution" effect due, for example, to fluctions in the number of photoelectrons created at the photocathode following absorption of a specific amount of light. The loss of efficiency, on the other hand, relates to such aspects as the reflectivity at the surfaces of the scintillator. Fluorescent light attenuation affects the overall neutron-detection measurement differently[42] than do fluctuation effects, as exhibited in Figure 9.

In this figure we suppose detection of a low-energy neutron by single-scattering events in the scintillator. Output electronic pulse heights are measured (and the information recorded) for a sufficient number of incident neutrons so that an energy distribution of pulses is recorded. For an ideal situation the measured result will be very similar to that result schematically represented in the top drawing of Figure 9. It is this ideal condition that we attempt to simulate when we do a detector calibration to determine a "light-unit" calibration curve. When we fold in fluctuation effects as discussed above, these "resolution" effects will result in modifying the ideal response measurement in the region of the maximum-sized pulses as exhibited in the middle drawing of Figure 9. There will be pulses observed to be larger than one would observe in the classical "ideal" measurement of the top drawing; however, these will be compensated for by an equal loss of lower-energy pulses. In fact, in setting up a detection system, one is never able to obtain an "ideal" measurement. Hence, one does not determine empirically the maximum value of E' corresponding to the "ideal" determination. One rather obtains something that resembles the middle drawing and then one finds the "ideal" maximum energy by determining that point in high-energy portion of the measured response that corresponds to a $Y(E')$ equal to about half of the $Y(E')$ measured for smaller values of E'.

The bottom drawing of Figure 9 exhibits the light attenuation effect[42] on an "ideal" measurement. Light attenuation always shifts the measured pulse height to smaller values; there can not be any pulses larger than the maximum obtained from the "ideal" measurement. Furthermore, the overall shape of the total measured response is different as the bottom drawing attempts to indicate. Again, however, we can not measure the "ideal" response, and so we do not know the value of the maximum E' for the ideal case. It must be evident from the bottom drawing that if an actual calibration measurement is affected by both light attenuation and

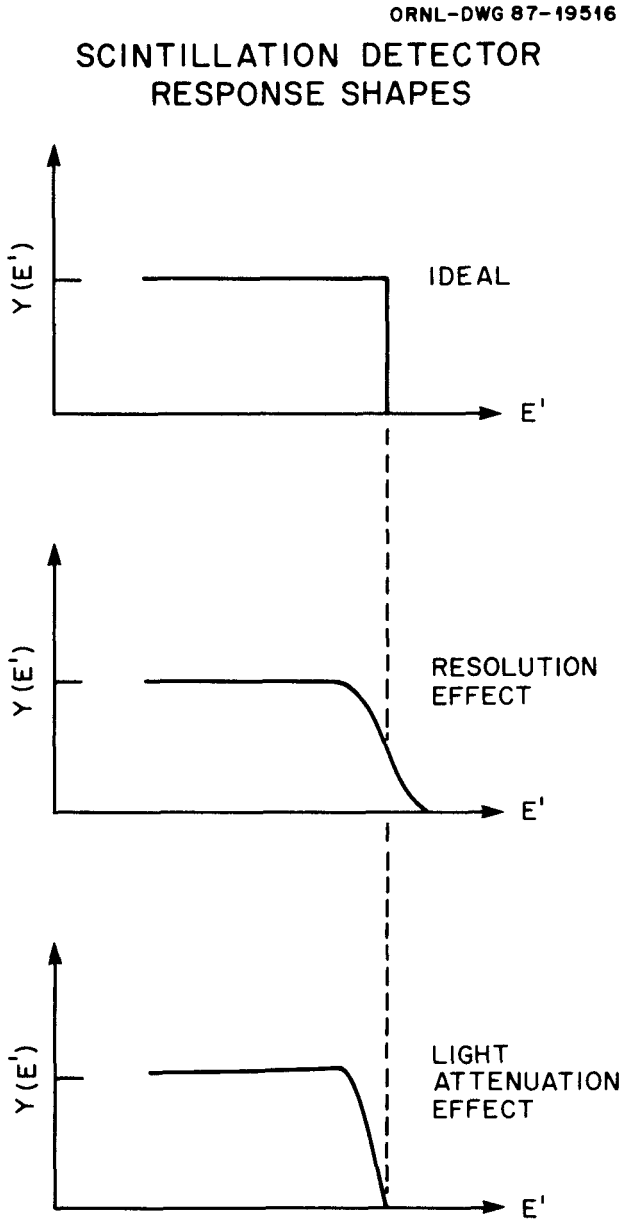

Fig. 9. Spectral distribution, $Y(E')$, of pulse heights, E', expected for neutrons incident upon a scintillation detector. The number of incident neutrons should be sufficient so that an "ideal" spectrum (top figure) could be theoretically realized. In practice one may obtain a spectrum similar to that shown in the middle figure from which may be deduced the maximum value of E' corresponding to the ideal case. However, as discussed in the text, attenuation of the fluorescent light by the detector skews the spectrum toward smaller pulse heights and definitely complicates an analysis to determine the maximum value of E' corresponding to the ideal case.

resolution one will simply not obtain a correct value of the E' corresponding to the ideal situation.

Now the point to this discussion may be stated, and that is that the many experimental reports[12,21,46–51] of "light" units versus proton (or other charged ion) energy are essentially devoid of any consideration of this problem of the efficiency of fluorescent light collection. In these experiments the detector is "calibrated" using gamma ray sources,[48] and then the pulse height with respect to said calibration is reported for different energy protons (neutrons) incident onto the face of the detector. The assumption is implicitly made that the incident protons (neutrons) will create light throughout the volume of the detector with exactly the same probability as the calibrating gamma-ray sources create light throughout the volume of the detector, an assumption that is very likely to be wrong for most of the "light-unit" calibration measurements so far reported, and quite wrong for at least a few of them. It is little wonder, then, that there is poor agreement to within the usual assigned uncertainties on one "light" unit in the literature.

These concerns bear upon the development of the light-unit conversions in SCINFUL. Light-unit values are tabulated[15] in SCINFUL for protons, deuterons, alphas, and carbon ions having energies between 0 and 100 MeV. For protons SCINFUL uses the values of light given by Verbinski et al.[52] for $0.1 < E_p < 40$ MeV; for E_p between 40 and 100 MeV the light-unit values were obtained from the current version of the O5S program[1] which are not reported in the Verbinski et al. paper.[52] Uwamino et al.[12] have reported measurements of $L(p)$ for monoenergetic neutrons of 22.6, 27.6, and 48.7 MeV (no ΔE_n quoted). Their results, given in graphical form, are compared to $L(p)$ used in SCINFUL in Table 1.

Table 1. Comparison of light-unit values used in SCINFUL with measurements of Uwamino et al. (ref. 12)

Proton Energy (MeV)	$L(p)$ SCINFUL	$L(p)$ Measurement	Ratio S/M
22.7	12.61	12.08 ± 0.36	1.044
27.6	16.00	15.87 ± 0.48	1.008
48.7	30.99	31.15 ± 0.94	0.995

Similarly, light-unit values for carbon ions were taken from Verbinski, et al.[52] for E_C up to 40 MeV and from the O5S program[1] for E_C up to 100 MeV. A justification for accepting the Verbinski et al.[1,52] proton values lies in that fact that for most of our studies at the ORELA, pulse-height calibration using the white neutron source of the ORELA will be the definitive calibration, and the justification for accepting the Verbinski et al.[1,52] values for carbon ions is simply that the light-unit values are so small that for our practical applications it does not matter much if the values for carbon are not exact.

Light-unit values in SCINFUL for alpha particles also used the reported Verbinski et al.[52] and from the O5S program[1] values for E_α between 0.1 and 100 MeV. However, comparisons of computed responses with measured responses for E_n between 14 and 22 MeV indicated that for $E_\alpha < \sim 10$ MeV, the Verbinski et al.[52] alpha-particle light-unit values were too small. The SCINFUL values are, therefore, somewhat larger so as to provide a computed response in better agreement with measurements regarding the pulse height position observed for the alpha contributions to these spectra.

Deuteron light-unit values in SCINFUL were estimated from measurements of Bechetti et al.[32] The values in SCINFUL were checked by comparing measured responses with computed responses and thus identifying the deuteron contributions to the measured responses. As best as can thus be determined the comparisons are in satisfactory agreement.

All of these tabulations are for the scintillator NE-213. For NE-110, Renner et al.[14] showed that although proton light for this scintillator is the same as proton light for NE-213*, carbon light is larger by about a factor of 3. In addition, comparisons of SCINFUL responses calculated for NE-110 with measured responses for NE-110 indicate that alpha light for NE-110 is larger than alpha light for NE-213, and that deuteron light for NE-110 is larger than deuteron light for NE-213. Consequently, one of the first steps in a SCINFUL calculation for NE-110 is to increase the tabulated carbon light by a factor of 3, increase the tabulated alpha light by a factor of 1.75, and increase the tabulated deuteron light by a factor of 1.52.

* This equivalence is an artifact of the definition of a "light" unit. According to the manufacturer (Nuclear Enterprises, Inc.) the absolute light output for NE-110 is ~75% of the absolute light output for NE-213.

Finally, for other charged particles that are obtained at the larger incident neutron energies, SCINFUL includes simple multiplicative factors with respect to one of the sets of tabulated values. These factors were deduced also from the measurements of Bechetti et al.[32] They are as follows:

Boron light = 1.2 times carbon light.

Beryllium light = 1.33 times carbon light.

Lithium light = $(2.6 - 0.006 * E_n)$ times carbon light.

^{3}He light = 1.25 times alpha light.

Triton light = 0.8 times deuteron light.

It is essentially impossible to validate these multiplicative values by comparisons of response calculations with experiment; however, such being the case the values used are certainly representative and adequate for the purpose intended.

7. OTHER FEATURES IN SCINFUL

There are several other features in SCINFUL which should be mentioned. First, impinging neutrons are assumed to emanate from a point. The point source may be placed at any location with respect to the detector, even inside it. However, a source placed behind the detector is moved to an equivalent position in front of the detector, since no provisions are made in the program to compute effects of any attached light pipe, photomultiplier tube or other peripheral material.

A second feature is the ability to define a "collimator" for the front face of the detector, i.e., a centered circular area smaller than the circular area of the front face. This infinitely-absorbing, zero-thickness "collimator" may also be used to mask the curved surface of the detector from a source placed at an angle with respect to the detector axis such that emanating neutrons illuminate both the front face and the curved surface.

A third useful feature is the ability to choose from a neutron distribution as well as to being able to specify a monoenergetic source. The two distributions available are (a) a uniform distribution and (b) a Maxwellian distribution.

A fourth feature, for an NE-213 calculation, is the capability of performing the computational equivalent of electronic pulse-shape-discrimination (PSD). In this mode if any type of event in the detector (such as inelastic scattering from ^{12}C) is followed by photon production, and if the program determines that this photon subsequently interacts in the detector, then the complete history for that neutron is discarded, and the total number of recorded events is reduced by one from the total number specified by the (input) number of histories. The utility of this feature depends to a large extent on the operation of the real electronic PSD circuitry. Measurement of responses with and without PSD for $E_n \sim 7$ MeV should indicate whether or not the PSD circuitry is affecting observed detector response to 4.4-MeV gamma rays following inelastic scattering of neutrons by ^{12}C in the detector.

A fifth feature of the present program is the first-order computation of the attenuation of the fluorescent light by the detector before the light reaches the photocathode. As discussed above, it is evident from study of the literature that this contribution to the response is not well understood; one should probably not use this capability built into SCINFUL without careful study of the specific detector and source configuration being modeled by the calculation.

8. COMPARISONS WITH EXPERIMENTAL DATA AND OTHER PROGRAM CALCULATIONS

Extensive comparisons of data calculated using SCINFUL with experimental data have been carried out and are reported in this section of this report. In addition, some calculations reported in the literature due to other codes have also been compared to SCINFUL output; however, complete comparisons with all other such programs have not been attempted.

The first set of comparisons are with the spectral data of Subramanian et al.[20] and these comparisons are exhibited in Figures 10 through 23. The experiment reports spectral distributions of separated charged particles ($p, d, t, {}^3$He and α) presented as a function of outgoing angle. In reply to my inquiry one of the authors[53] kindly provided me with angle-integrated differential cross sections representing particle energy spectra. These are the data shown in the 14 figures. To compare with these data, an intermediate output was programmed into SCINFUL to provide a comparable set of angle-integrated particle energy spectra. The SCINFUL results are shown as histograms in these 14 figures. These data have already been mentioned above. In particular, the triton and ^{3}He spectral data were used directly in developing SCINFUL to provide cross section as well as angular distribution information for these reaction types. The proton and deuteron data, Figures 10, 11, 14, 15, 19 and 20, were important constraints along with other data in developing the cross section data used in SCINFUL for $E_n > 20$ MeV as well as the programming of the various multi-body breakup reactions. Preliminary versions of the program, for example, indicated a proton spectrum for $E_n = 27.4$ MeV at about 3 times larger than the experimental data shown in Figure 10. Because in the multi-body breakup programming of SCINFUL alpha particles are produced from events of the other major types (i.e., simultaneous with each of the other four charged particles) as well as in the ${}^{12}\mathrm{C}(n, n')3\alpha$ reaction, it became evident that the experimental alpha spectra, Figures 13, 18 and 23, would be of little help in determining places in the SCINFUL program needing improvement. All that could be done was to compare the computed alpha spectra with the experimental spectra to see how close the two were, and so in a sense these comparisons provide a quantitative test of how well the code performs at the nuclear physics level.

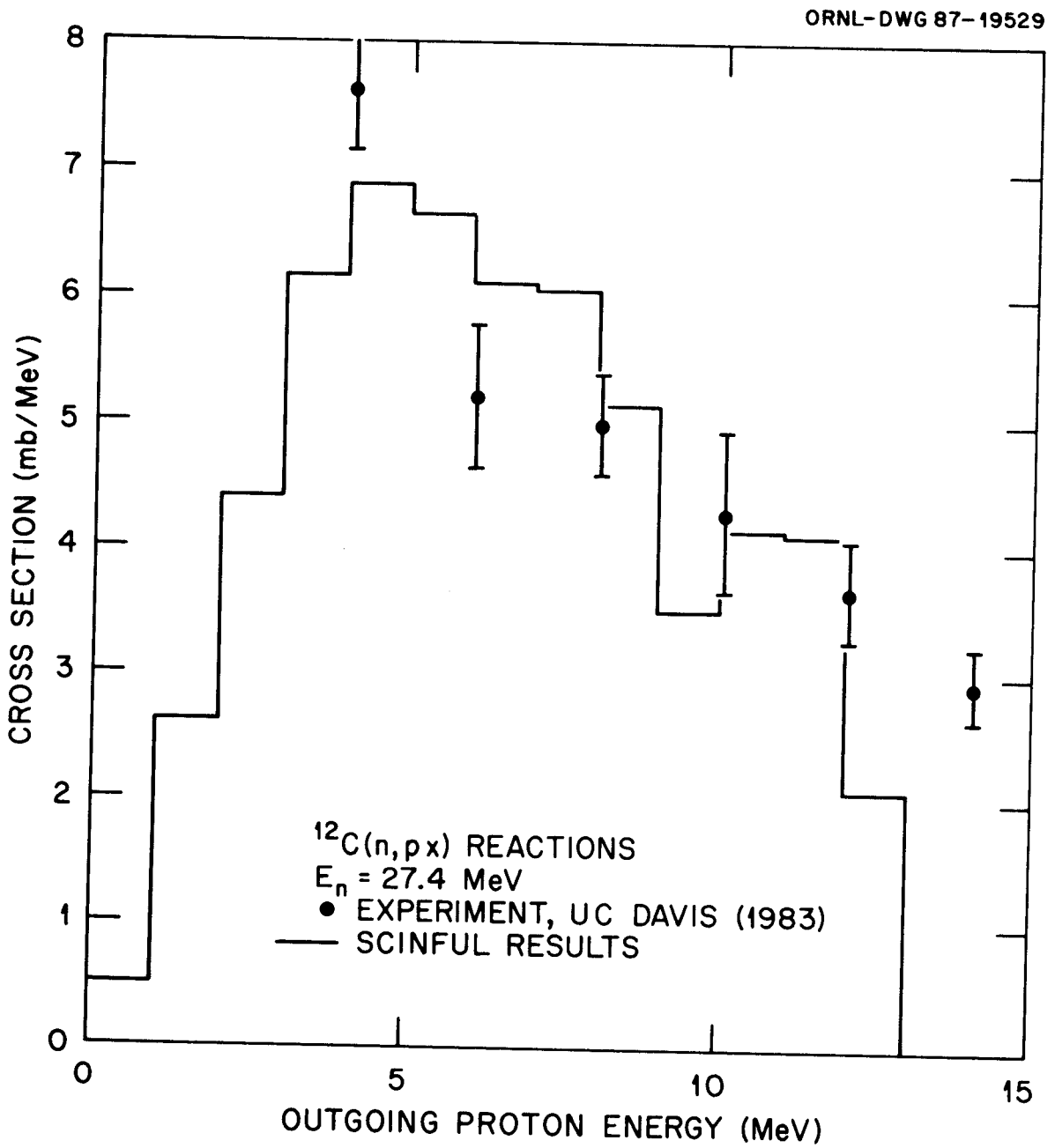

Fig. 10. Proton angle-integrated energy spectrum for 27.4-MeV neutrons incident on ^{12}C as measured by Subramanian et al. (refs. 20 and 53) compared with calculations using SCINFUL.

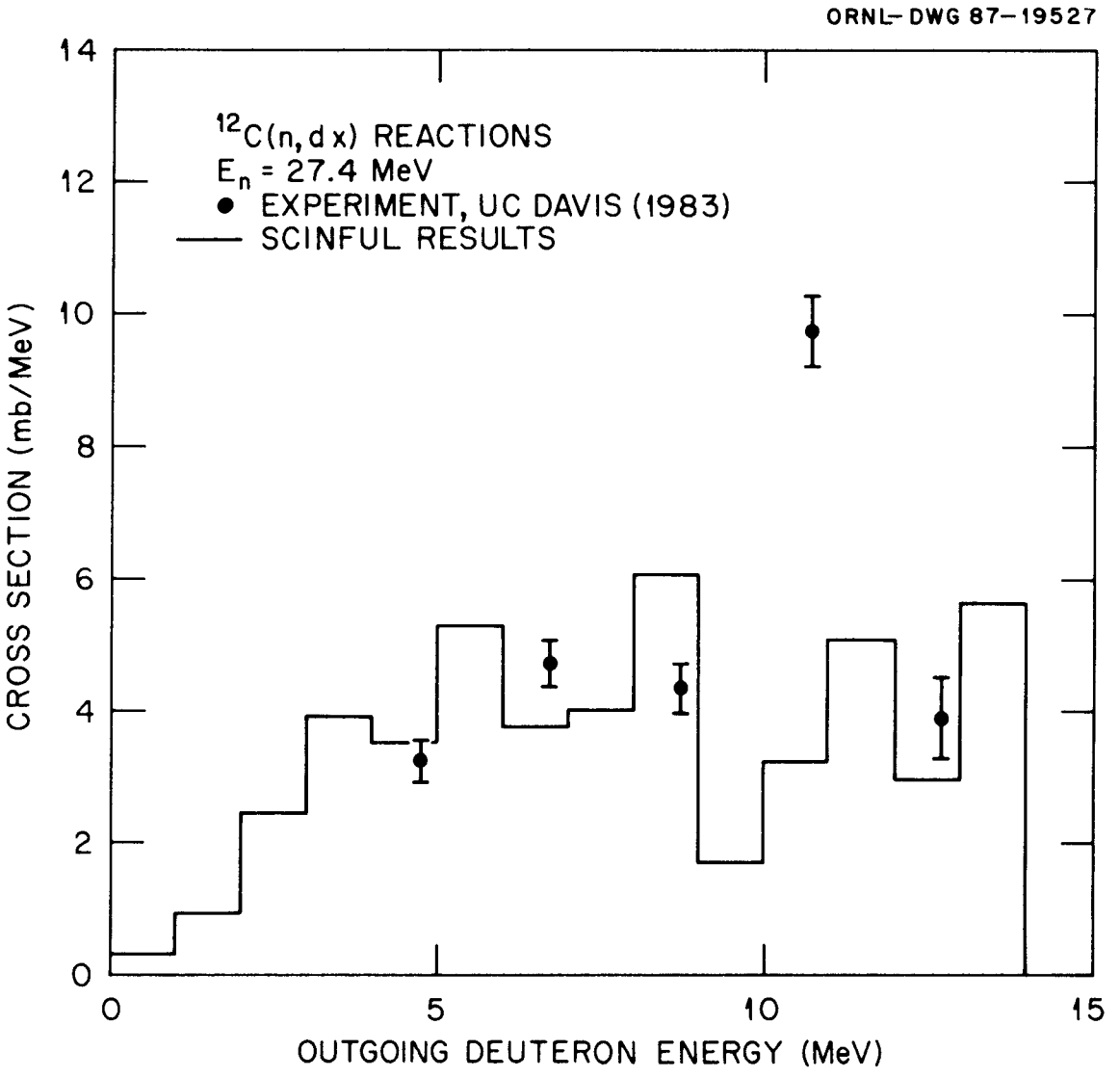

Fig. 11. Deuteron angle-integrated energy spectrum for 27.4-MeV neutrons incident on ^{12}C as measured by Subramanian et al. (refs. 20 and 53) compared with calculations using SCINFUL.

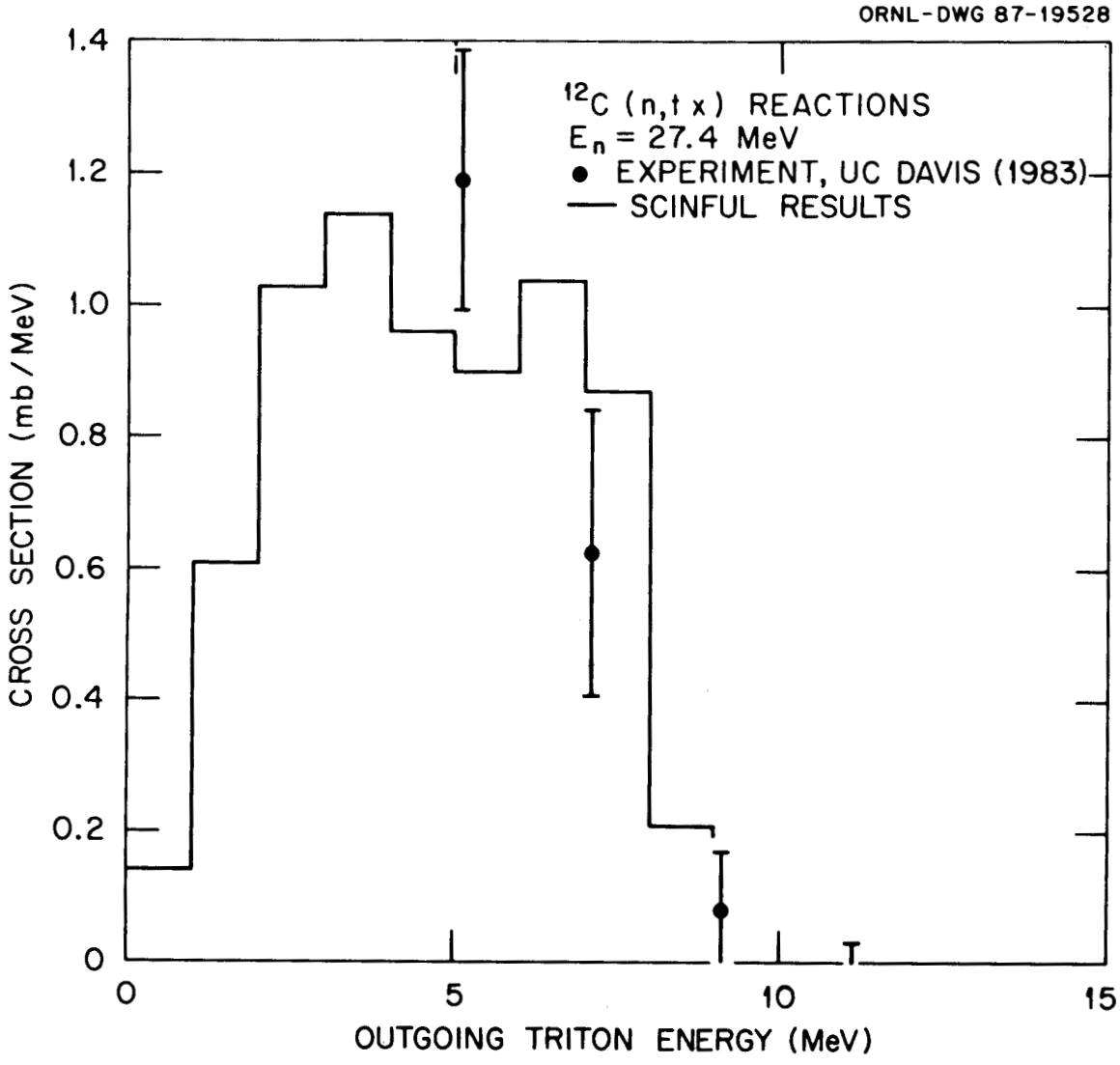

Fig. 12. Triton angle-integrated energy spectrum for 27.4-MeV neutrons incident on ^{12}C as measured by Subramanian et al. (refs. 20 and 53) compared with calculations using SCINFUL.

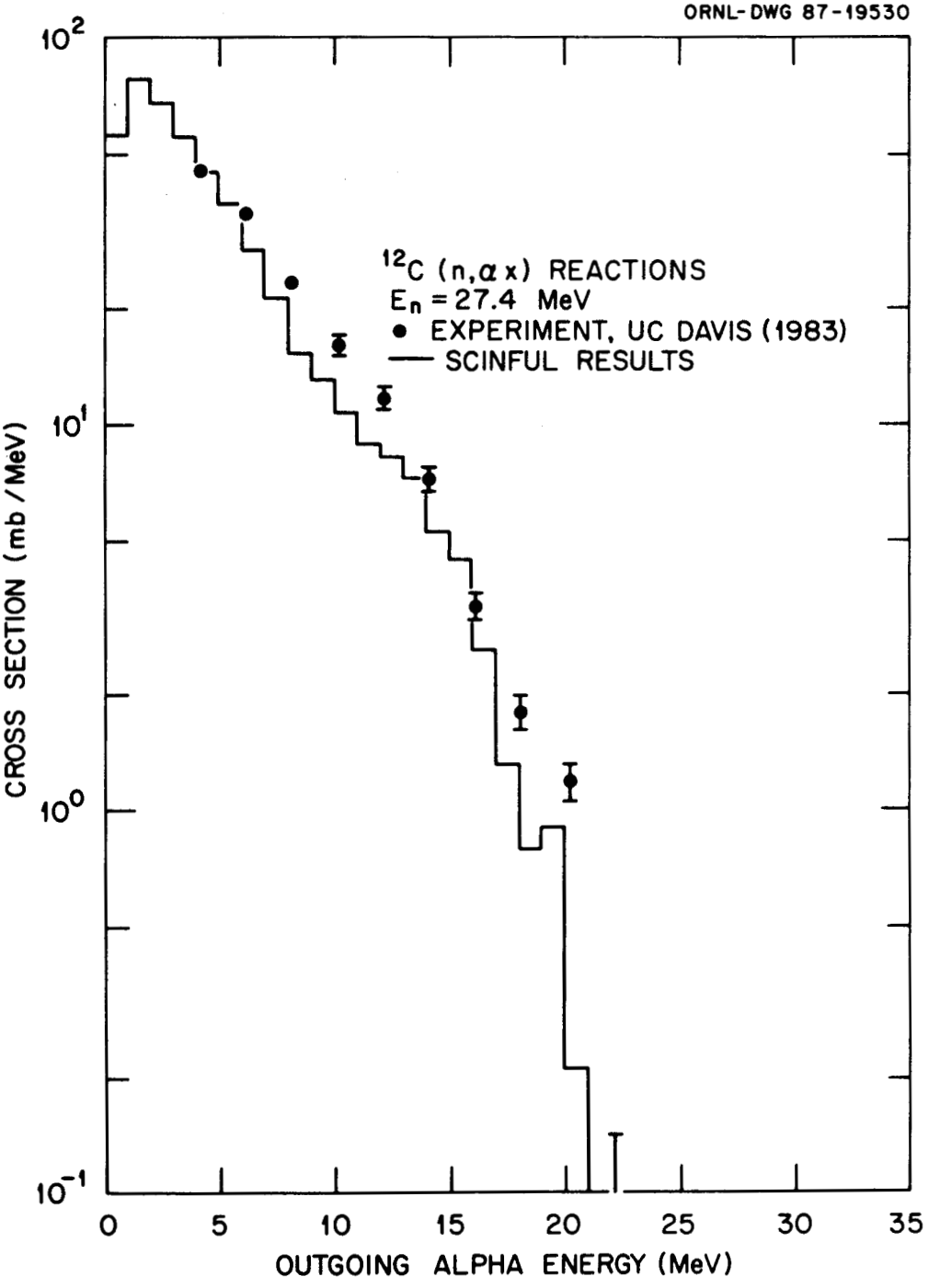

Fig. 13. Alpha angle-integrated energy spectrum for 27.4-MeV neutrons incident on ^{12}C as measured by Subramanian et al. (refs. 20 and 53) compared with calculations using SCINFUL.

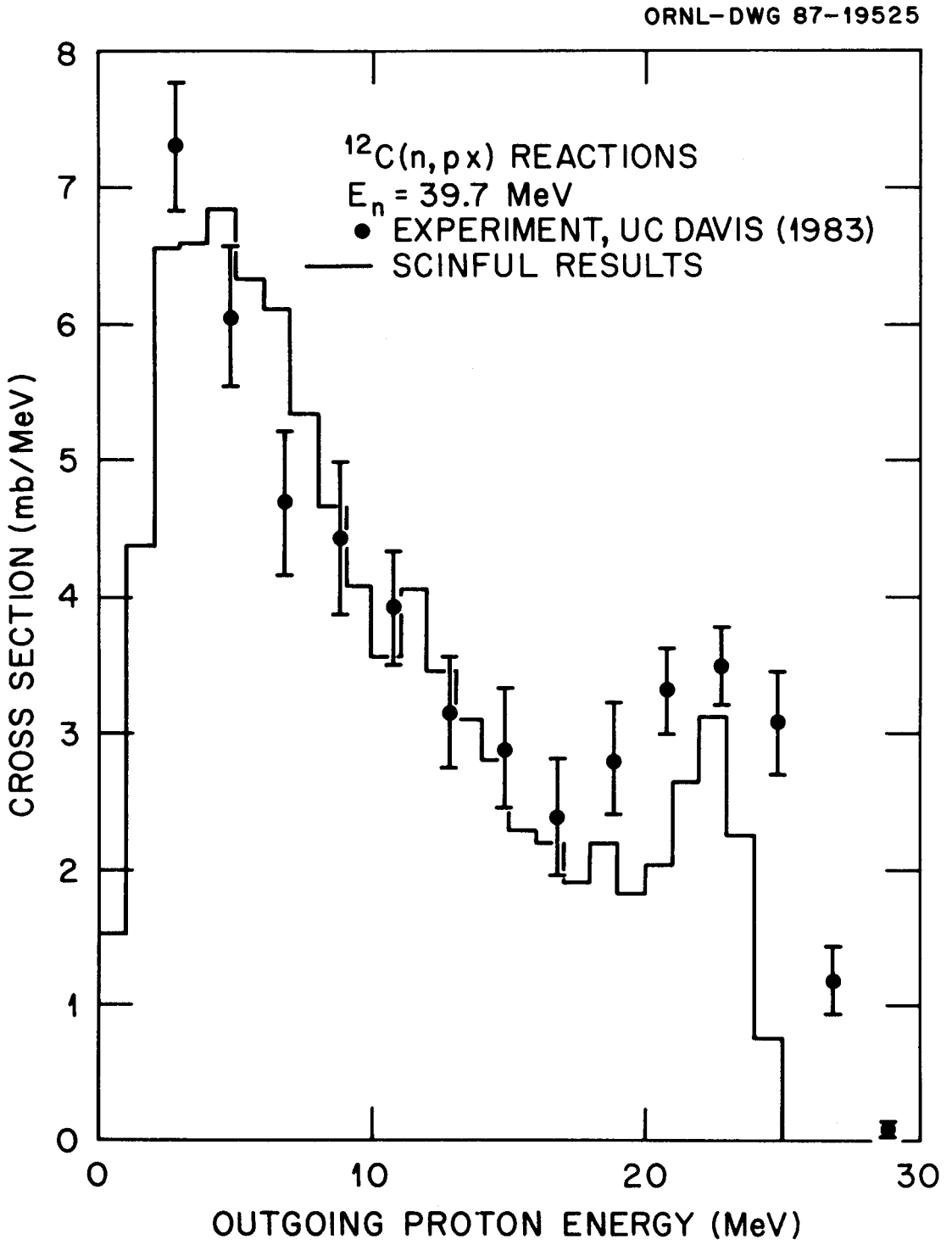

Fig. 14. Proton angle-integrated energy spectrum for 39.7-MeV neutrons incident on ^{12}C as measured by Subramanian et al. (refs. 20 and 53) compared with calculations using SCINFUL.

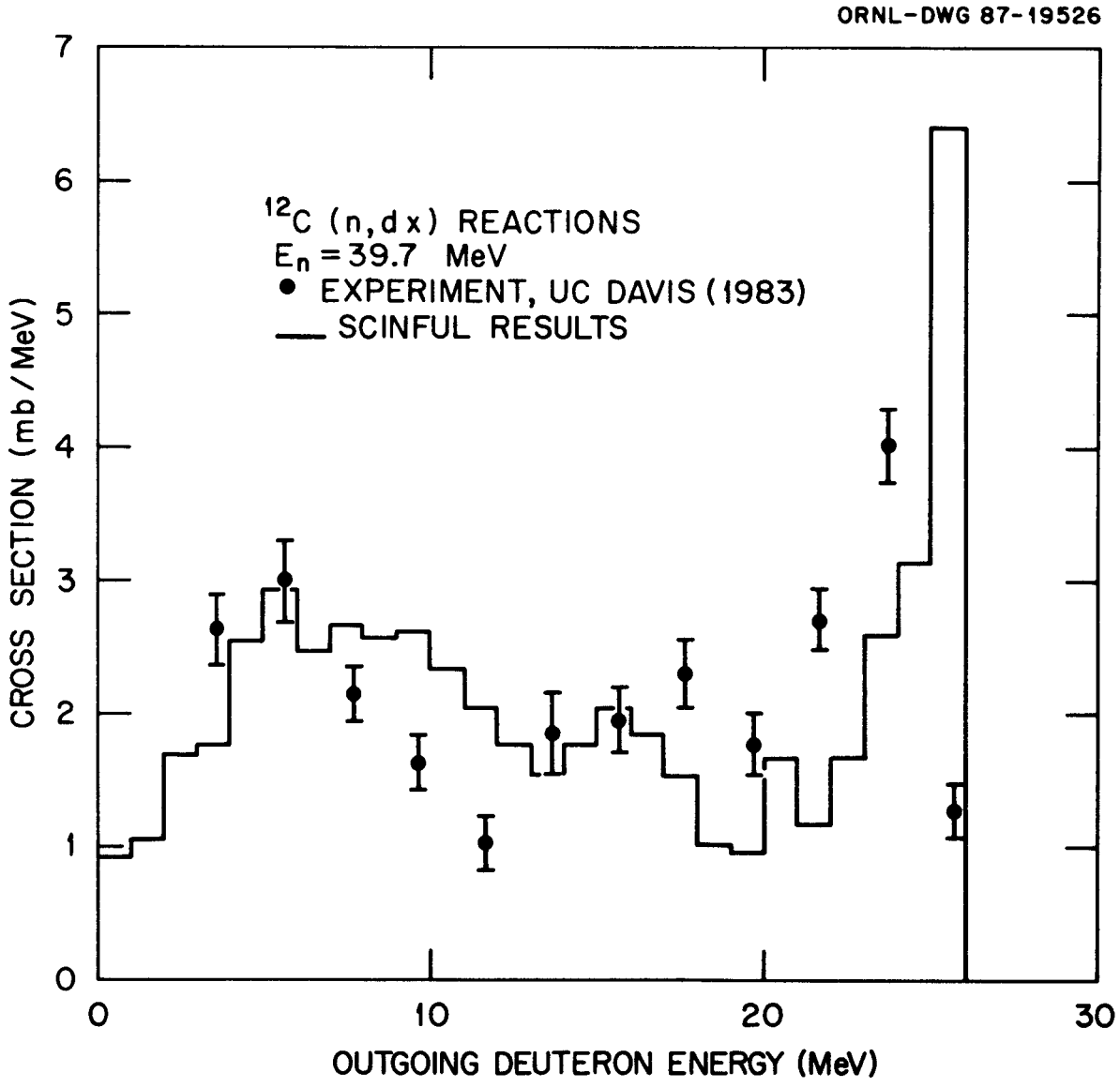

Fig. 15. Deuteron angle-integrated energy spectrum for 39.7-MeV neutrons incident on ^{12}C as measured by Subramanian et al. (refs. 20 and 53) compared with calculations using SCINFUL.

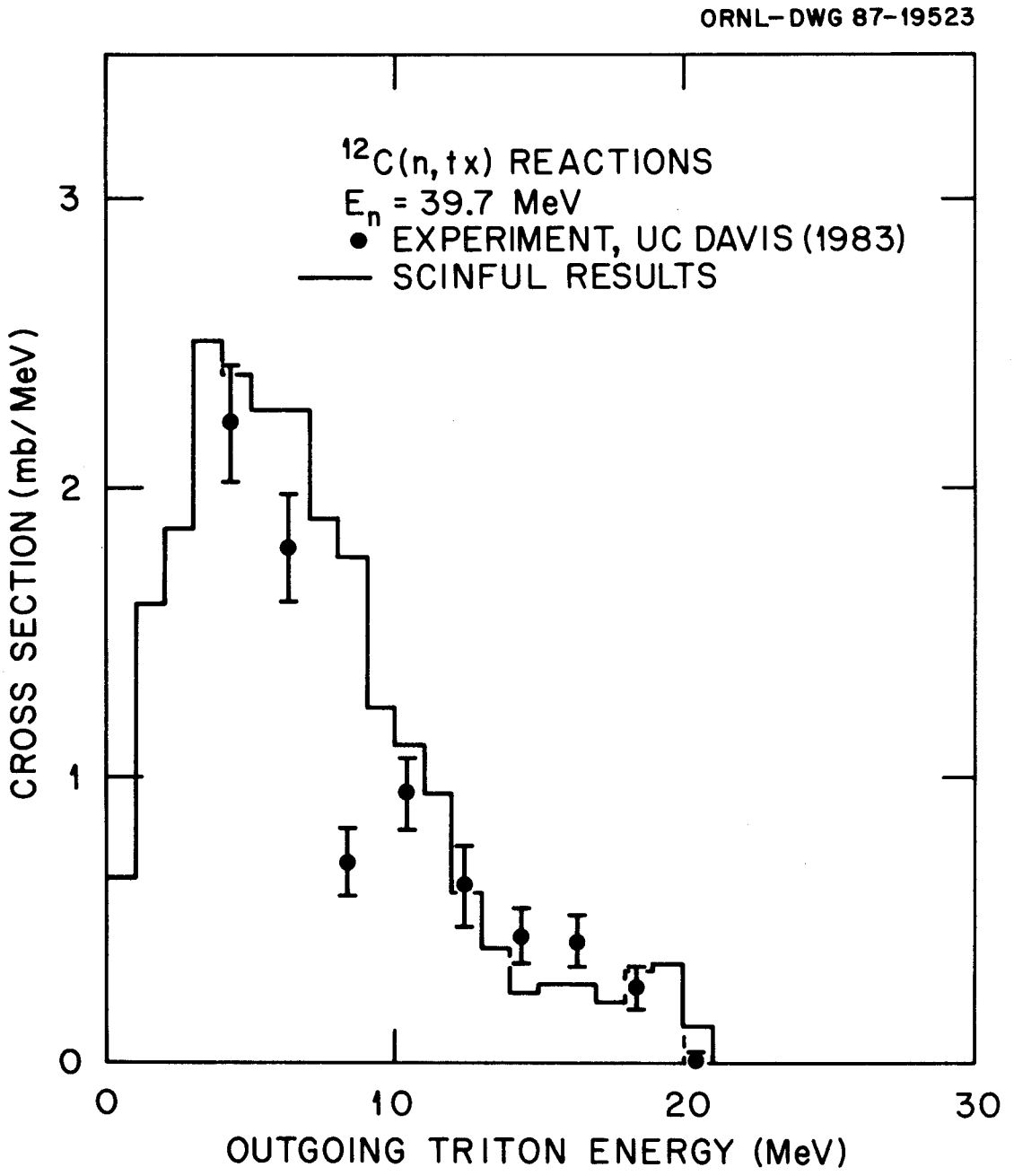

Fig. 16. Triton angle-integrated energy spectrum for 39.7-MeV neutrons incident on ^{12}C as measured by Subramanian et al. (refs. 20 and 53) compared with calculations using SCINFUL.

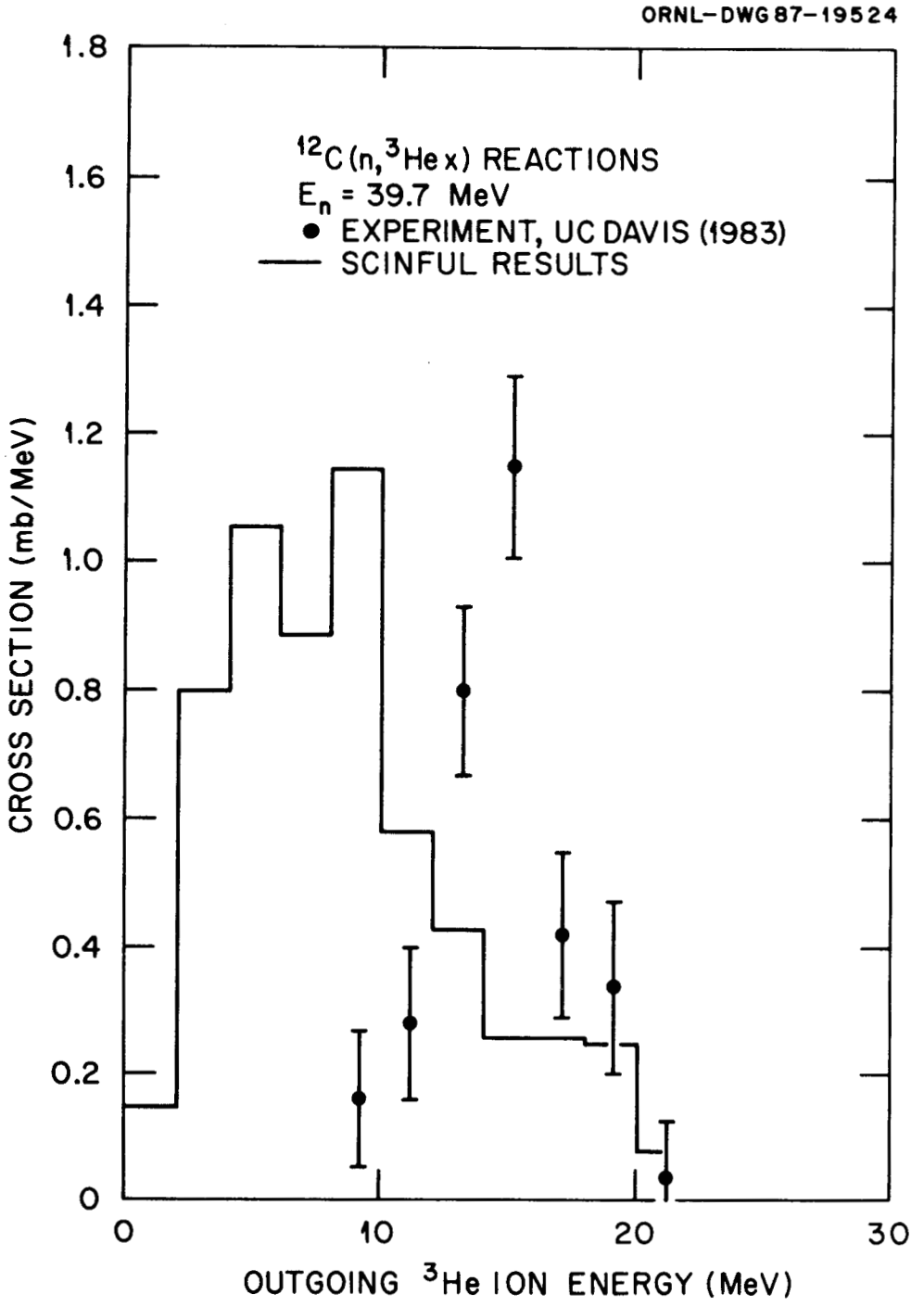

Fig. 17. ^{3}He ion angle-integrated energy spectrum for 39.7-MeV neutrons incident on ^{12}C as measured by Subramanian et al. (refs. 20 and 53) compared with calculations using SCINFUL.

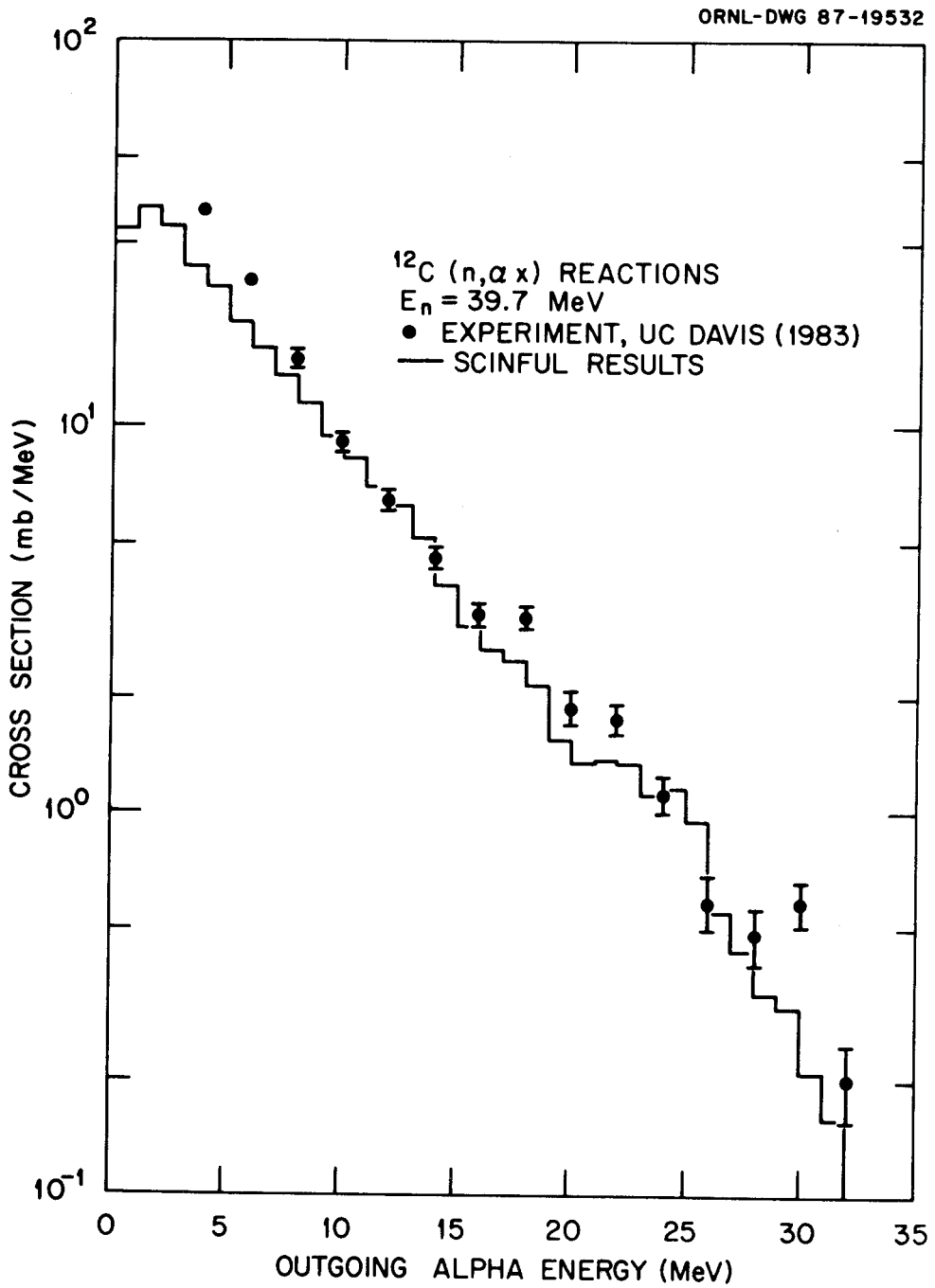

Fig. 18. Alpha angle-integrated energy spectrum for 39.7-MeV neutrons incident on ^{12}C as measured by Subramanian et al. (refs. 20 and 53) compared with calculations using SCINFUL.

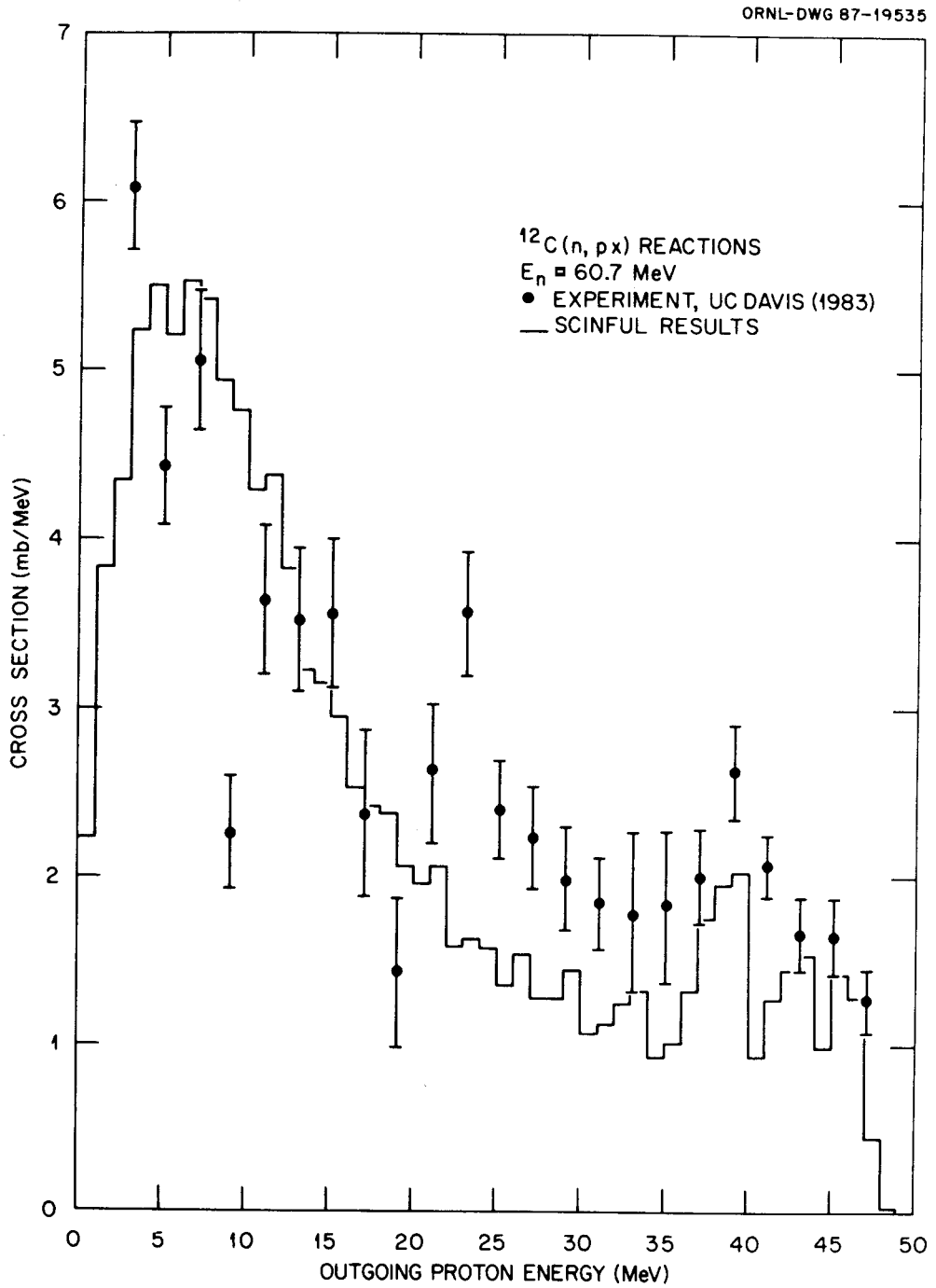

Fig. 19. Proton angle-integrated energy spectrum for 60.7-MeV neutrons incident on ^{12}C as measured by Subramanian et al. (refs. 20 and 53) compared with calculations using SCINFUL.

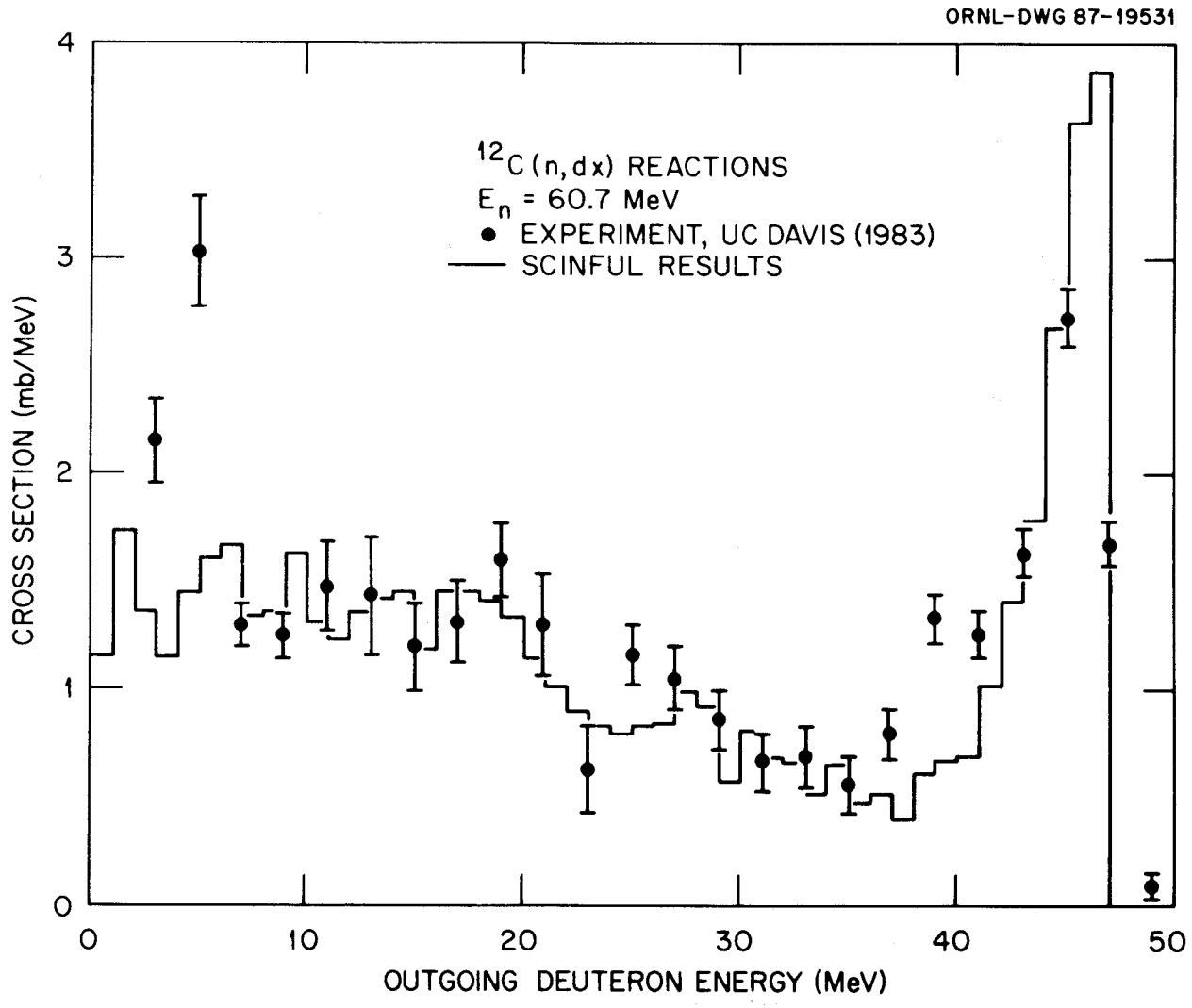

Fig. 20. Deuteron angle-integrated energy spectrum for 60.7-MeV neutrons incident on ^{12}C as measured by Subramanian et al. (refs. 20 and 53) compared with calculations using SCINFUL.

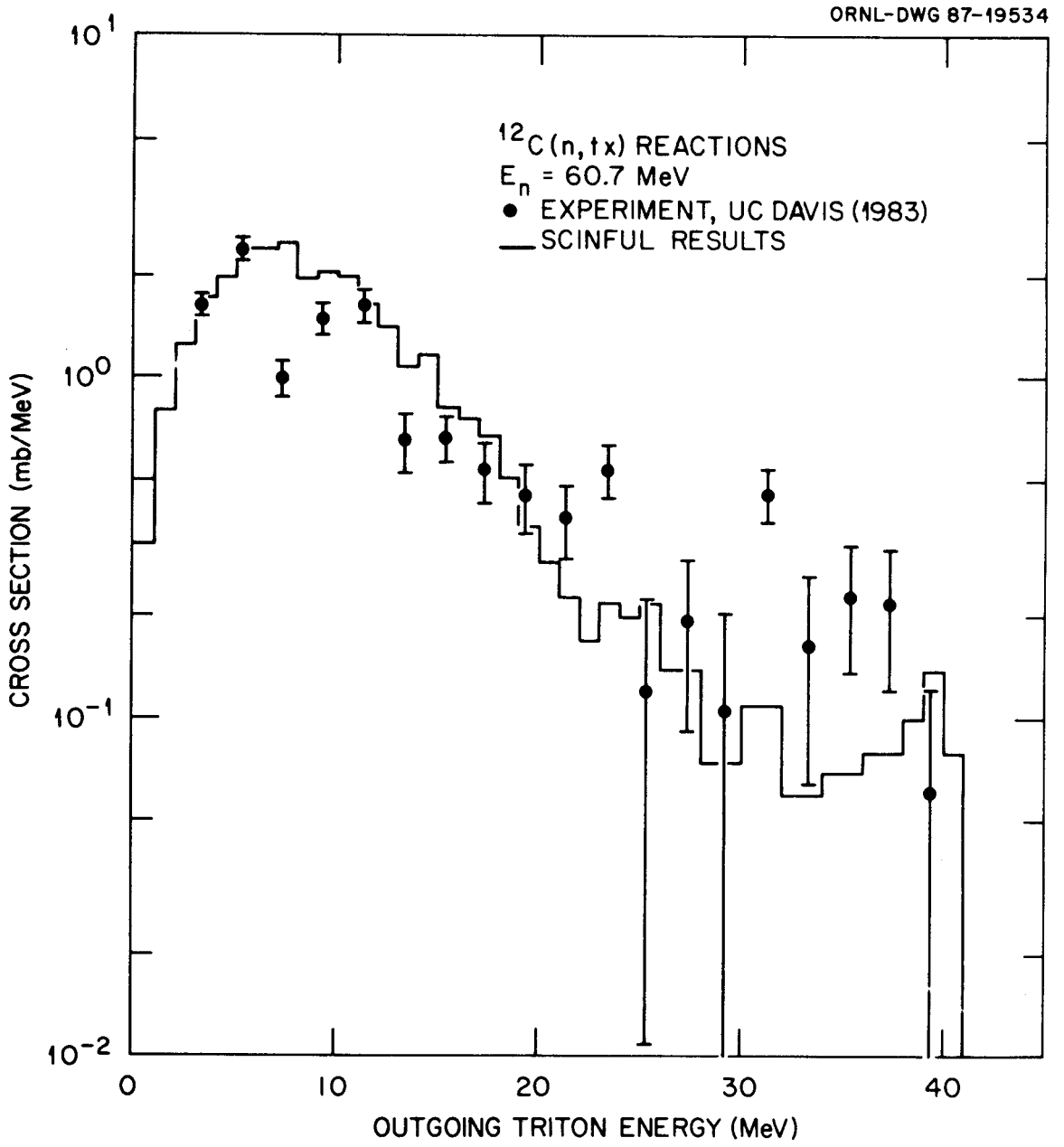

Fig. 21. Triton angle-integrated energy spectrum for 60.7-MeV neutrons incident on ^{12}C as measured by Subramanian et al. (refs. 20 and 53) compared with calculations using SCINFUL.

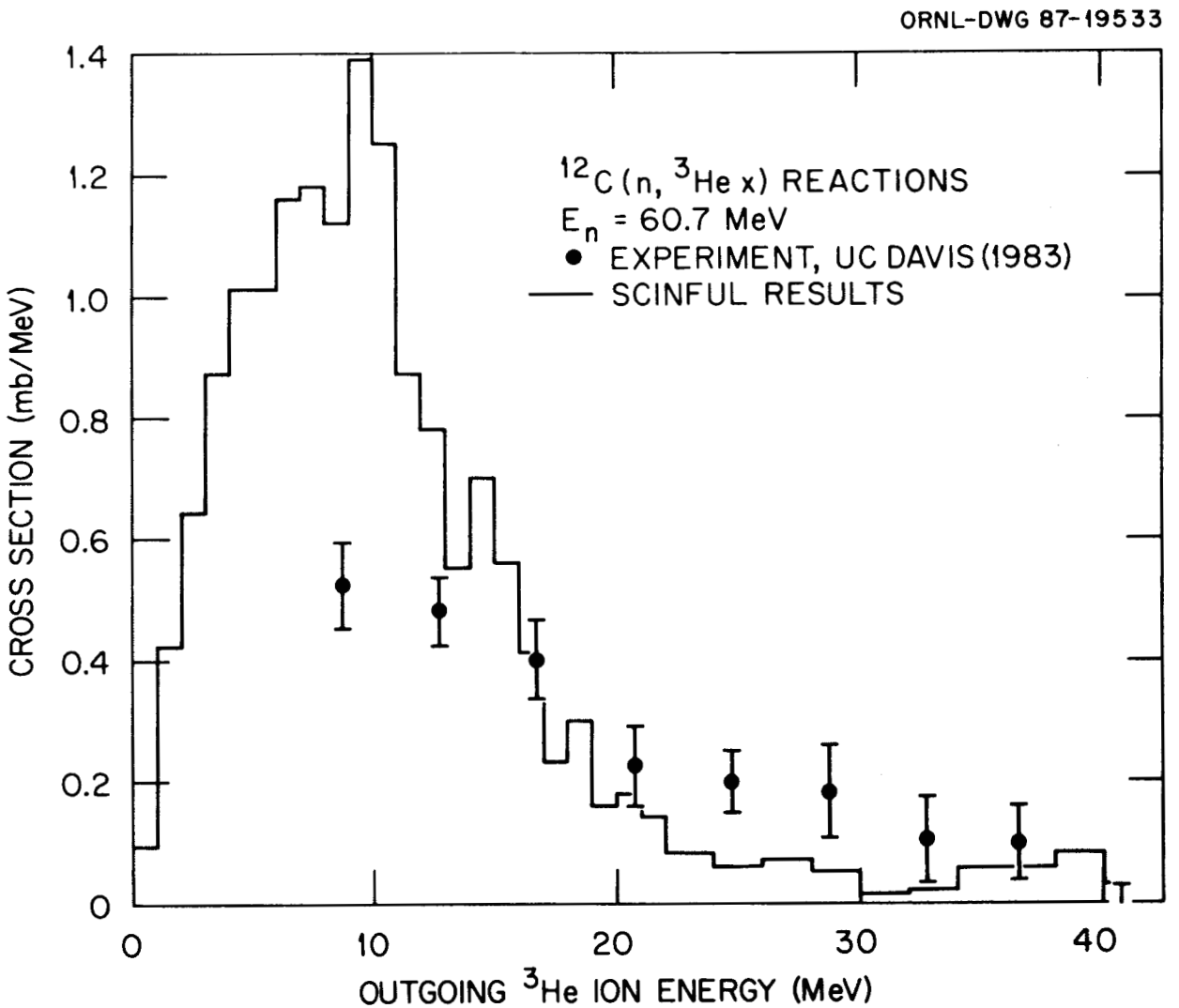

Fig. 22. ^{3}He ion angle-integrated energy spectrum for 60.7-MeV neutrons incident on ^{12}C as measured by Subramanian et al. (refs. 20 and 53) compared with calculations using SCINFUL.

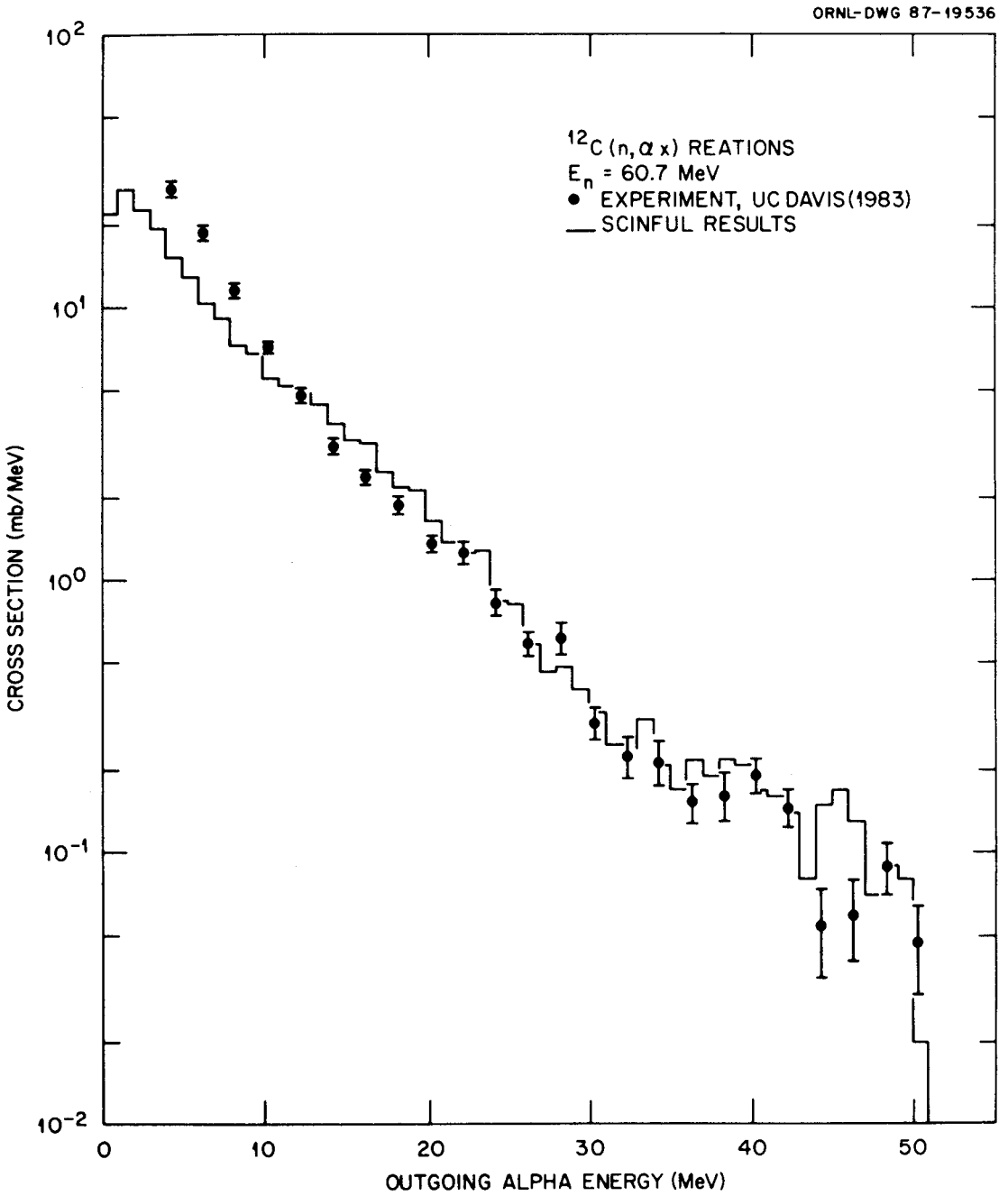

Fig. 23. Alpha angle-integrated energy spectrum for 60.7-MeV neutrons incident on ^{12}C as measured by Subramanian et al. (refs. 20 and 53) compared with calculations using SCINFUL.

Qualitatively the comparisons in Figures 10 through 23 are very good. Quantitatively there are a few misses. In Figure 11, there is essentially no way for the SCINFUL program to reproduce the large value at $E_d \sim 11$ MeV. In Figure 13, the ~25% miss for E_α between about 10 and 12 MeV could probably be lessened with small changes to the programming computing the $^{12}C(n,n')3\alpha$ reaction channel, but it is not likely such changes could be made without also worsening the comparisons for the p, d and t spectra. In Figure 14 the data for $E_p > 20$ MeV indicate that SCINFUL is underpredicting the $^{12}C(n,p)^{12}B$ (bound state) reaction by ~30%. In Figure 15, the high-energy deuteron data would be better represented if the SCINFUL results were folded with a detector resolution function. In Figure 17, SCINFUL does not predict enough high-energy ^{3}He ions; however, the cross sections are quite small compared to the alpha spectrum in Figure 18, and differences in Figure 17 are not likely to affect detector response calculations. The comparison in Figure 18 is really quite good. For protons at $E_n = 60.7$ MeV, the comparison in Figure 19 does suggest that the number of predicted high-energy outgoing protons is 20 to 25% too small, but again as for $E_n = 39.7$ MeV, nudging the program to improve the proton spectrum tends to worsen agreement with the other charged-particle spectra. In Figure 20, experimental data for $E_d < 5$ MeV are probably due to a multi-body breakup reaction not programmed into SCINFUL. And finally, the comparison of the alpha spectra in Figure 23 is quite good, with only the lowest outgoing alpha portion of the experiment being underpredicted.

The next set of data to compare SCINFUL calculations with are the cloud-chamber data of Kellogg[22] obtained over 30 years ago for $E_n = 90$ MeV. In this experiment neutrons interacted with carbon producing "stars" made up of the spiraling tracks of outgoing charged particles. These stars were photographed and analyzed to determine the break up of the ^{12}C into charged particles, p, d, t, ^{3}He, α, Li, Be and B, with each track, or prong, from the star center representing one such charged particle. The measurement could not record any outgoing neutrons. A total of 1029 stars were identified. For comparison, the SCINFUL program was run for about 60000 histories for a 90-MeV neutron incident on a thin detector, thin enough such that there would be very little multiple scattering of the incident neutrons. The total number of interactions which could be compared directly to Kellogg's data was 20476, or a factor of 19.9 times the experimental[22] number of stars. For the present study, the meaningful comparisons are given in Table 2.

Table 2. Charged-particle production for 90-MeV neutron interaction with carbon

Type of Data	Yield: Experiment	Yield: SCINFUL	Ratio SCIN/Exp
Total Events	1029	20476	19.9
Total p	781	15697	20.1 ± 0.8
Total d	410	4662	11.4 ± 0.6
Total t	99	2278	23.0 ± 2.4
Total ^{3}He	28	626	22.4 ± 4.3
Total α	543	13643	25.1 ± 1.1
Total Li	168	1025	6.1 ± 0.5
Total Be	138	3574	25.9 ± 2.3
Total B	542	9175	16.9 ± 0.8
$p(E_p > 20$ MeV)	378	8923	23.6 ± 1.3
$d(E_d > 27$ MeV)	108	2904	26.9 ± 2.7
$t(E_t > 33$ MeV)	13	137	10.5 ± 3.1
$p + B$	422	7000	16.5 ± 0.8
$d + B$	104	2084	20.0 ± 2.0
$t + B$	16	91	5.7 ± 1.6
^{3}He + Be	0	47	
α + Be	11 ± 2	206	17.0 ± 0.8
Total 2 Prong	553	9428	17.0 ± 0.8
Total 3 Prong	318	6717	21.1 ± 1.2
Total 4 Prong	151	4469	29.6 ± 2.5
Total 5 Prong	7	not programmed	

If SCINFUL were capable of well-reproducing the data then one would expect the ratios of the various comparisons all to be very close to 20. In fact most of the ratios are between 16 and 25, which is heartening and suggests that for E_n up to

90 MeV the calculational methods plus estimated cross sections are combining to provide a reasonable representation of the nuclear physics results. On the other hand the observed differences are sufficient to warrant caution with regard to computed detector responses, and, indeed, the insufficiency in agreement for several of the data types in Table 1 was the principal reason for terminating the present program's range at 80 MeV rather than at 90 or perhaps 100 MeV.

Now we go on to the next step in the response computation which is to include the fluorescent light output. In the next two tables and nine figures SCINFUL predictions of detector efficiency above selected biases will be compared with experimental results from 10 different experiments. In quick summary these experiments are:

Table 3:	Renner et al.[14] at Oak Ridge. NE-110, rad = 5.1 cm, ht = 6.6 cm at the center of a curved back surface. Beam collimated to 0.8 cm
Figure 24:	Dekempeneer et al.[11] at GEEL. NE-213, rad = 2.54 cm, ht = 5 cm.
Figure 25:	Brede et al.[54] at Physikalisch-Technische Bundesanstalt. NE-213, rad = 2.54 cm, ht = 2.54 cm.
Figure 26:	Fowler et al.[55] at the AERE. NE-213, rad = 2.54 cm, ht = 3.81 cm.
Figure 27:	Olsson and Trostell at Studsvik.[33] NE-213, rad = 6.25 cm, ht = 5.1 cm. Source-to-detector distance = 4 m.
Figure 28:	As Figure 27, only source-to-detector distance = 2.5 m.
Figure 29:	Hunt et al.[56] at Rutherford. NE-102 detector calculated as NE-110. Rad = 5.14 cm, ht = 5.08 cm.
Figure 30:	McNaughton et al.[57] at the Crocker Nuclear Lab. at UC-Davis. NE-102 calculated as NE-110, rad = 3.55 cm, ht = 15.2 cm.
Figure 31:	Riddle et al.[58] at Maryland. NE-102 calculated as NE-110. Rad = 8.86 cm, ht = 7.63 cm, beam collimated to 2.54 cm radius.

Table 3. NE-110 Detector Efficiency Comparisons

Neutron Energy (keV)	Zero-bias Efficiency		ORNL (78) Bias (L.U.)	Efficiency above ORNL Bias	
	ORNL (78)	SCINFUL		ORNL (78)	SCINFUL
82	0.998	0.998	0.003	0.843	0.926
128	0.997	0.996	0.003	0.910	0.935
137*	0.996	0.995	0.003	0.916	0.928
168	0.994	0.992	0.003	0.920	0.930
184	0.993	0.992	0.003	0.923	0.922
219	0.991	0.989	0.004	0.904	0.913
244	0.989	0.984	0.005	0.894	0.897
274*	0.987	0.982	0.005	0.895	0.890
311	0.985	0.978	0.005	0.891	0.883
352	0.981	0.979	0.006	0.880	0.877
376	0.979	0.974	0.007	0.866	0.868
439	0.974	0.966	0.01	0.837	0.846
467*	0.972	0.961	0.01	0.829	0.832
704	0.926	0.945	0.02	0.739	0.759

*Spectrum obtained and compared with SCINFUL calculation.

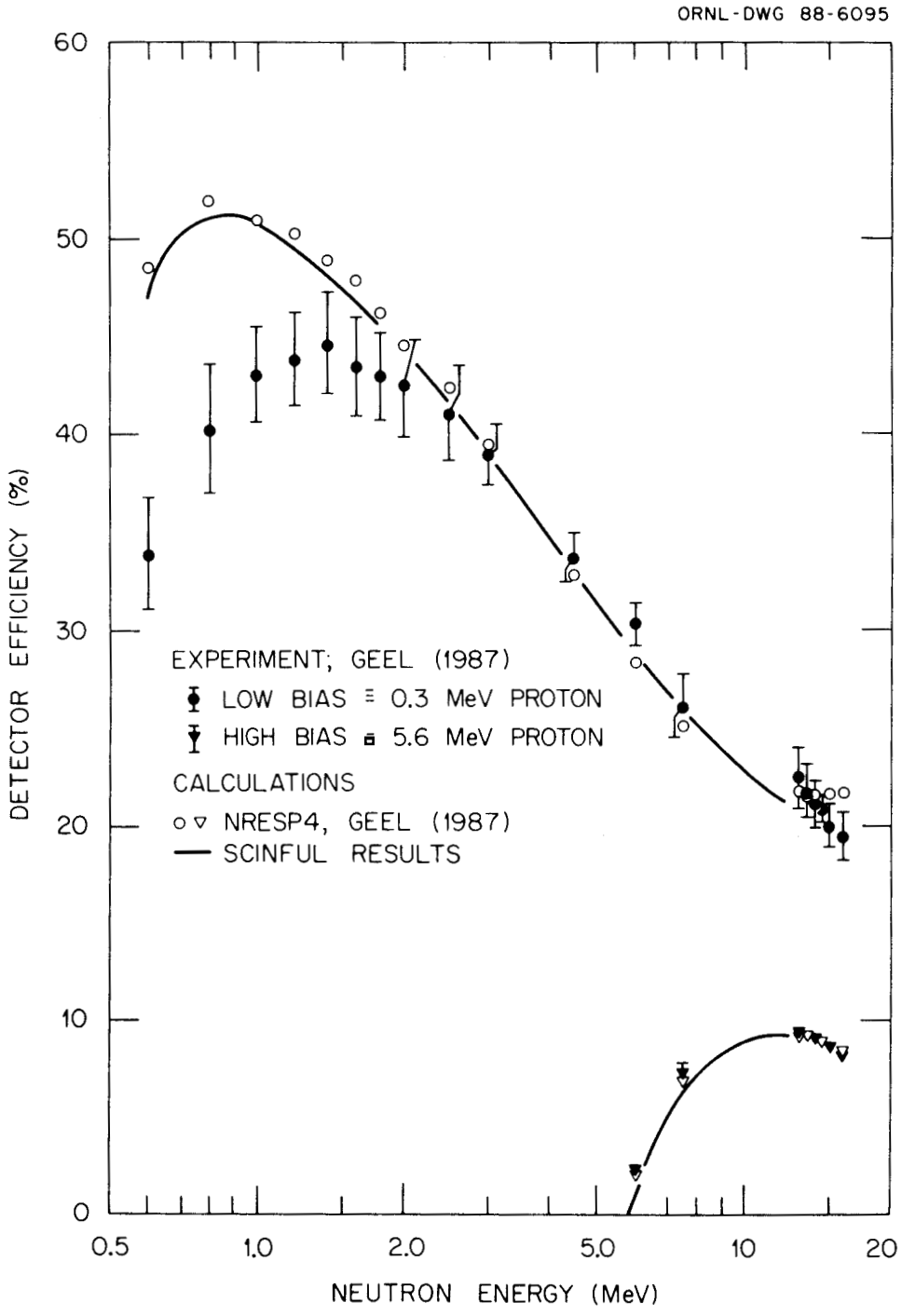

Fig. 24. Detector efficiency as a function of neutron energy for the data of Dekempeneer et al. (ref. 11) for two different electronic thresholds. Also shown are predictions of the NRESP4 code (ref. 10) as given in ref. 11.

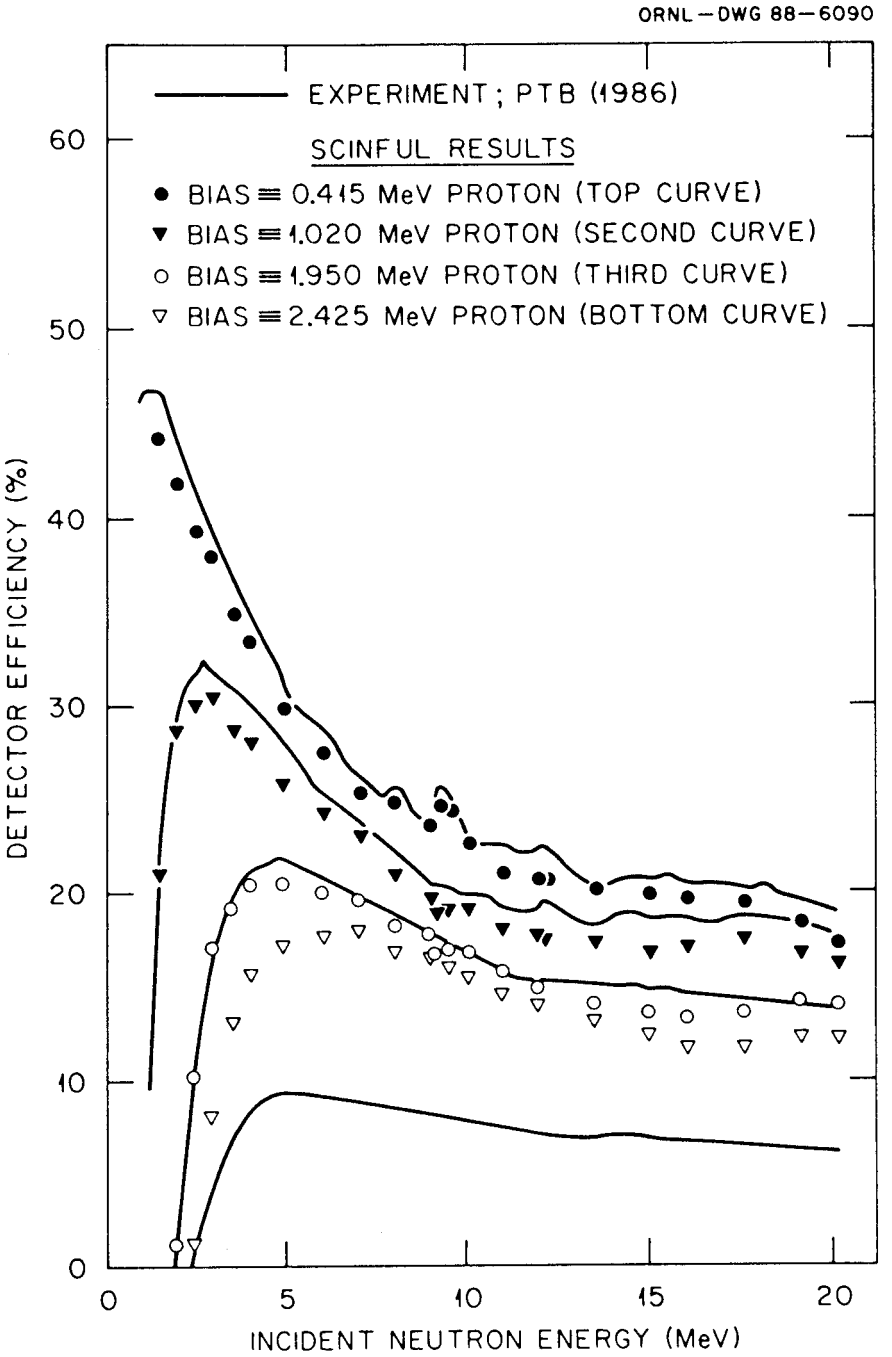

Fig. 25. Detector efficiency as a function of neutron energy for the data of Brede et al. (ref. 54) for four different electronic thresholds. There is a complete miss in the SCINFUL predictions, as given by the open triangles for the largest bias, and the experimental data, as given by the bottom curve.

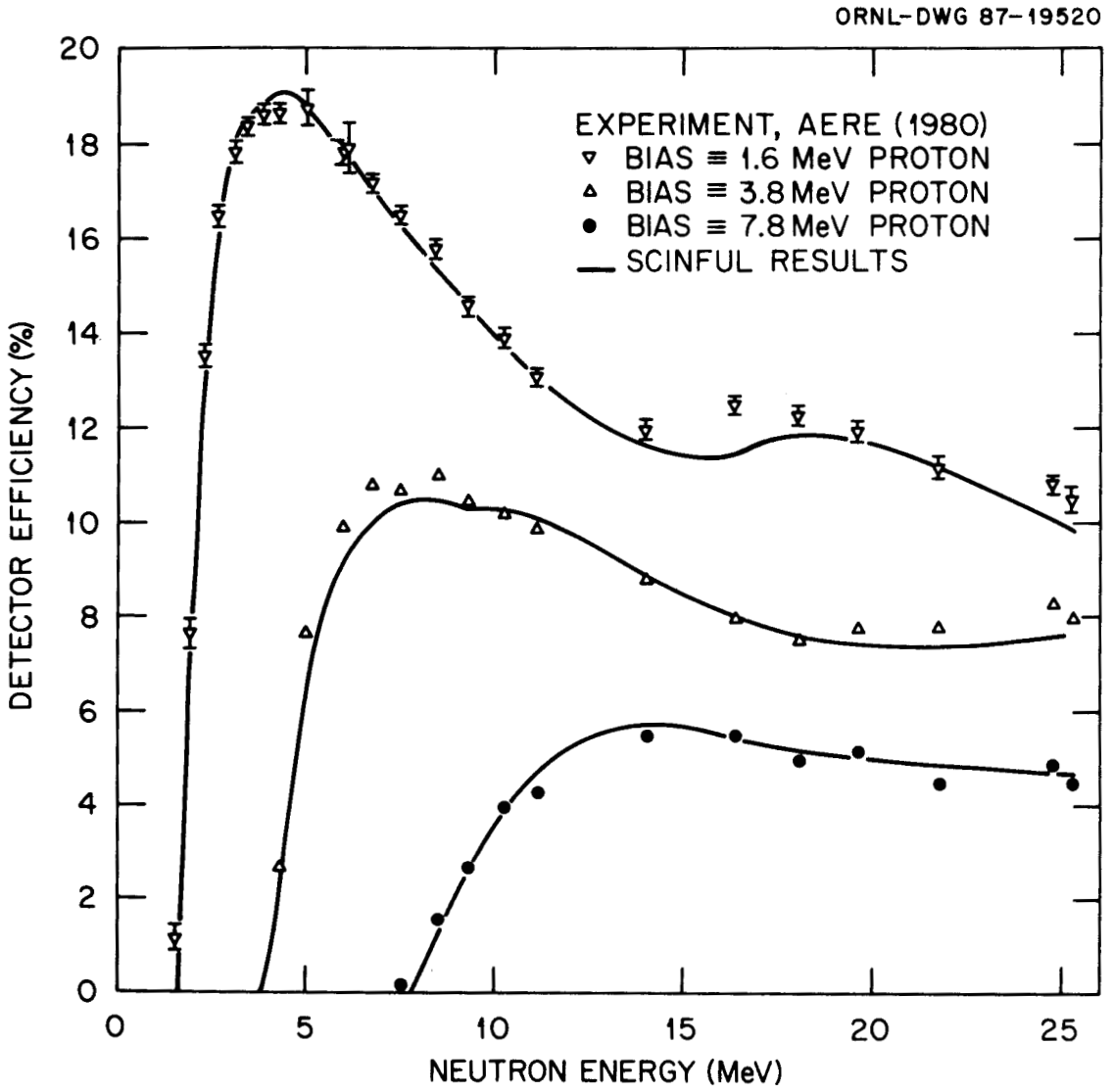

Fig. 26. Detector efficiency as a function of neutron energy for the data of Fowler et al. (ref. 55) for three different electronic thresholds. The more exact geometry description in SCINFUL provides a better fit to the lowest-bias data for $E_n < 10$ MeV than obtained from other codes.

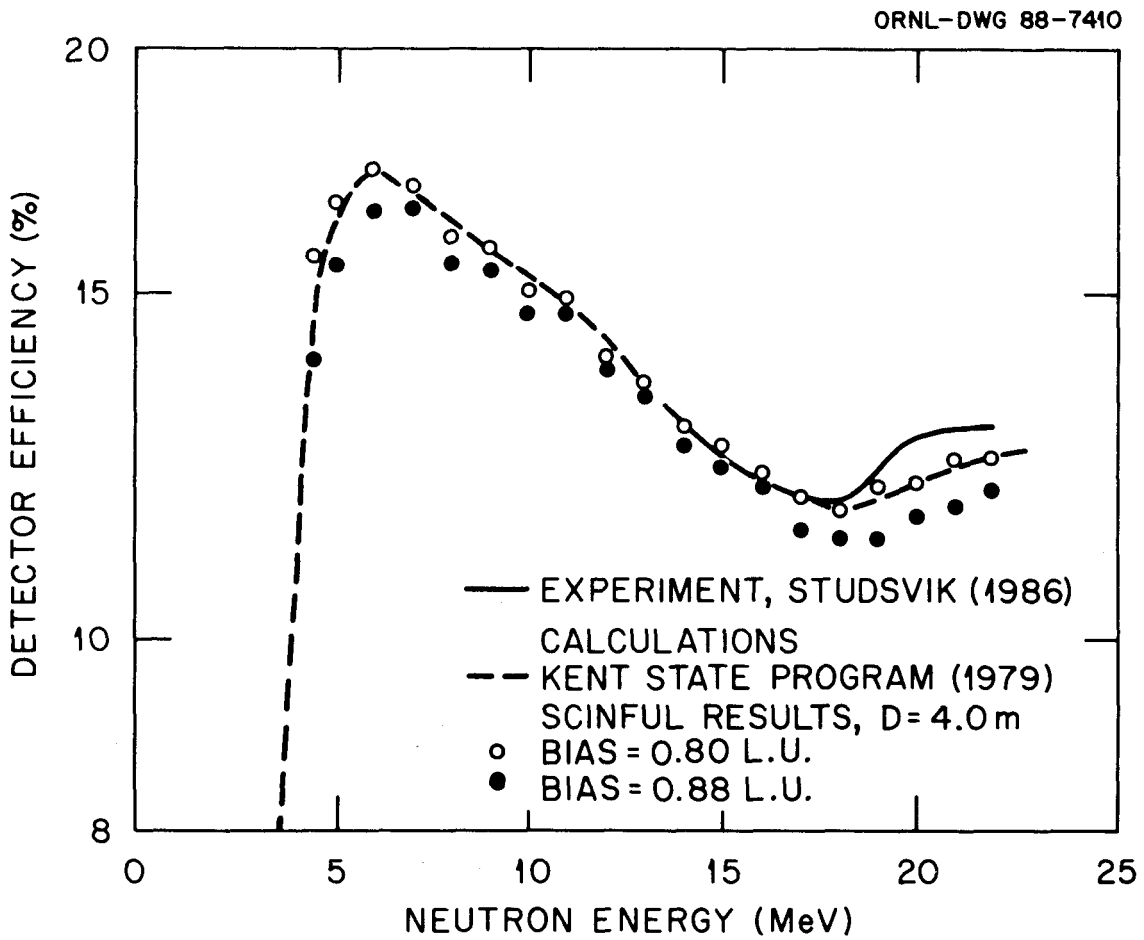

Fig. 27. Detector efficiency as a function of neutron energy for the data of Olsson and Trostell (ref. 33). In this figure the SCINFUL calculations were for a source-to-detector distance of 4 m wherein the full face of the detector was exposed. The 0.88-light-unit bias is that expected from the description given in ref. 33; however, the 0.80-light-unit bias gives a much better representation of the calculation using the code of Cecil et al. (ref. 8), shown by the dashed line, as reported in ref. 33. The experimental results between 13.5 and 22 MeV incident neutron energy were normalized to the dashed-line calculations for E_n between 13.5 and 16 MeV. However, as Olsson and Trostell point out, the dashed-line calculation does not reproduce the experimental increase between 18 and 20 MeV. Neither does either SCINFUL calculation for this geometry.

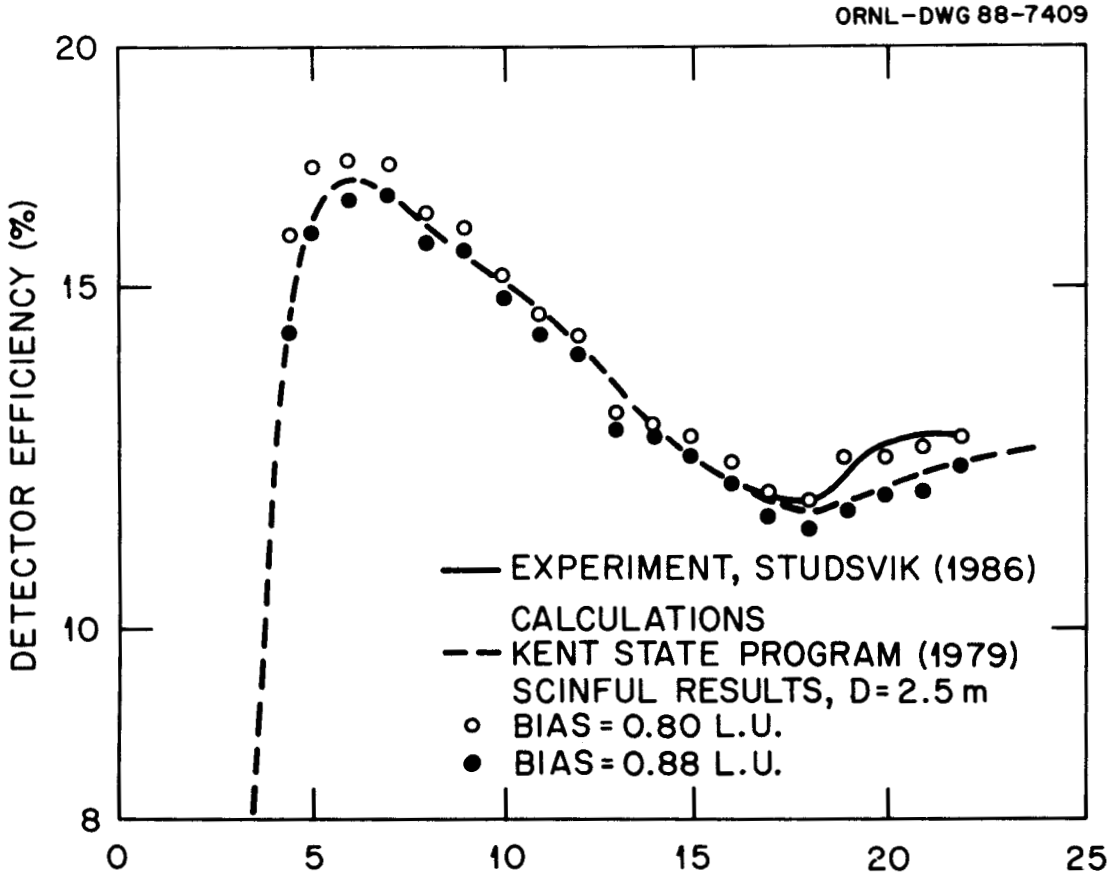

Fig. 28. Same as Figure 27, only now for a source-to-detector distance of 2.5 m which not only has the detector a little closer but also, because of the collimation exhibited in ref. 33, has the detector's outer periphery shielded. In this new geometry the 0.80-light-unit SCINFUL calculations reproduce quite well the experimental results. Also in this geometry the 0.88-light-unit SCINFUL results closely resemble the dashed-line calculations using the Cecil et al. (ref. 8) code.

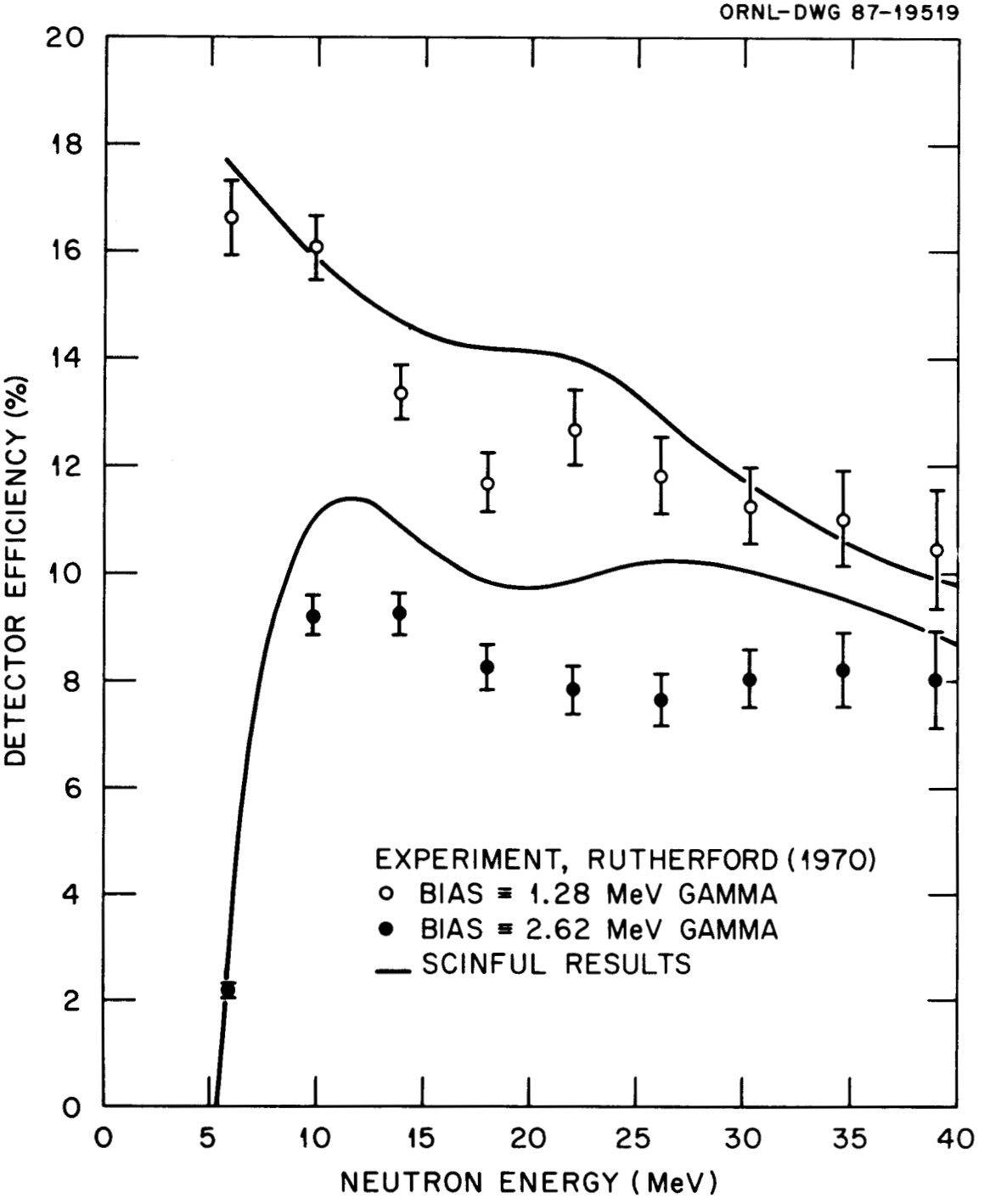

Fig. 29. Detector efficiency for an NE-102 scintillator as a function of neutron energy for the data of Hunt et al. (ref. 56) for two different electronic thresholds. The SCINFUL results are for NE-110. The agreement is the worst of any in this report.

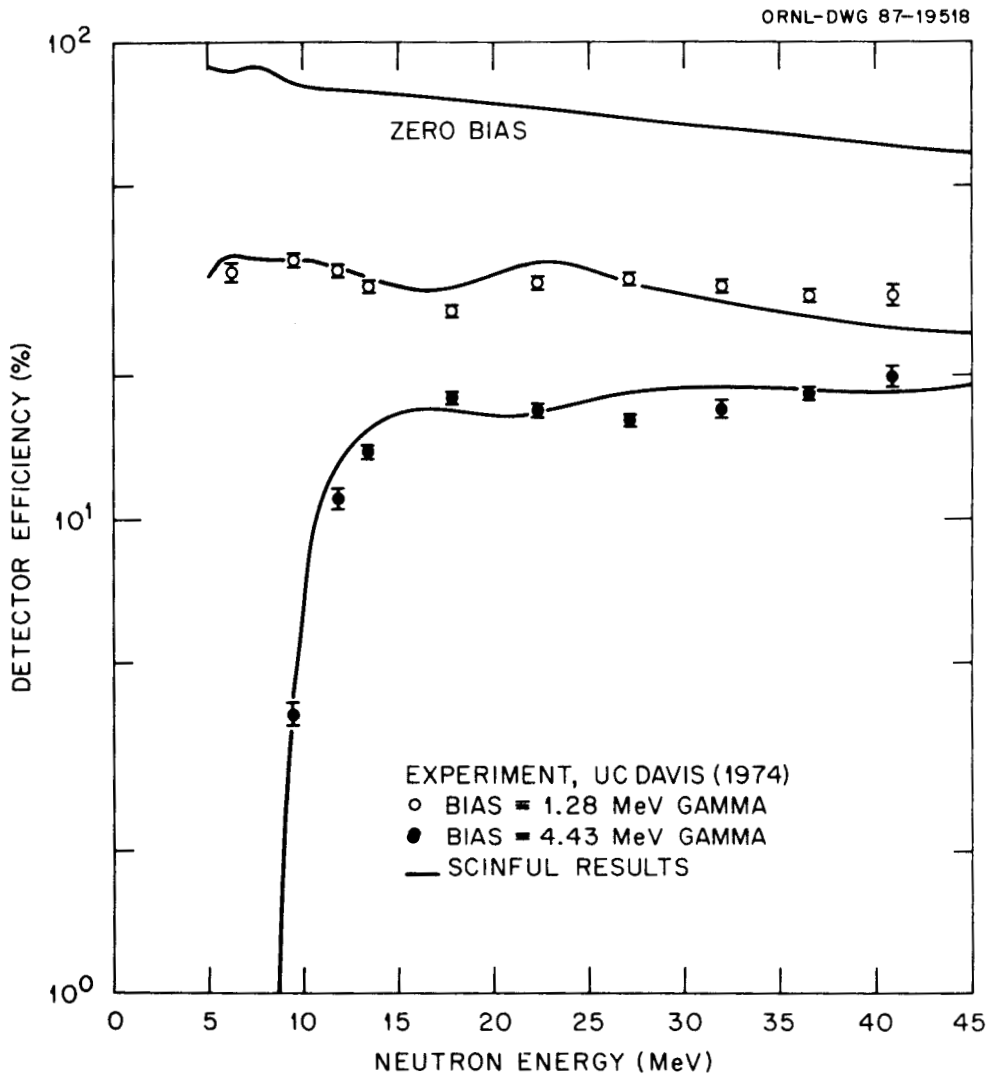

Fig. 30. Detector efficiency for an NE-102 scintillator as a function of neutron energy for the data of McNaughton et al. (ref. 57) for two different electronic thresholds. The SCINFUL results are for NE-110.

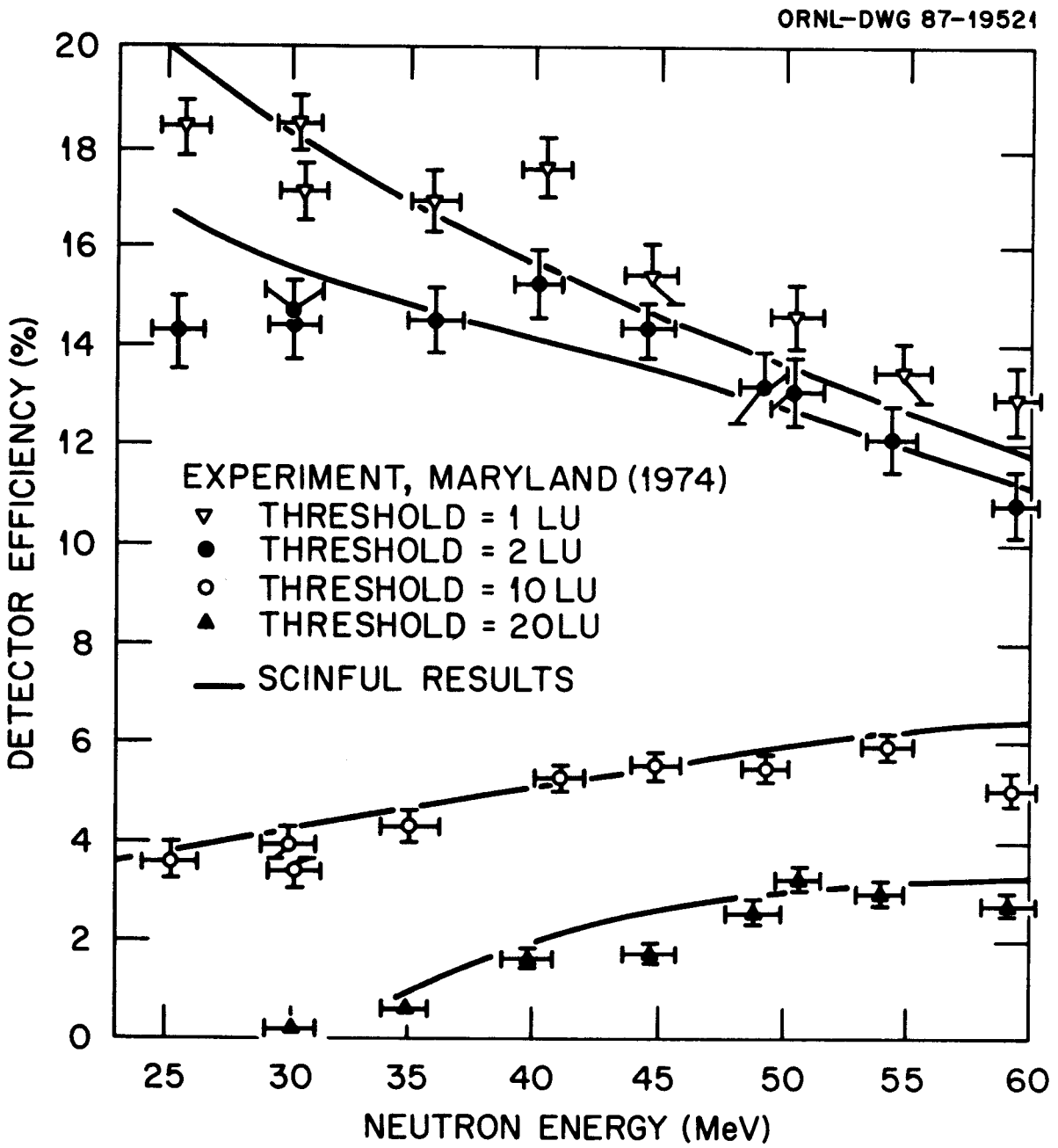

Fig. 31. Detector efficiency for an NE-102 scintillator as a function of neutron energy for the data of Riddle et al. (ref. 58) for four different electronic thresholds. The SCINFUL results are for NE-110.

Table 4: Cierjacks et al.[59] at Karlsruhe. NE-213, rad = 2.25 cm, ht = 3 cm. Collimator radius = 1.8 cm to approximate the neutron "cone" striking the detector.

Figure 32: Wiegand et al.[60] at Lawrence Radiation Laboratory. Large plastic slabs from 10 cm by 20 cm by 15 cm thick to 20 x 80 x 15 cm. Calculated as NE-110, rad = 10 cm, ht = 15 cm, collimator rad = 7 cm. Their bias setting, stated to be set so that their counter would be able to detect ≈20% of the 1.28-MeV gamma rays from a ^{22}Na source, was estimated for SCINFUL calculations to be 0.89 light units.

Except for the 18-yr old Rutherford results in Figure 29, the overall agreement of the SCINFUL calculations with the measurements is quite good. There are, however, several specifics that warrant further discussion.

The Renner et al.[14] data in Table 2 are for a detector which is "black" to the $E_n < 1$ MeV neutrons being detected, and so the efficiencies are all large. Most of the slight differences between calculation and experiment are probably due to the curved back surface of the detector which is not modelled in the program; the program used the thinnest distance in the calculation.

For the GEEL data[11] in Figure 24, the disagreement for $E_n < 1.5$ MeV is very likely experimental. The predictions of the NRESP4 program[10] agree quite well with the SCINFUL results except at the highest E_n for the lower bias.

The SCINFUL results tend to slightly underpredict the PTB experimental results[54] in Figure 25 except for the bottom curve. This complete miss between calculation and experiment is not understood. One small victory for the calculational method is the agreement in the small increase in efficiency noted for E_n between 9 and 10 MeV for the lowest bias (top curve). The increase is not observed in the calculation for the two intermediate-bias curves.

The Fowler et al.[55] results at the AERE are interesting because the computation used the experimental source-to-detector distance of 20 cm, which was necessary to get the good agreement shown in Figure 26. Using the "parallel beam" of neutrons as required in O5S,[1] for example, will result in underpredicting nearly all of the experimental data.

Table 4. Efficiency comparisons with NE-213 Measurements at Karlsruhe (ref. 59). Efficiencies are in percent.

E_n (MeV)	Experiment	SCINFUL	Ratio
	Zero Bias		
49.5		12.41 ± 0.17	
75.4		8.54 ± 0.12	
	Bias = 0.6 MeV_e		
49.5	4.98 ± 0.15	4.71 ± 0.11	1.06 ± 0.04
75.4	3.82 ± 0.25	3.34 ± 0.08	1.14 ± 0.08
	Bias = 4.2 MeV_e		
49.5	4.01 ± 0.15	3.35 ± 0.09	1.19 ± 0.03
75.4	2.86 ± 0.25	2.71 ± 0.07	1.06 ± 0.10
	Bias = 17.5 MeV_e		
49.5	0.86 ± 0.10	0.78 ± 0.05	1.10 ± 0.15
75.4	1.06 ± 0.10	0.95 ± 0.04	1.12 ± 0.12

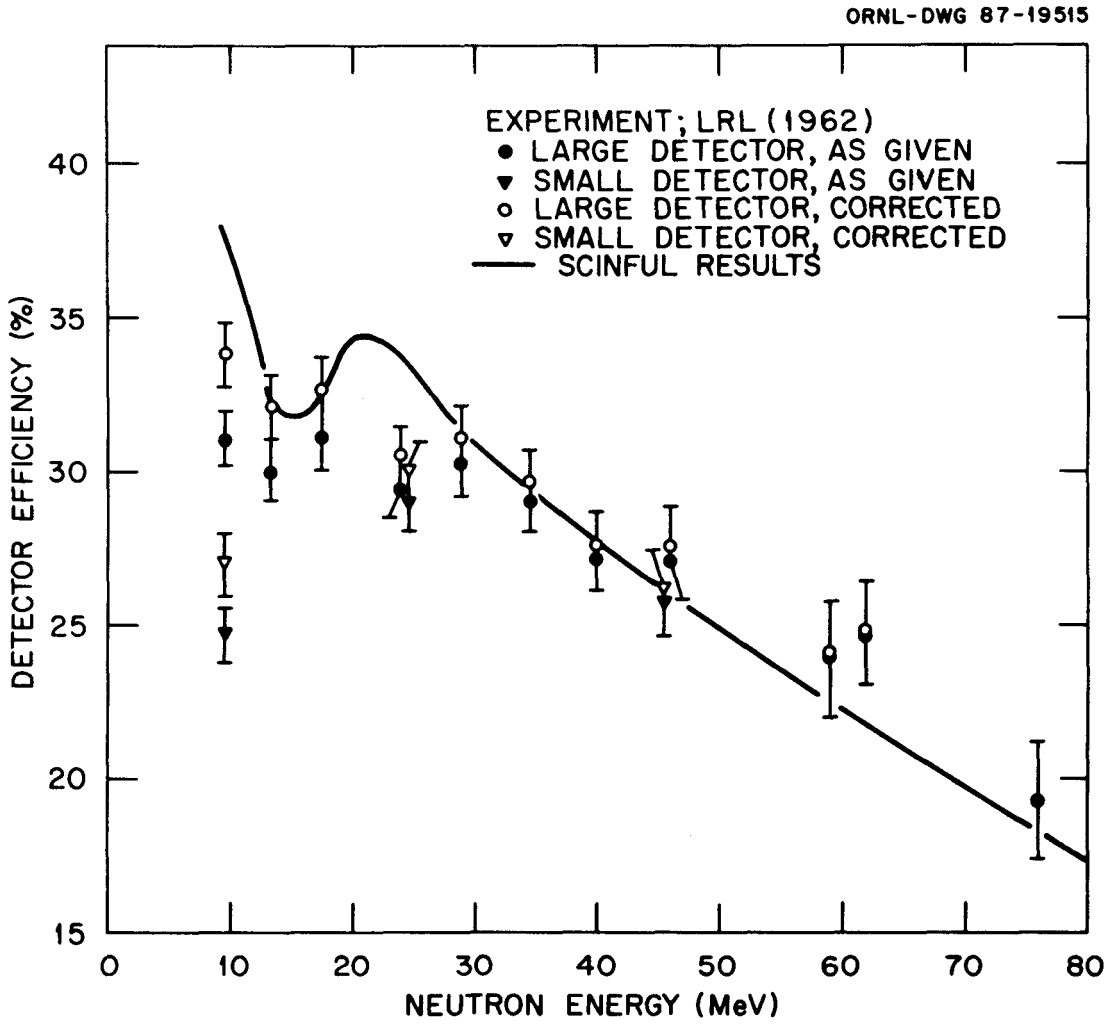

Fig. 32. Detector efficiency for plastic scintillator of rectangular shape as a function of neutron energy for the data of Wiegand et al. (ref. 60) for an assumed electronic threshold. The SCINFUL results are for NE-110 and a cylindrical detector for which the outer edges were masked by a collimator. Apparently the 15-cm thickness is the most important parameter, at least for $E_n > 13$ MeV. SCINFUL was not able to differentiate between the two experimental detector sizes. However, the overestimates of the SCINFUL results for $E_n < 35$ MeV prompted a study of the experiment to search for a possible correction to the data. One possibility not discussed by Wiegand et al. was a loss of re-scattered neutrons at the source. If such be a valid correction, the resulting experimental efficiencies should be increased by about the amounts exhibited in the figure. The agreement with SCINFUL is improved with this possible correction.

The recent Studsvik[33] data were obtained relatively for E_n between 13.5 and 22 MeV, and then normalized by comparison with calculations using a code developed at Kent State.[8] The authors stated that their bias was determined by a ^{60}Co source, which, in SCINFUL, would be 0.88 light units. The authors also stated that their detector could be positioned between 2.5 and 4 m with respect to the neutron source. In Figure 27 are shown calculations for a 4-m distance and two biases. It seems apparent that the earlier calculation is well reproduced by the present calculations for the lower bias of 0.8 light units. Indeed, also using the 4-m distance better reproduces the "parallel beam" of neutrons probably implicit in the Kent State code.[8] The experimental rise in efficiency for $E_n > 19$ MeV is not reproduced at either bias. However, reducing the distance to 2.5 m, which also results in somewhat shielding the outer circumference of the Studsvik detector, can be modelled in SCINFUL rather accurately, and the computed results for both biases are shown in Figure 28. The SCINFUL program reproduces the experiment for $E_n > 19$ MeV. It is in this energy region that the ^{12}C(n, d) reaction exhibits a sharp rise in cross section (recall Figure 8) and the ground-state deuterons are yielding enough fluorescent light to contribute above the bias of 0.8 light units. Based on present results, however, the authors' assertion[33] that they know their efficiency to $\pm 2\%$ seems quite optimistic.

Data in the next Figures 29, 30 and 31 were obtained for detectors of NE-102 or NE-102A, and are compared with calculations using the NE-110 parameters in SCINFUL. Although density and H:C ratio are same, light output is slightly different and the comparisons, therefore, may not be strictly valid. However, it seems unlikely that the differences in scintillator material are the root of the large discrepancies in Figure 29 for the Rutherford[56] data in view of the much better agreements observed in Figures 30 and 31 for the Davis[57] and Maryland[58] data.

The comparisons given in Table 3 are important because the detector is only 3 cm thick, and so at $E_n = 75.4$ MeV there is a substantial amount of recoil proton escape. The SCINFUL program does well at all three biases.

Lastly, Figure 32 exhibits results[60] for an undefined-material plastic detector, which is not in the cylindrical geometry of Figure 1. The calculations are for the NE-110 parameters in SCINFUL for large detectors, however, avoiding edge effects. For $E_n > 40$ MeV the calculations agree well with the efficiency data, probably better than they ought, but for $E_n < 40$ MeV the calculations systematically overpredict

the experimental results. A study of the published report[60] suggested the possibility that the authors did not take into consideration outscattering of neutrons from their liquid hydrogen source. Assuming a correction due to this effect was needed yielded the open-symbol "experimental" results shown in Figure 32. The agreement of the corrected experimental results is much better with the SCINFUL calculations, although the discrepancy for $E_n \sim 25$ MeV is a little worrisome. The experimentally smaller efficiencies for $E_n = 10$ MeV probably indicate that geometrical effects are important for lower energy neutrons, effects which are not modelled in SCINFUL.

Comparisons were also made with efficiencies reported by Leleux et al.[61] for a 2-cm height NE-102 detector and E_n between 7 and 14 MeV, and with a large detector (12.7-cm diameter by 30.5-cm height) by Grady et al.[62] For the Leleux et al.[61] data, the SCINFUL calculations agreed with the data at $E_n = 7$ MeV, but underpredicted the reported data for $E_n > 10$ MeV by ~10%. As for the Brady et al.[62] data, the SCINFUL calculations were unable to reproduce the variations of efficiency exhibited by the reported experimental data. A likely source of discrepancy is the present inability to correctly model the detector geometry. Hence a figure exhibiting "comparisons" is not given.

The next data comparisons are for complete detector responses, and the experimental data, from 6 experiments, span the incident neutron energy range from 0.137 to 74.3 MeV.

Renner, et al.[14] published results for $E_n < 1$ MeV for data taken with NE-110 detectors. Two detectors were used; one was 0.64 cm thick by 1.25 cm radius and the neutron beam struck the entire front face, and the other was 5.1 cm in radius by 6.6-7.6 cm thick (the back surface was curved) and the incident neutron beam was collimated to a 1.6-cm-diam spot centered on the front face of the detector. The absolute pulse-height calibration and yield determinations were determined by an iterative series of comparisons with calculated spectra using the O5S program.[1] To reproduce these data using the SCINFUL program required a step beyond the program itself, and that was to fold a "resolution" function into the SCINFUL output. The assumption was made that the resolution function was a Gaussian, and a parameter, R, called the full width at half maximum, was defined. This parameter is related to the width parameter, σ, of a Gaussian function by,

$$\sigma = R * E/2.355 \tag{5}$$

where E is centroid parameter, in this case energy (in MeV), of the Gaussian function. Renner et al.[14] do not give any values for R but state that it ranged between 18 and 20% at all neutron energies. After some trial and error, a relationship for R was deduced which appears to be satisfactory;

$$R^2 = 0.01 + 0.013/E + 0.0067/E^2 \ . \tag{6}$$

Figure 33 exhibits a comparison of experiment using the thinner detector with a SCINFUL calculation folded with the resolution function of equation (6). For the thicker detector, spectra were obtained at 0.137, 0.274 and 0.467 MeV, and these data are exhibited in Figures 34, 35 and 36. The first calculations with the SCINFUL code produced a small surprise, namely that the calculated spectra were shifted to slightly larger absolute pulse heights compared to the data. As a test of the fluorescent-light attenuation feature built into the program, a small (0.01/cm) attenuation was tried. After folding in the resolution the calculated results agree well with the data, as shown in the figures. It is apparent, however, that for some reason the O5S calculations (used by Renner et al.[14] to normalize these data), which don't have this light attenuation capability, do not quite agree with the SCINFUL results for these low energy neutrons. Consequently there may be some question about the absolute pulse-height calibration in light units of the data. Clearly the program SCINFUL can be modelled for this detector configuration such that the results are in excellent agreement with the spectra as published by these authors. At this juncture further claims for either the experimental data or the calculations cannot be justified.

The next experimental responses were obtained at GEEL as part of the same experiment[11] already discussed above for Figure 24. The spectral data are exhibited in this reference[11] as absolute yields/channel vs channel, that is, the authors do not give a pulse-height calibration in light units. Hence, for comparisons with SCINFUL it was necessary to make assumptions about the experimental gain calibration. In addition, as may be observed in Figure 37, the SCINFUL results do not have any resolution folded into the them, and so the calculated results exhibit a less "rounded" character for the largest pulse heights near channel 21. Overall for $E_n = 1$ MeV the SCINFUL calculation agrees well with the experiment for the upper 75% of the spectrum, but disagrees somewhat with the NRESP4[10] calculation

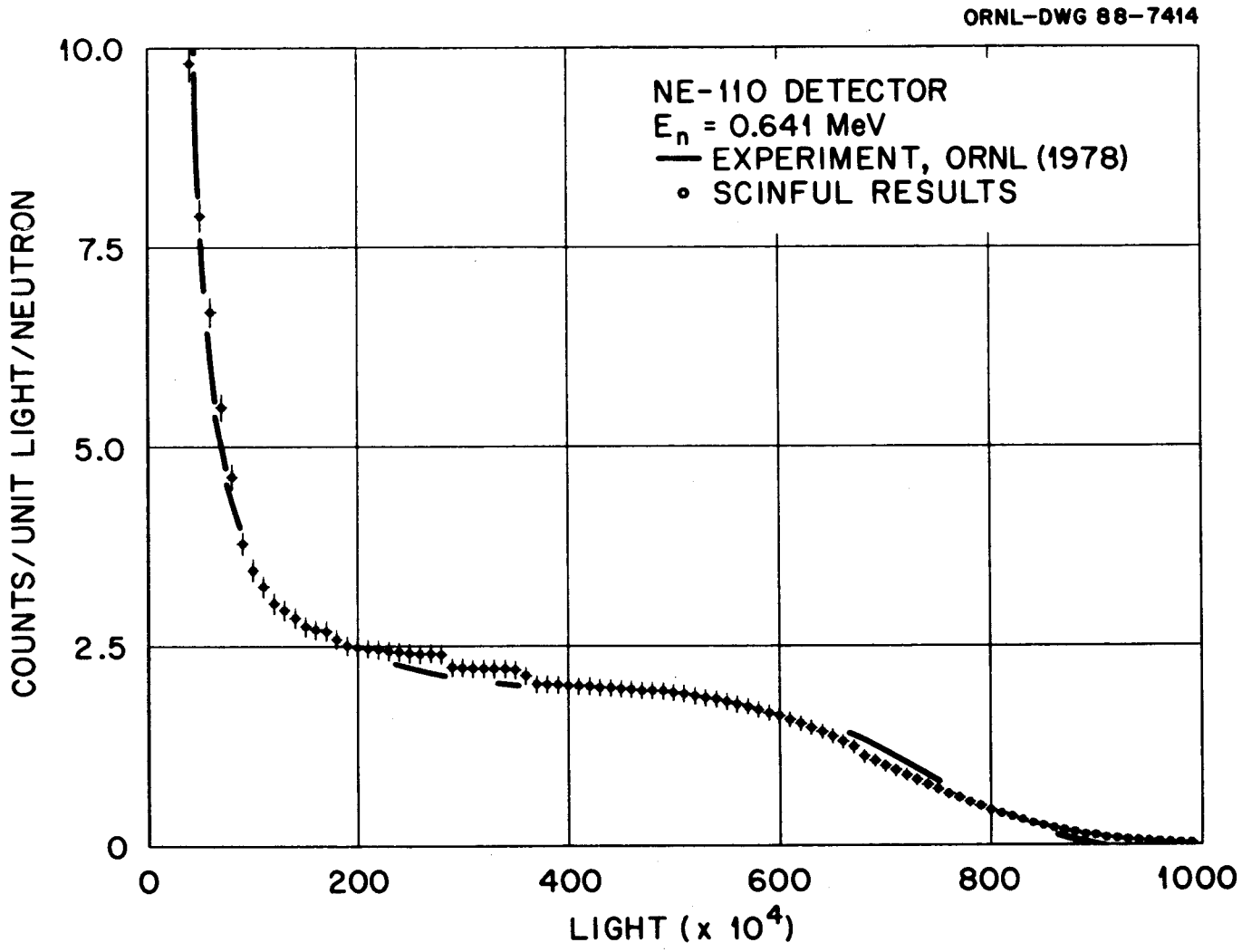

Fig. 33. Comparison of an experimental response measurement for $E_n = 0.641$ MeV by Renner et al. (ref. 14) and results of a SCINFUL calculation for their thin detector configuration. As discussed in the text, the SCINFUL results have an empirically deduced resolution folded into them.

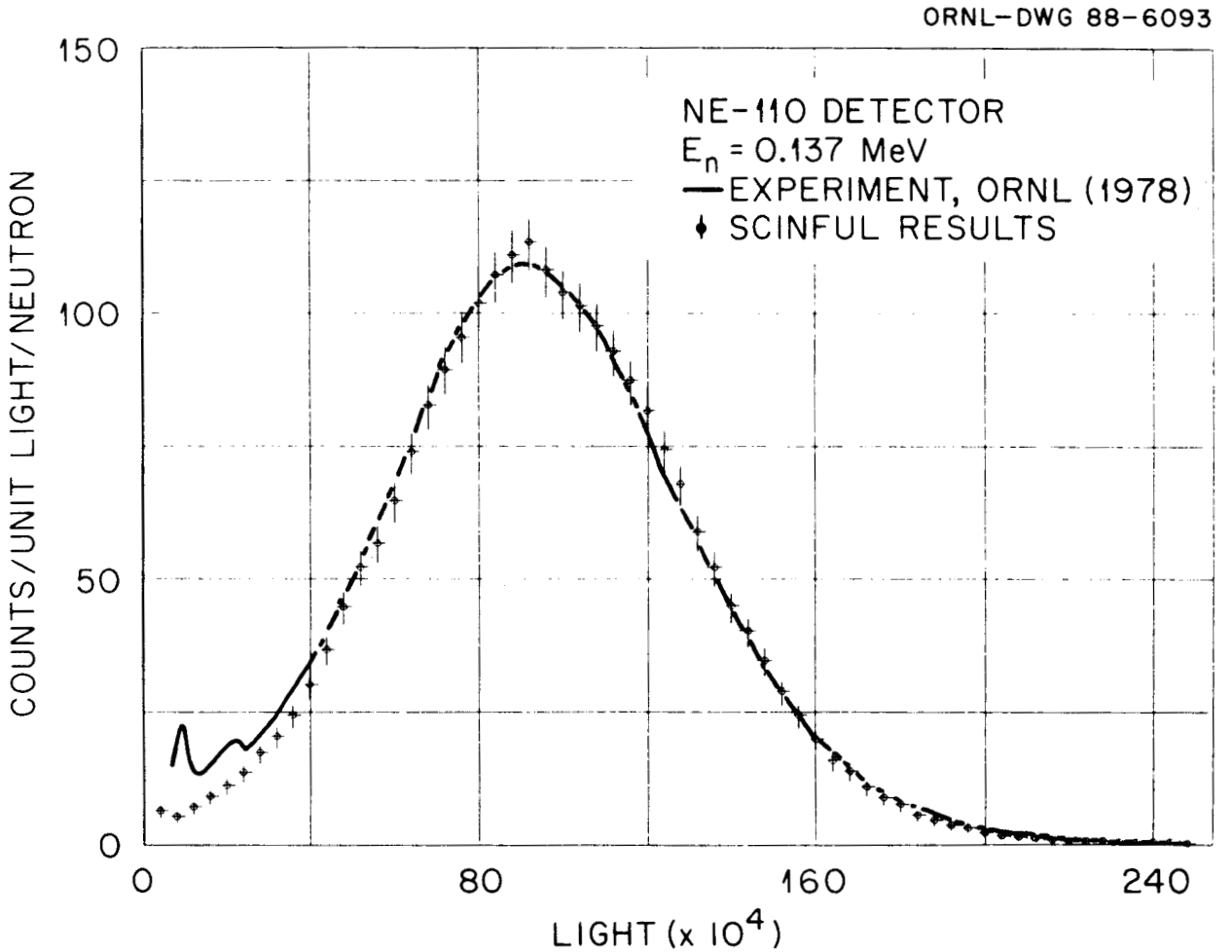

Fig. 34. Comparison of an experimental response measurement for $E_n = 0.137$ MeV by Renner et al. (ref. 14) and results of a SCINFUL calculation for their thick detector configuration. In this case, also, a resolution function has been folded into the SCINFUL results.

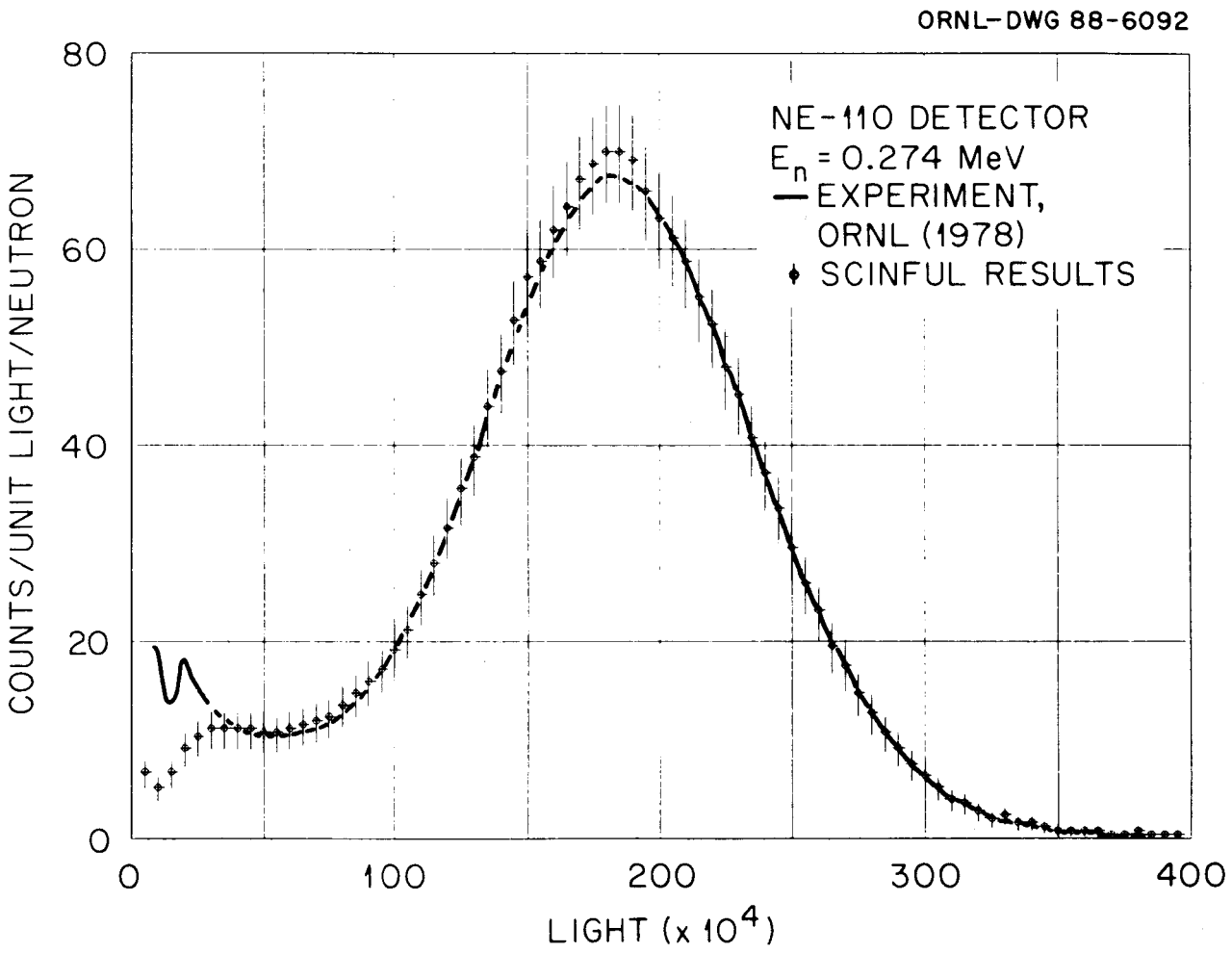

Fig. 35. Comparison of an experimental response measurement for $E_n = 0.274$ MeV by Renner et al. (ref. 14) and results of a SCINFUL calculation similar to Figure 34.

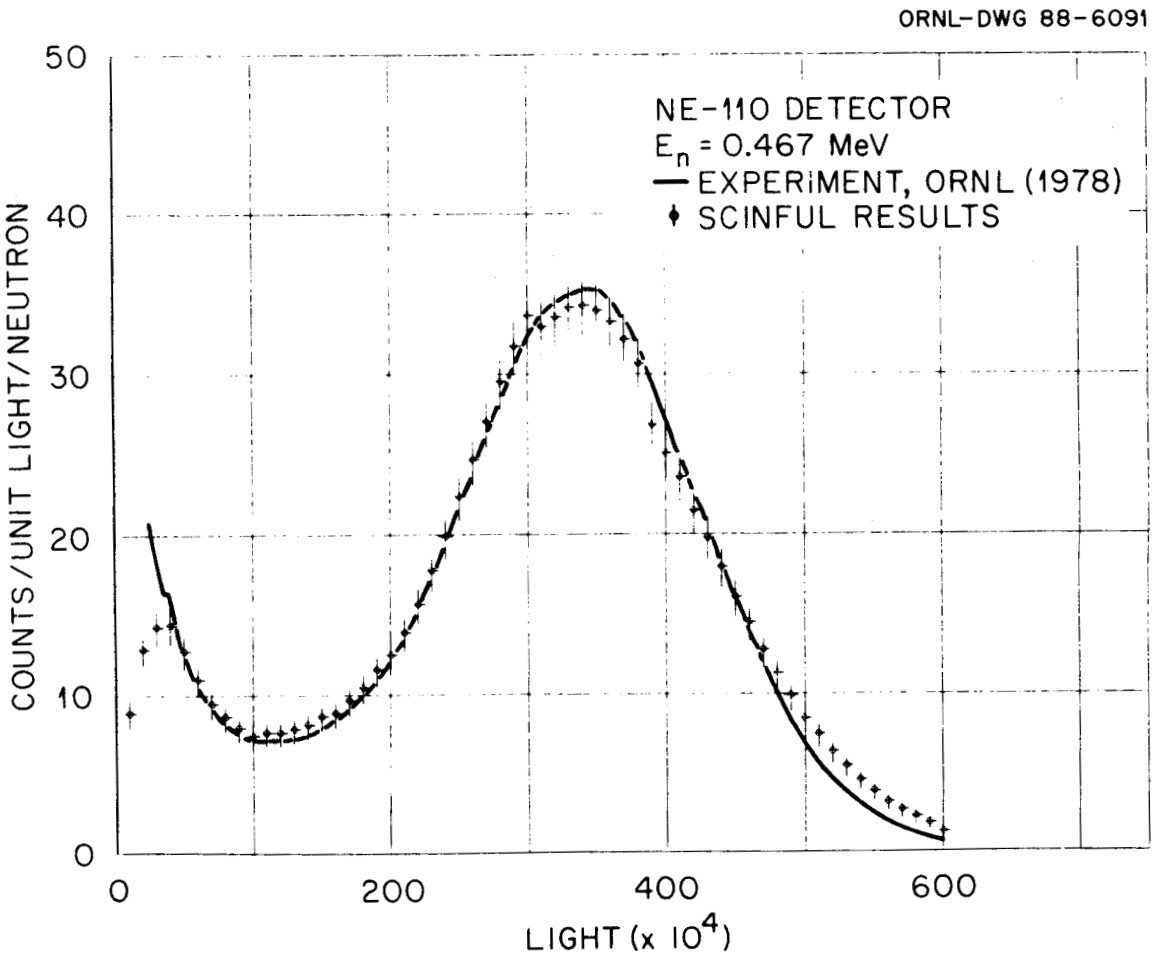

Fig. 36. Comparison of an experimental response measurement for $E_n = 0.467$ MeV by Renner et al. (ref. 14) and results of a SCINFUL calculation similar to Figure 34.

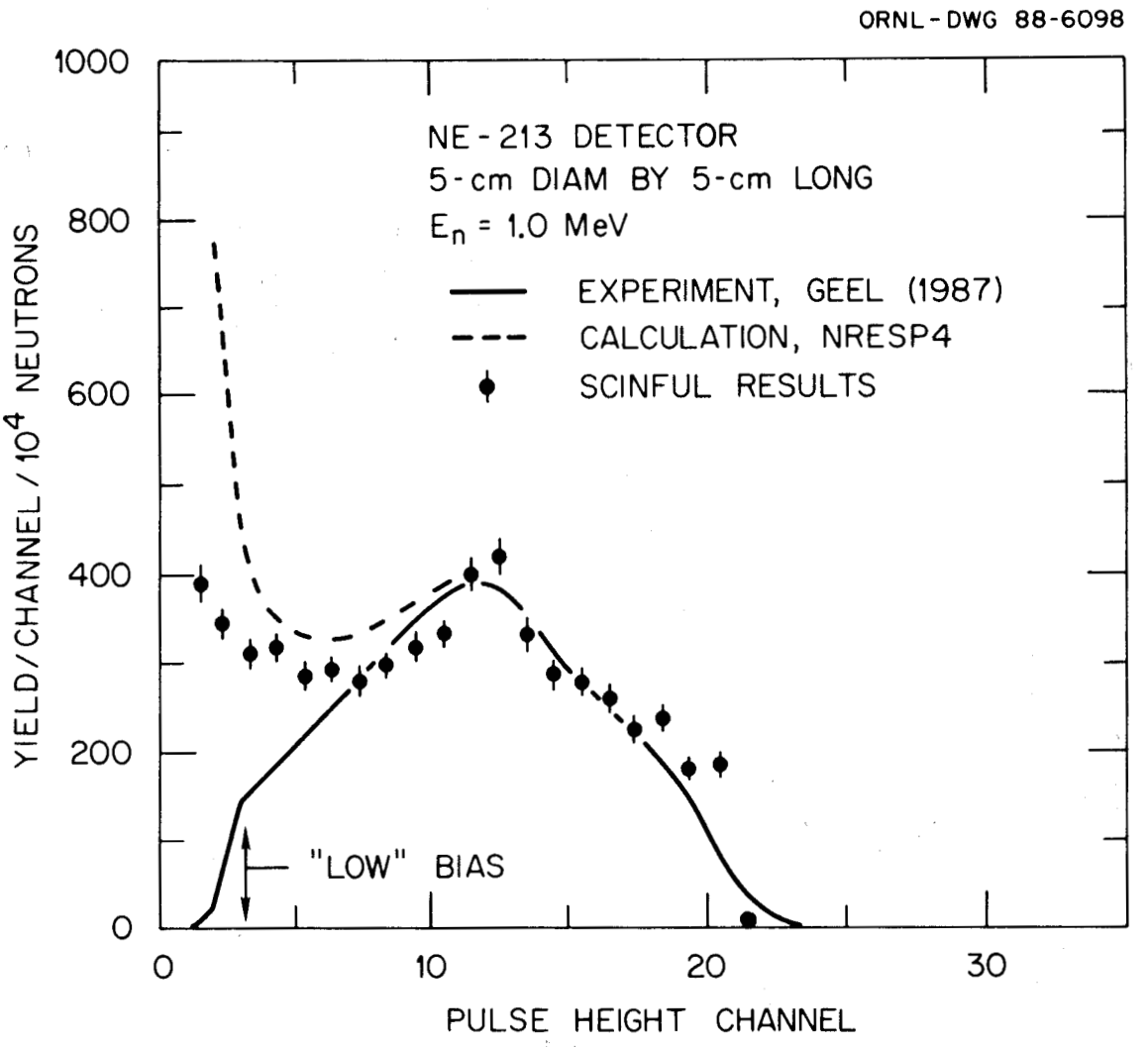

Fig. 37. Comparison of an experimental response measurement for $E_n = 1.0$ MeV by Dekempeneer et al. (ref. 11) and results of a SCINFUL calculation. Also shown are results of a calculation attributed to the NRESP4 code of ref. 10 by the authors of ref. 11. Since the experiment was reported in units of pulse height it was necessary to estimate the channel-to-light-unit conversion for comparison with SCINFUL results for the data in this figure and in the next three figures.

for the lower half of the pulse-height distribution. For $E_n = 2$ MeV, as shown in Figure 38, the SCINFUL results slightly underpredict by ~7% the experimental data while reproducing the "shape" of the spectrum quite well. For $E_n = 7.8$ MeV the SCINFUL results reproduce the spectrum very well; both calculations somewhat overpredict the spectral data for the smallest 10-15% of the pulse-height distribution. For $E_n = 15.6$ MeV, as exhibited in Figure 40, moderate differences are observed. The NRESP4 program[10] exhibits a "peak" in the vicinity of channel 125 which appears to be that associated with the $^{12}C(n,\alpha)^9Be$ ground-state reaction; the same contribution in the experiment is apparently manifest as the peak in the vicinity of channel 45. The equivalent peak in the SCINFUL calculation could be in the vicinity of channel 20, but it is not clear. The SCINFUL results are in quite good agreement with the experiment between channels 100 and 900, although slightly underpredicting the experimental data at the largest pulse heights. The shape of the experimental response in this region, however, is about what one would expect[42] from the discussion of fluorescent light attenuation. All in all, the SCINFUL program provides a good representation of the experimental response for ~85% of the pulse height, and might be improved if the light attenuation capability in SCINFUL were utilized.

The next experiment[63] to be discussed was performed at ORNL and consisted of careful absolute measurements of responses to two different thickness of NE-213 detector and for two different incident neutron energies. The associated-particle technique was used to determine absolute yields; the pulse-height calibration was determined absolutely with the experimental spectral distributions of ^{60}Co gamma rays being plotted in the report[63] of this experiment. The data are compared not as spectral response distributions but rather as integral efficiencies. The SCINFUL calculations do not have any resolution folded in, but they do include a fluorescent light attenuation factor deduced from the reported ^{60}Co gamma-ray responses. The exact geometry of the experiment was modelled closely, since the source-to-detector distance is given in the report[63] and the cone of neutrons on the front face of the detectors could be deduced from the reported geometries. As a consequence there are no adjustments either to the experimental data or to the SCINFUL calculations. The agreement for $E_n = 2.7$ MeV is excellent for both detectors as shown in Figure 41. (The agreement is better than that shown in reference 63 for O5S calculations, those calculations having to be made for a parallel beam of neutrons

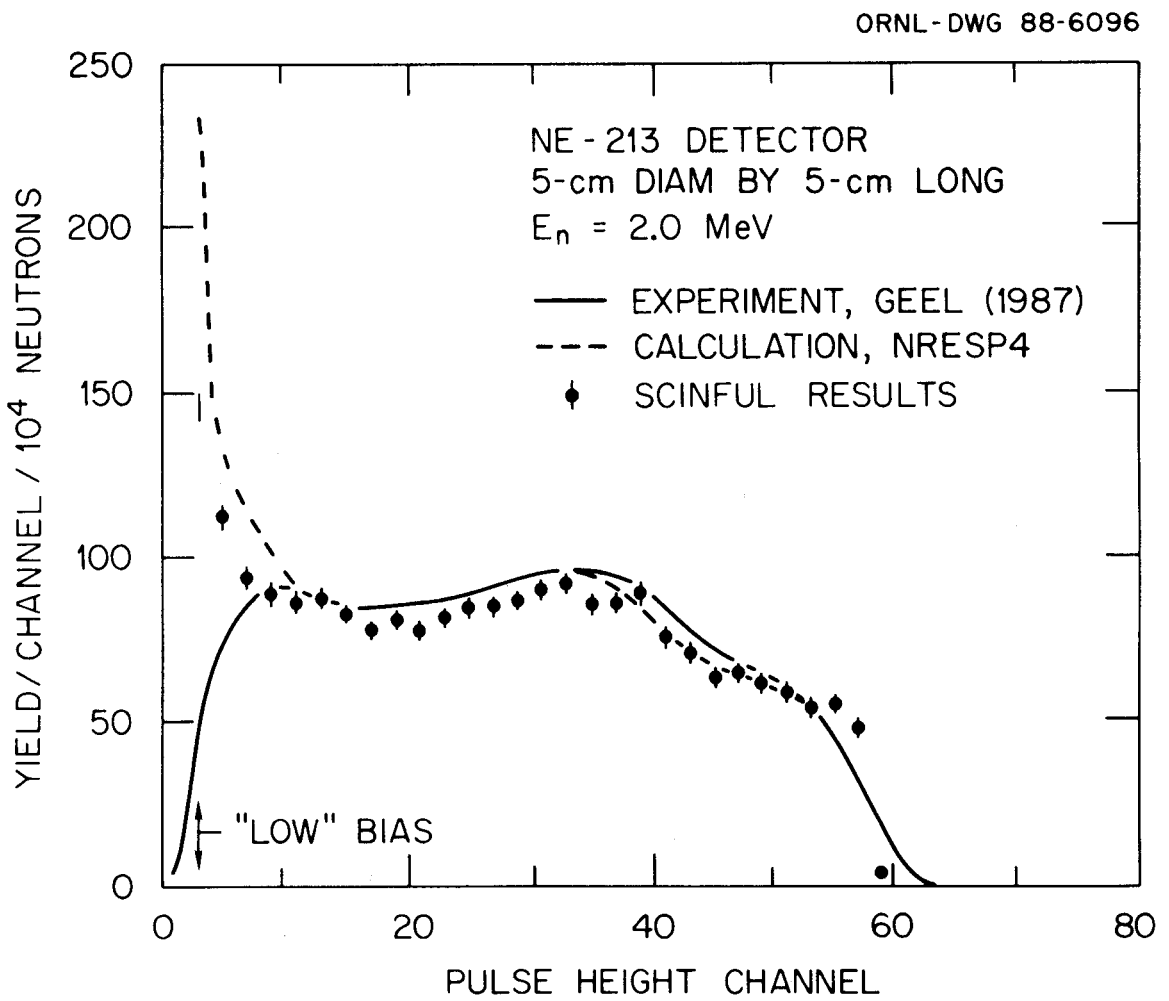

Fig. 38. Comparison of an experimental response measurement for $E_n = 2.0$ MeV by Dekempeneer et al. (ref. 11) and results of a SCINFUL calculation. Also shown are results of a calculation attributed to the NRESP4 code of ref. 10.

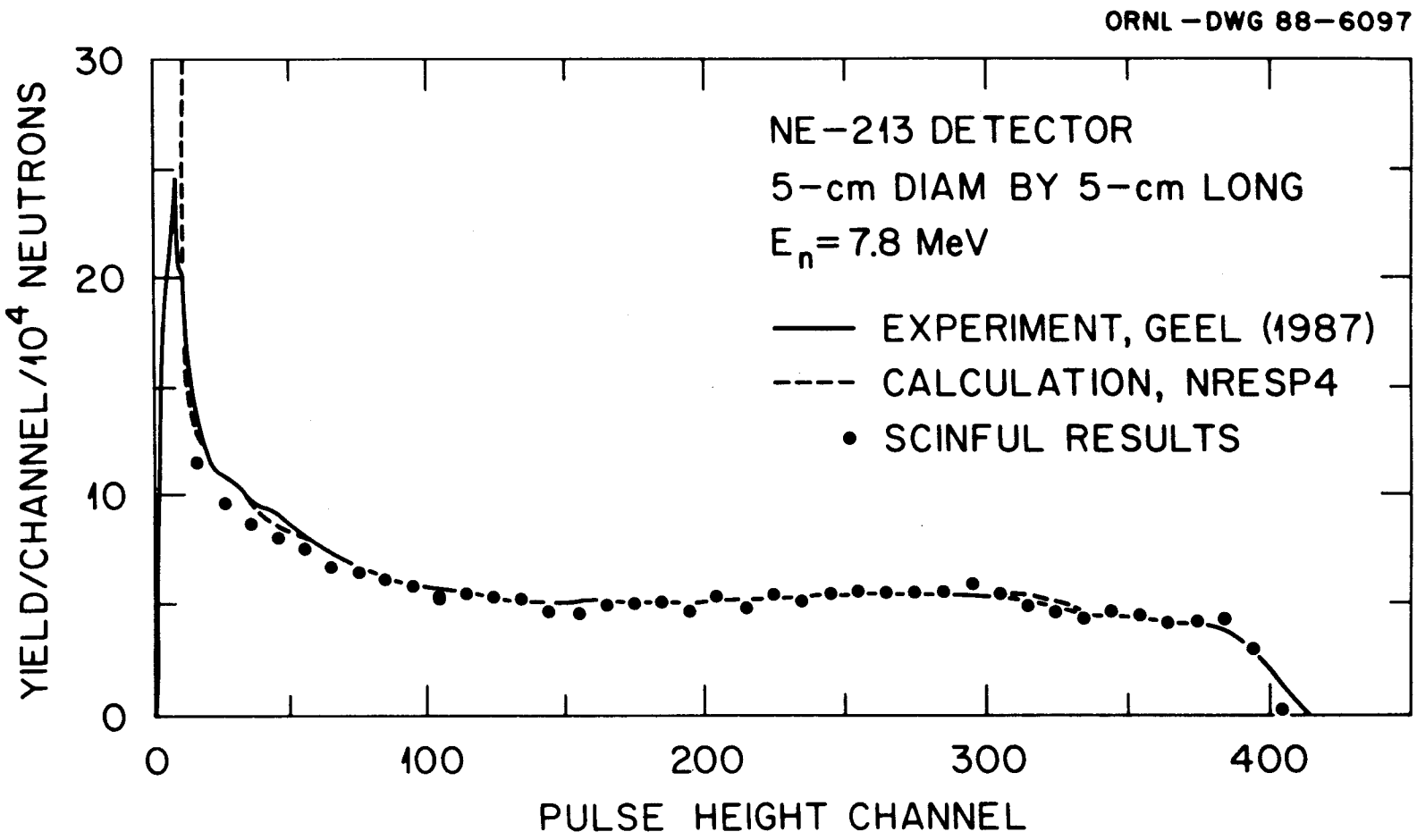

Fig. 39. Comparison of an experimental response measurement for $E_n = 7.8$ MeV by Dekempeneer et al. (ref. 11) and results of a SCINFUL calculation. Also shown are results of a calculation attributed to the NRESP4 code of ref. 10.

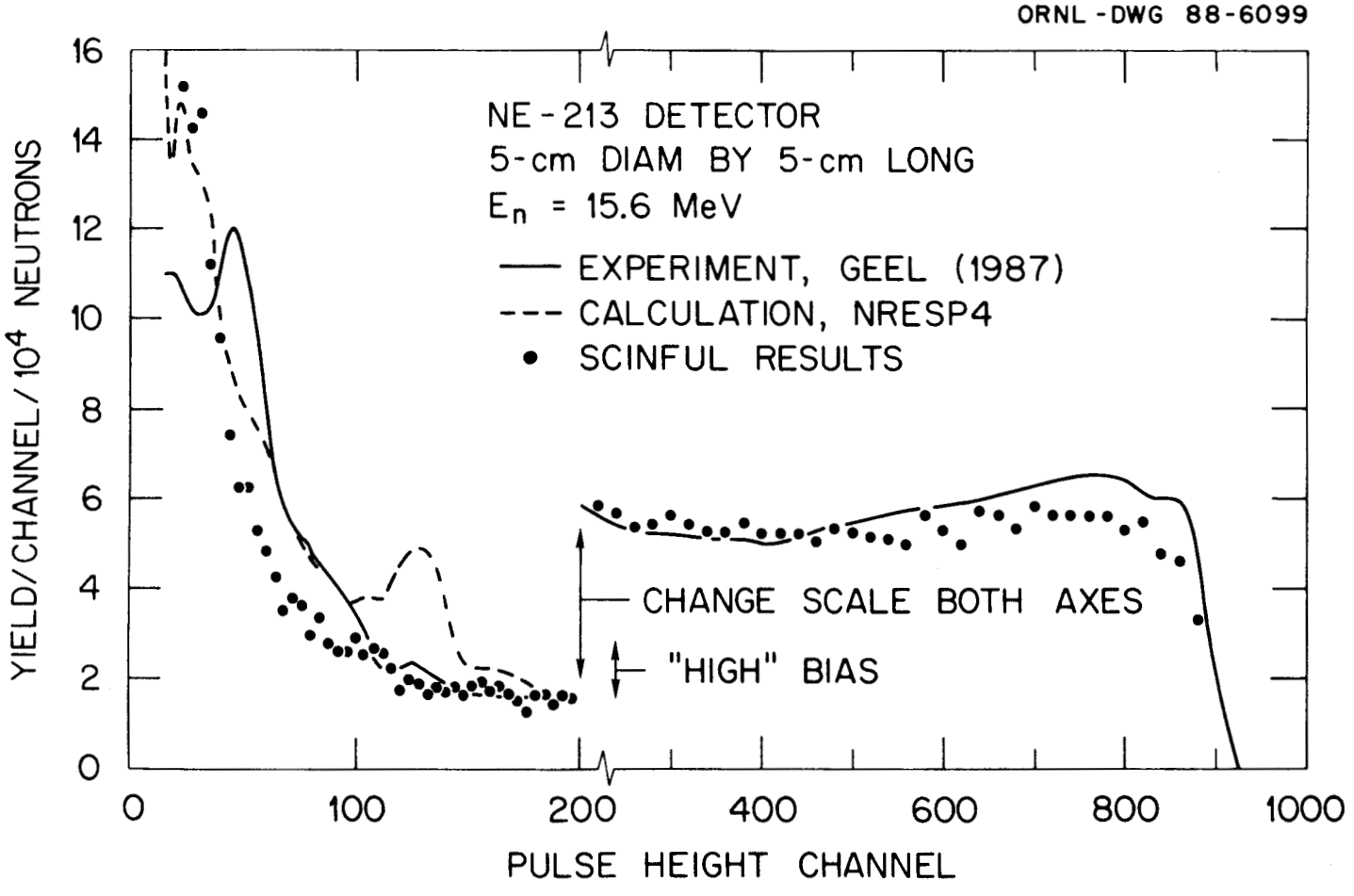

Fig. 40. Comparison of an experimental response measurement for $E_n = 15.6$ MeV by Dekempeneer et al. (ref. 11) and results of a SCINFUL calculation. Also shown are results of a calculation attributed to the NRESP4 code of ref. 10. As discussed in the text the shape of the experimental spectrum for pulse heights > 500 channels could indicate a small-to-moderate fluorescent light attenuation in the scintillation detector.

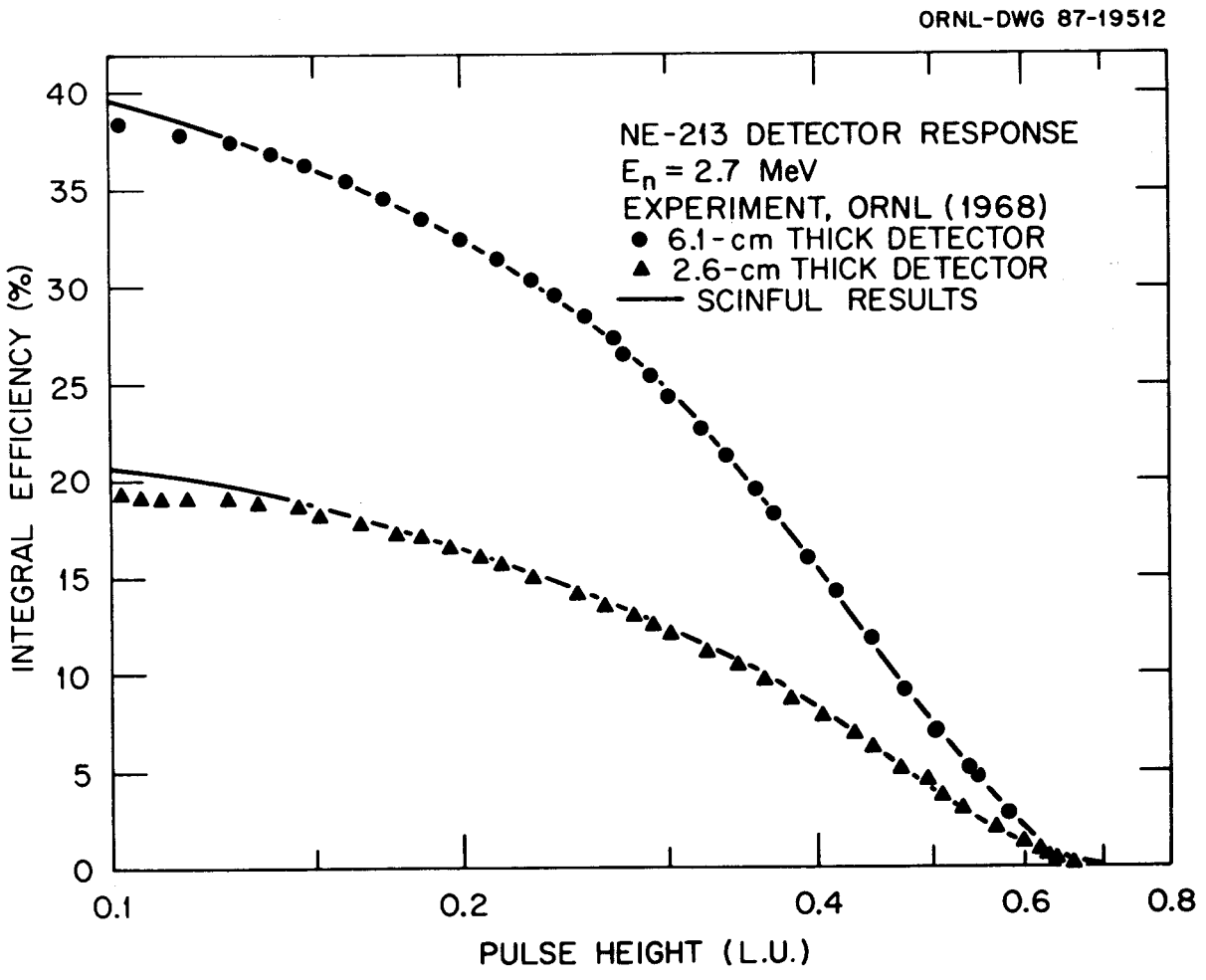

Fig. 41. Comparison of an experimental response measurement for $E_n = 2.7$ MeV by Love et al. (ref. 63) and results of a SCINFUL calculation. The data and calculations are shown as integral efficiencies for the plotted pulse-height values for two different detectors.

incident over the front face of the detector.) In Figure 42 are exhibited experiment and calculations for $E_n = 14.5$ MeV using the thinner detector, and again the agreement is excellent over most of the pulse-height region. For $E_n = 14.5$ MeV and the thicker detector, as shown in Figure 43, the agreement is excellent for pulse heights greater than 1 light unit, and, as for the thinner detector data exhibited in Figure 42, the calculation somewhat underpredicts integral efficiency at the smaller pulse heights. Interestingly, this characteristic is opposite that observed in Figure 40 for the GEEL data[11] at $E_n = 15.8$ MeV. Overall, the agreement between SCINFUL results and experiment in Figures 41-43 is very comforting, and suggests that when the experimental configuration is well known the calculated results using SCINFUL reproduce the experimental results.

The next experiment[52] to be discussed was also performed at ORNL. It is the only experiment wherein the detected neutrons impinged upon the curved surface of the detector, that is, normal to the detector axis. The detector was NE-213, rad = 2.3 cm, ht = 4.6 cm. Neutrons were created using a Van de Graaff accelerator. Absolute normalization of the response spectra were determined by comparing with O5S calculations[1] at larger pulse heights dominated in the calculation by $n + H$ scattering. The SCINFUL results were folded with a resolution parameter, R, given by

$$R^2 = 0.004 + 0.02/E \ , \tag{7}$$

where E is neutron energy in MeV. Comparison of the SCINFUL calculated response with experiment is shown in Figure 44 for $E_n = 3.238$ MeV. The agreement is good for the larger pulse heights, but for pulse heights $< \sim 0.3$ light units SCINFUL apparently underpredicts the measurements. Very likely the experiment includes scattering from the light pipe connected to the bottom of the scintillator, a configuration of external influence which is not included in the SCINFUL program. More interesting comparisons are exhibited in Figures 45 through 48 and for E_n between 14 and 22 MeV. For $E_n = 14$ MeV, as shown in Figure 45, the SCINFUL results compare well for pulse heights > 1.5 light units, and may be considered very adequate for pulse heights > 0.25 light units. The peaks in both the data and calculation near 0.7 light units are due to detection of the ground-state alphas, and it appears that the slight difference in the centroids of the peaks, experiment vis-a-vis

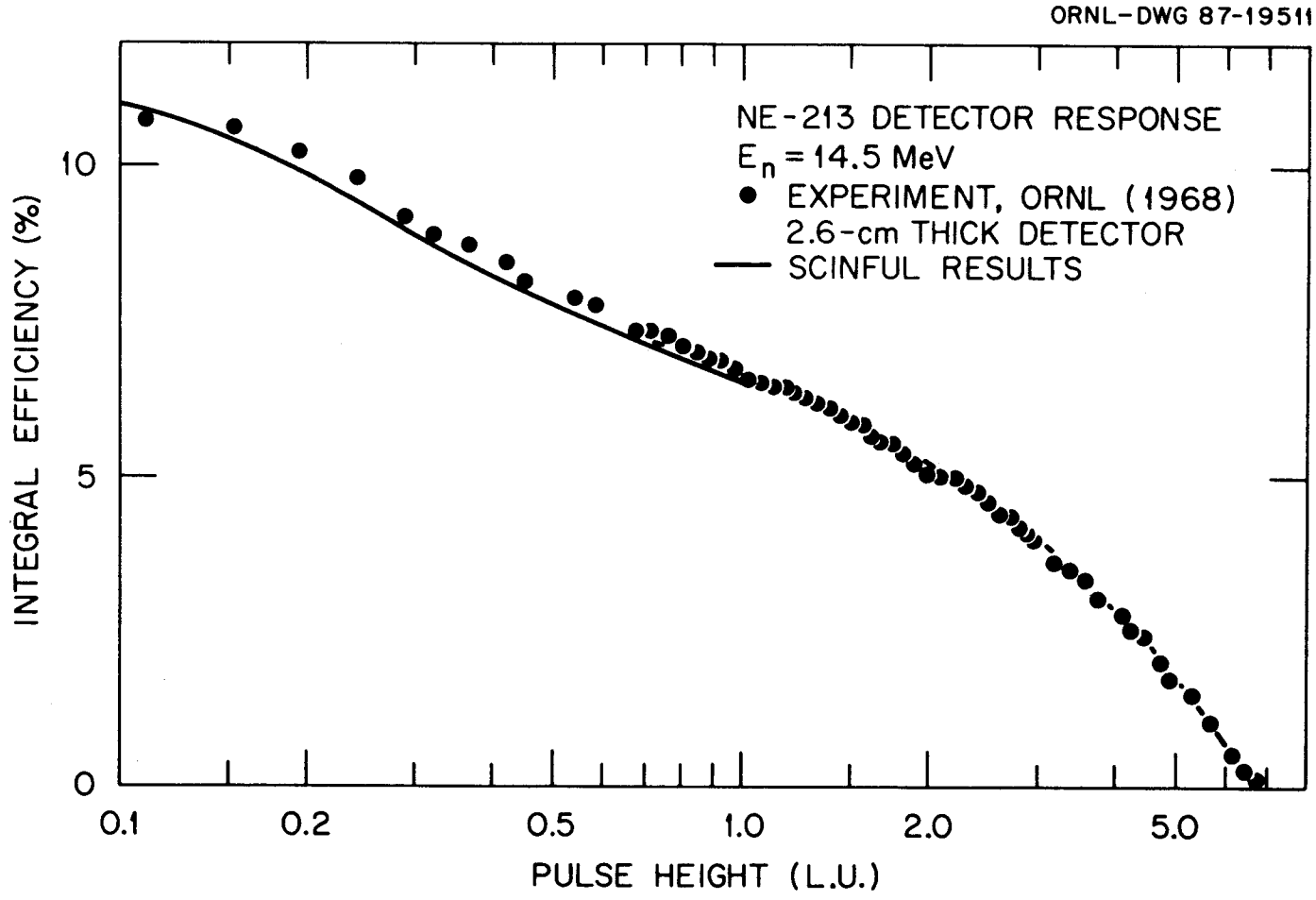

Fig. 42. Comparison of an experimental response measurement for $E_n = 14.5$ MeV by Love et al. (ref. 63) and results of a SCINFUL calculation, again shown as integral efficiencies, for the thin detector.

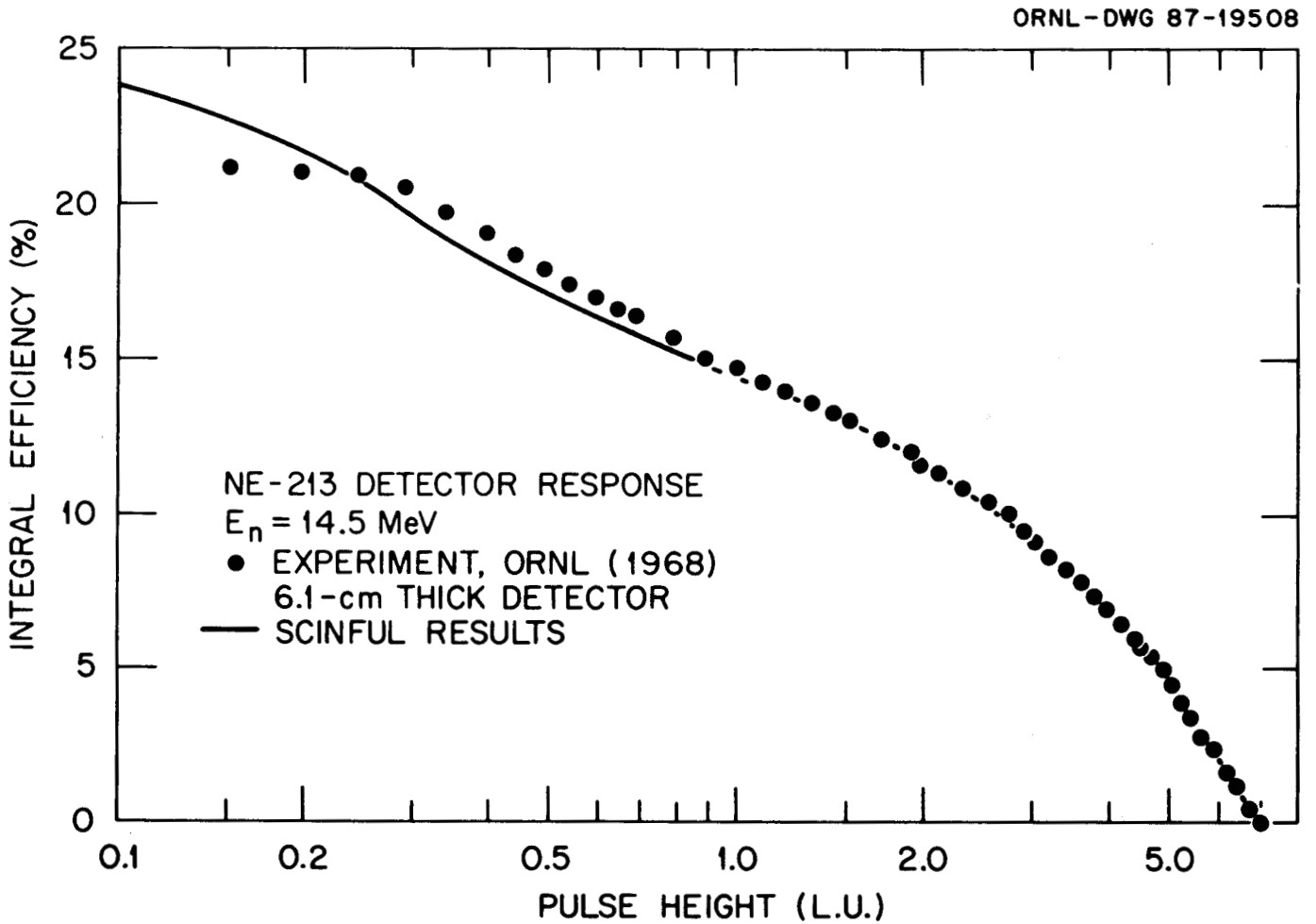

Fig. 43. Comparison of an experimental response measurement for $E_n = 14.5$ MeV by Love et al. (ref. 63) and results of a SCINFUL calculation, again shown as integral efficiencies, this time for the thick detector.

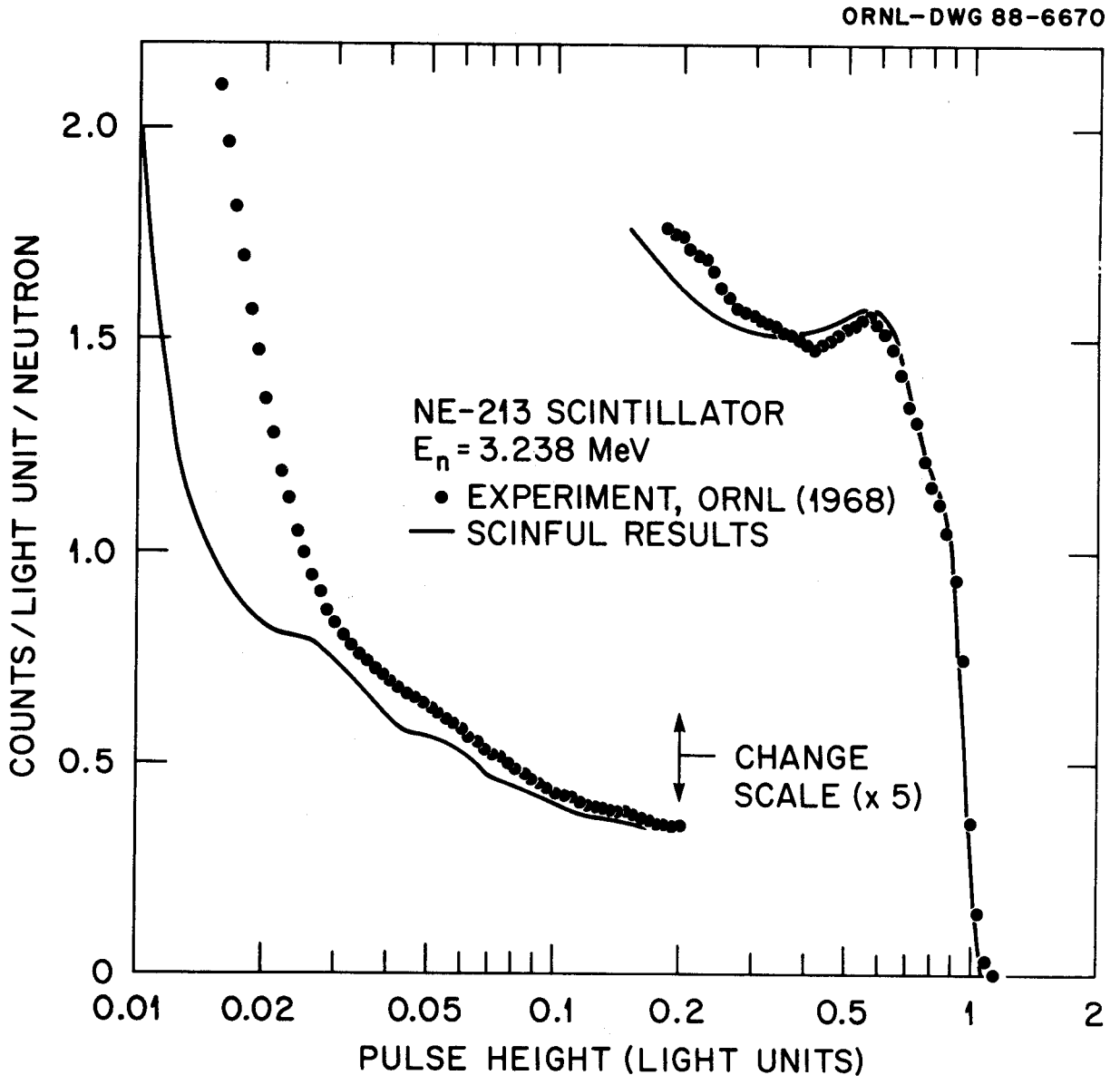

Fig. 44. Comparison of an experimental response measurement for $E_n = 3.238$ MeV by Verbinski et al. (ref. 52) and results of a SCINFUL calculation after folding in an empirically determined resolution as discussed in the text. The discrepancy for very low pulse heights (<0.03 light units) may be due to neutron scattering from the environs of the detector, in particular, from the attached light pipe.

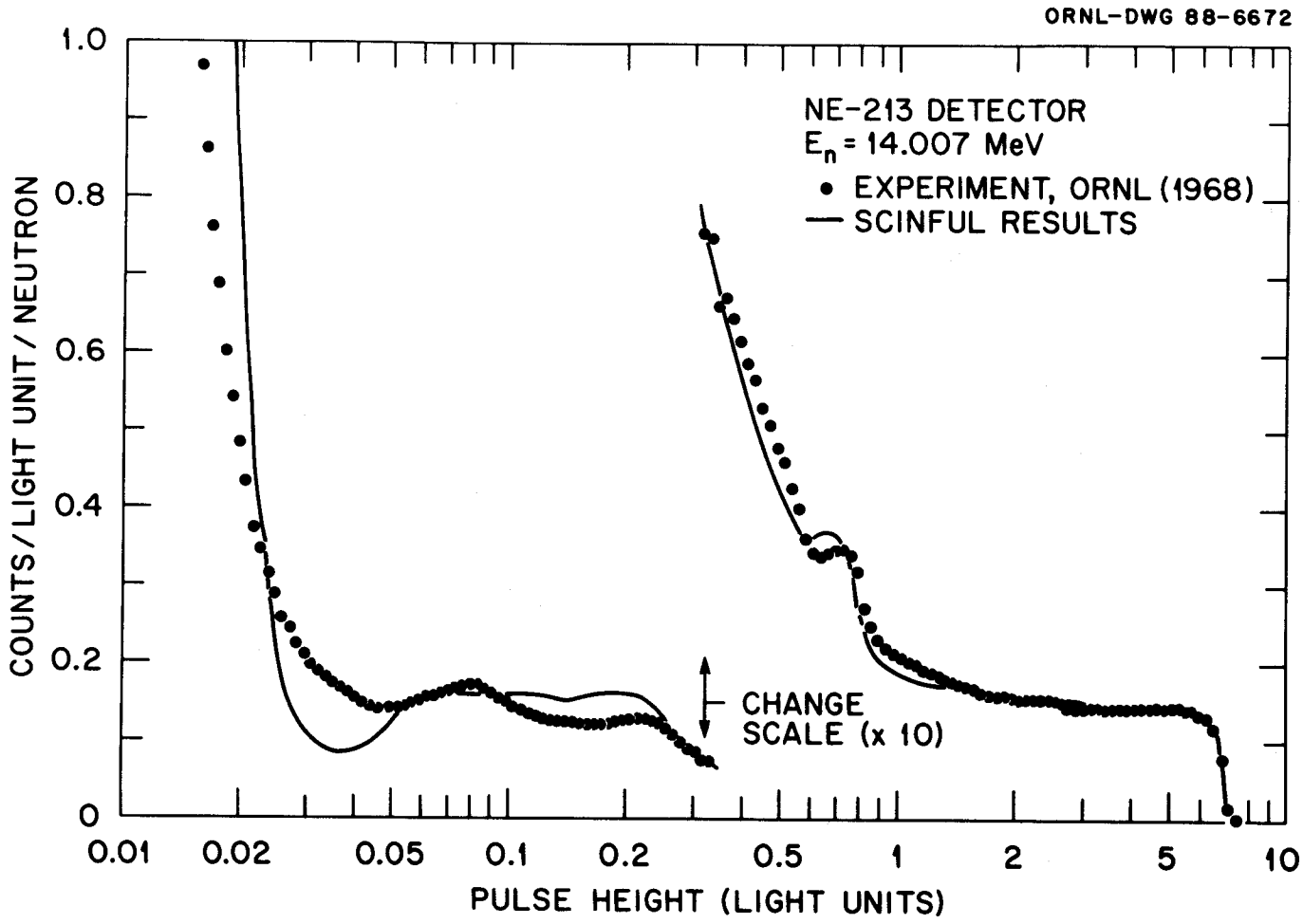

Fig. 45. Comparison of an experimental response measurement for $E_n = 14.007$ MeV by Verbinski et al. (ref. 52) and results of a SCINFUL calculation following folding in of a resolution function. The little peak in the data and calculation vicinity 0.7 light units is due to detection of alphas from the ground-state $^{12}C(n,\alpha)^9Be$ reaction. The response between 0.04 and 0.5 light units is dominated by alphas from the 3α breakup reaction.

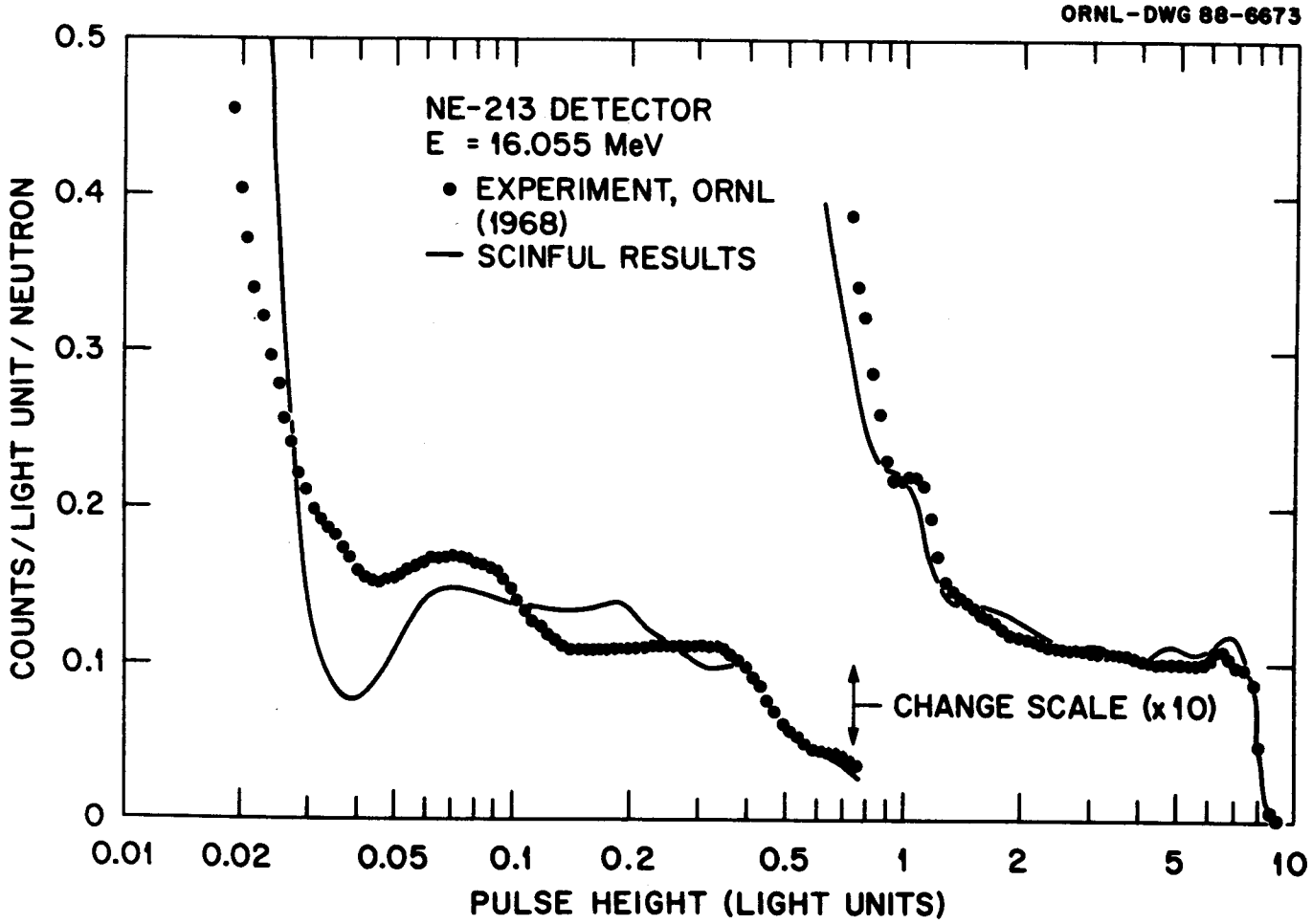

Fig. 46. Comparison of an experimental response measurement for $E_n = 16.055$ MeV by Verbinski et al. (ref. 52) and results of a SCINFUL calculation following folding in of a resolution function.

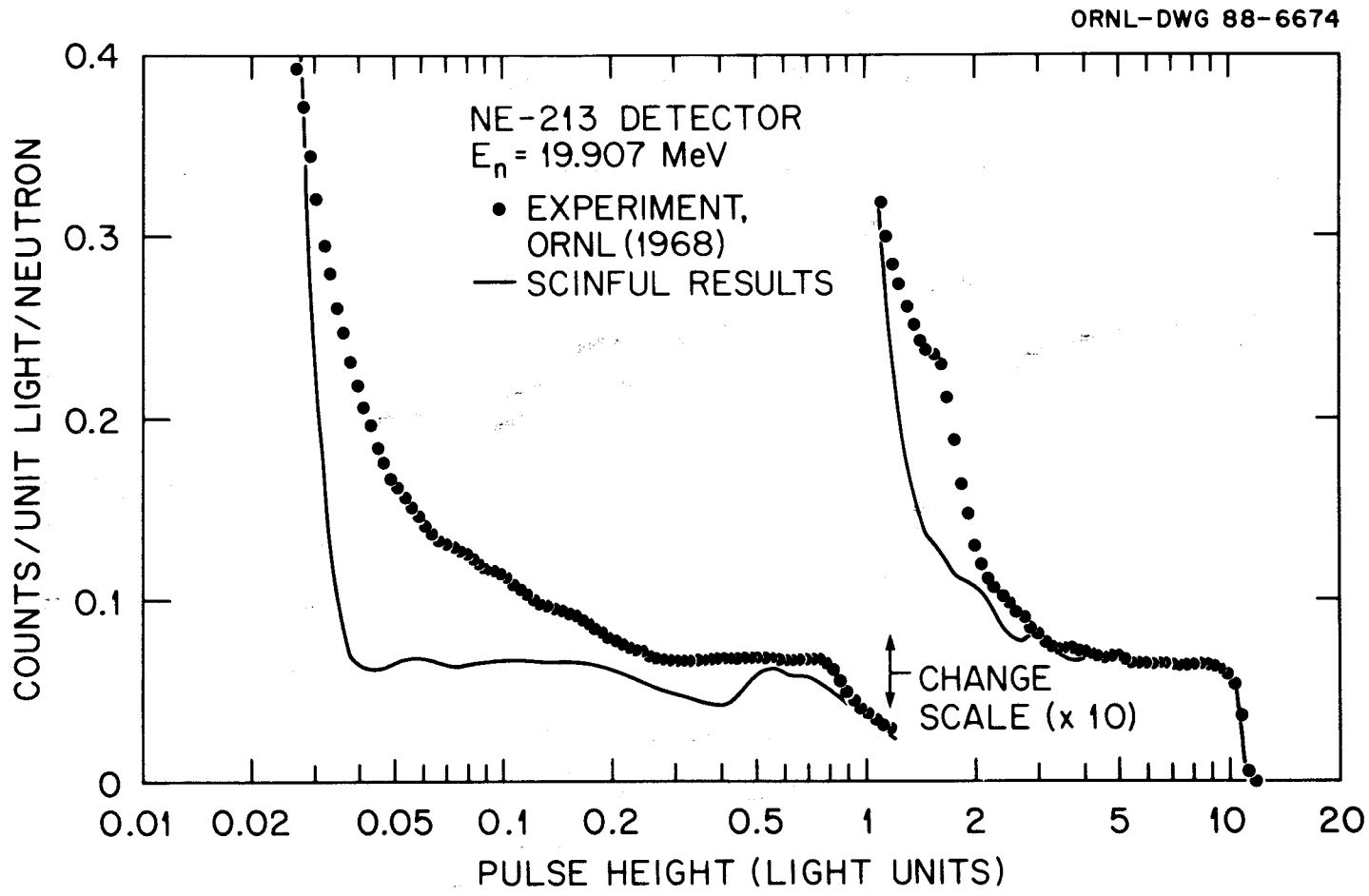

Fig. 47. Comparison of an experimental response measurement for $E_n = 19.907$ MeV by Verbinski et al. (ref. 52) and results of a SCINFUL calculation following folding in of a resolution function. The near peak in the experimental data vicinity 1.7 light units cannot be reproduced by any sensible set of parameters in the SCINFUL program.

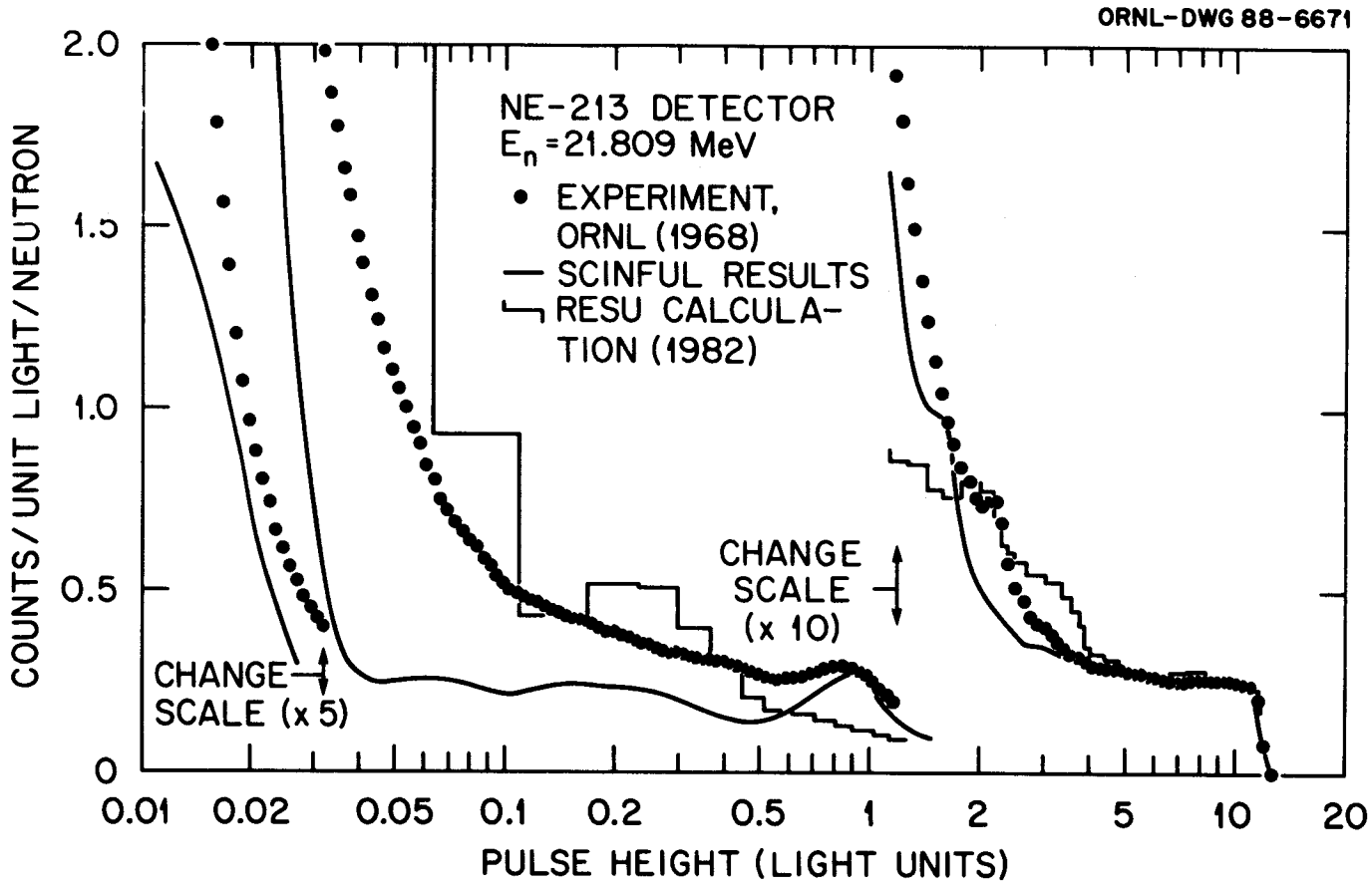

Fig. 48. Comparison of an experimental response measurement for $E_n = 21.809$ MeV by Verbinski et al. (ref. 52) and results of a SCINFUL calculation following folding in of a resolution function. Also shown as the histogram is a calculation using the RESU code (ref. 12). Similar to the data in Figure 47, the little peak in the experiment vicinity 2.2 light units cannot be reproduced by the SCINFUL program. As discussed later in the text the overestimate of the RESU calculation vicinity 3 to 4 light units is due to a likely incorrect analysis of proton energies following $n + {}^{12}C \rightarrow p + \ldots$ reactions.

calculation, could be reduced by increasing somewhat the fluorescent light generated by the alpha in the detector. The main contribution to the response for pulse heights between 0.05 and 0.25 is due to detection of alphas from the $^{12}C(n,n')3\alpha$ breakup reaction, and the moderate difference (of ~20%) observed between calculation and experiment might be reduced by altering somewhat the partitioning of energy among the four outgoing particles in this reaction. The disagreement between calculation and experiment becomes larger as the incident neutron energy is increased from 16 MeV (Figure 46) to 20 MeV (Figure 47) and to 22 MeV (Figure 48). The disagreements observed may be due partly to interactions with detector environs as discussed above for the 3.2-MeV spectrum, but there is also the very real possibility that a second lower-energy neutron group is being generated in the experiment by beam-deuteron interactions with deuterium driven into the tritium target during prior runs at lower deuteron beam energies. The histograms in Figure 48 are taken from a calculation using a program named RESU,[12] and will be discussed later on.

Two pulse-height spectra were reported[58] by the Maryland groups that reported the efficiency data shown in Figure 31. Their response spectrum for $E_n = 30$ MeV is shown in Figure 49, and for $E_n = 45$ MeV in Figure 50. The shapes of the largest pulse height portions of both spectra suggested including a small amount of fluorescent light attenuation in the calculation, and so calculations were performed using a small attenuation coefficient of 0.01/cm. Then the gains, in pulse-height light-units vs channel number were adjusted at the largest pulse heights in order to display the calculated responses with the experimental responses. The agreement for $E_n = 30$ MeV in Figure 49 is very satisfying. The comparison for $E_n = 45$ MeV in Figure 50 is not so favorable, particularly for channels 60 through 80. It is in this pulse-height region that protons from the $n + {}^{12}C \rightarrow p + ...$ reactions and deuterons from the $n + {}^{12}C \rightarrow d + ...$ reactions contribute. The peak near channel 86 in the calculation represents proton contributions from the first reaction, and it is at slightly too large pulse heights. Perhaps the incident energy is somewhat less than 45 MeV?

The last response experiment to be discussed is that of Lockwood et al.[25] at Michigan State. These experimenters used pulse-shape-discrimination electronic techniques not only to eliminate gamma-ray interactions, but they also determined that they could electronically eliminate alpha interactions, leaving only the proton

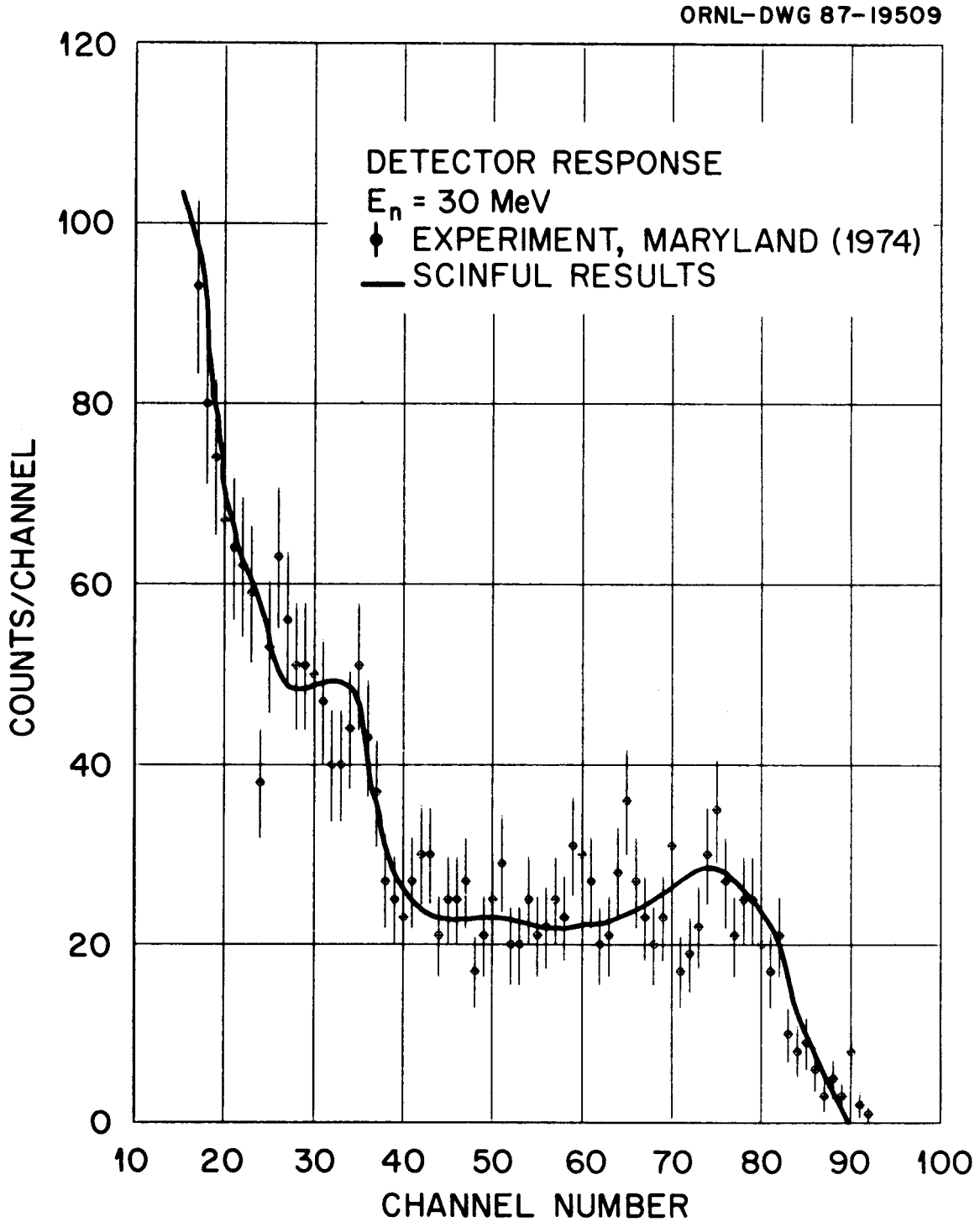

Fig. 49. Comparison of an experimental response measurement for $E_n = 30$ MeV by Riddle et al. (ref. 58) and results of a SCINFUL calculation. A channel-number-to-light-unit calibration was assumed in order to exhibit this comparison.

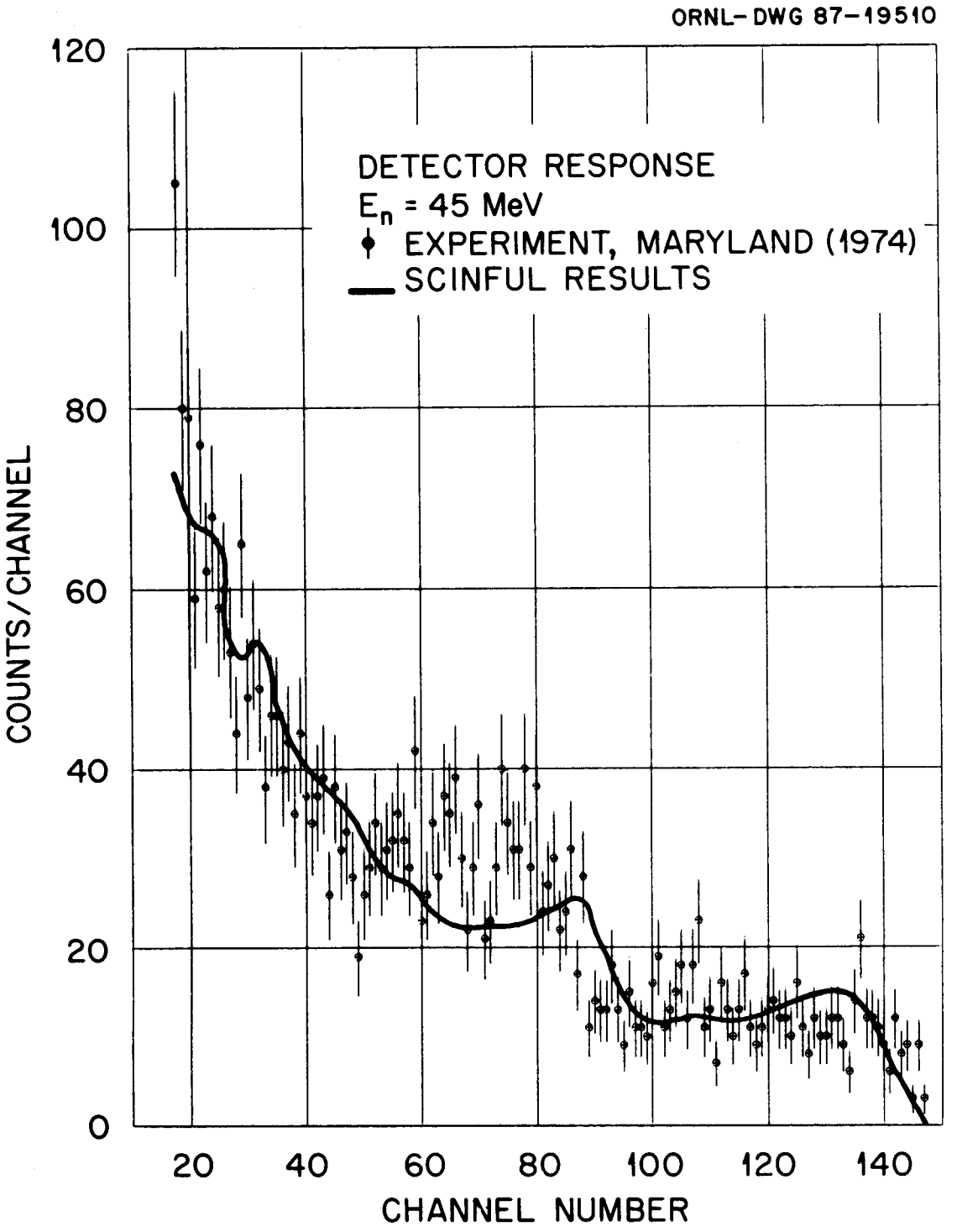

Fig. 50. Comparison of an experimental response measurement for $E_n = 45$ MeV by Riddle et al. (ref. 58) and results of a SCINFUL calculation. A channel-number-to-light-unit calibration was assumed to exhibit this comparison.

interactions in the detector to be recorded. Their hope was in this manner for E_n between 25 and 75 MeV to isolate the contributions to the response from the protons created in the $n + {}^{12}\mathrm{C} \rightarrow p + \ldots$ reactions and thus determine cross sections for this reaction channel. They used two different sized detectors of NE-213. For $E_n < 28$ MeV the detector was 2.5 cm radius by 5.0 cm height, and for $E_n > 28$ MeV the detector was 6.25 cm radius by 12.5 cm height. The resulting responses were plotted as a function of proton energy and reported in absolute yields per unit proton energy. There were some difficulties in comparing SCINFUL results with these experimental responses. The major one was the "calibration" of the pulse-height axis, for it appeared that the experiment was yielding protons of energies larger than the available energy. Furthermore it was going to be difficult to determine a resolution parameter, $R = R(E)$, that might be used to fold a resolution into the SCINFUL results for a better comparison with the measurements. Ultimately it was decided (1) to revise the calibration of the experimental proton-energy axis by about 8% and (2) to forego folding in of a response. The SCINFUL calculations were recast into equal proton energy intervals, and, at first only events labelled "protons" in the SCINFUL calculation were kept. Comparisons with experimental results for $E_n = 4.85$ MeV in Figure 51, for $E_n = 9.55$ MeV in Figure 52, and for $E_n = 14.7$ MeV in Figure 53 all show reasonable agreement, generally <10% difference between calculation and experiment, ignoring somewhat the experimental peak at around 2-MeV proton energy in Figure 53 which is probably due to experimentally misidentified alpha events. For $E_n = 27.4$ MeV in Figure 54 the agreement is quite good for pulse heights > 14 MeV; however, for lower pulse heights the SCINFUL results for just proton events (shown by the open rectangles) clearly underestimate the experimental data. However, including all $Z = 1$ ions gives a much better representation of the experimental data, at least for pulse heights between 7 and 14 MeV. In all of these last 4 figures, by the way, the absolute calibration of the yields is as given by the experimenters but corrected to reflect the ~8% change in the pulse height axis. The small numbers in parentheses along the horizontal axis indicate the original experimental pulse height calibration.

On the basis of the results just discussed as exhibited in Figure 54, the remaining SCINFUL calculations included p, d, and t events for comparison with the experimental data. The results for $E_n = 39.4$ MeV are shown in Figure 55, and except for the lack of folding a resolution into the calculated response, the agreement

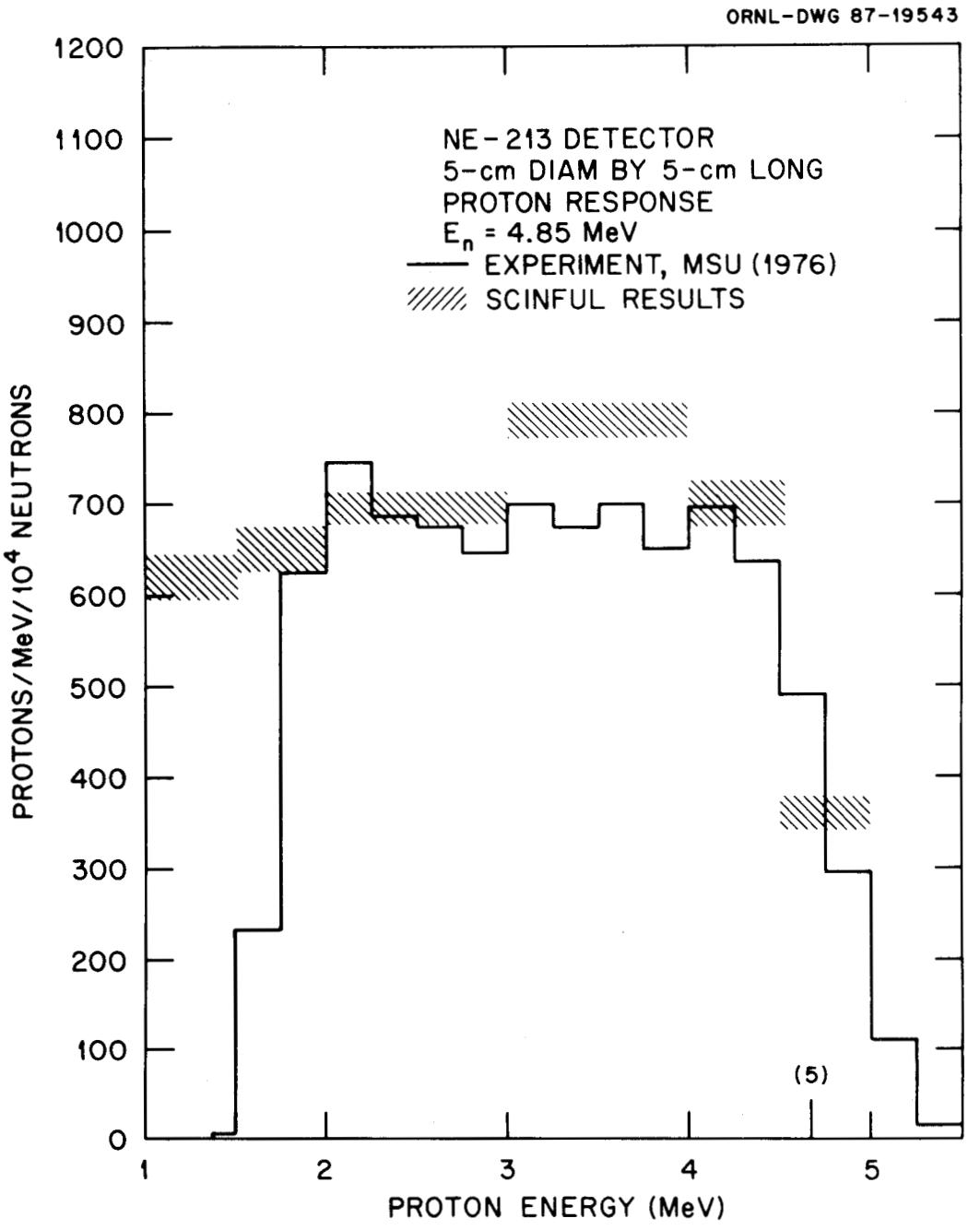

Fig. 51. Comparison of an experimental response measurement for $E_n = 4.85$ MeV by Lockwood et al. (ref. 25) and results of a SCINFUL calculation. The experimental pulse-height calibration for these data (and in the succeeding 8 figures) appears to be in error by about 8%. The small figure 5 in parentheses indicates the pulse-height calibration given in ref. 25.

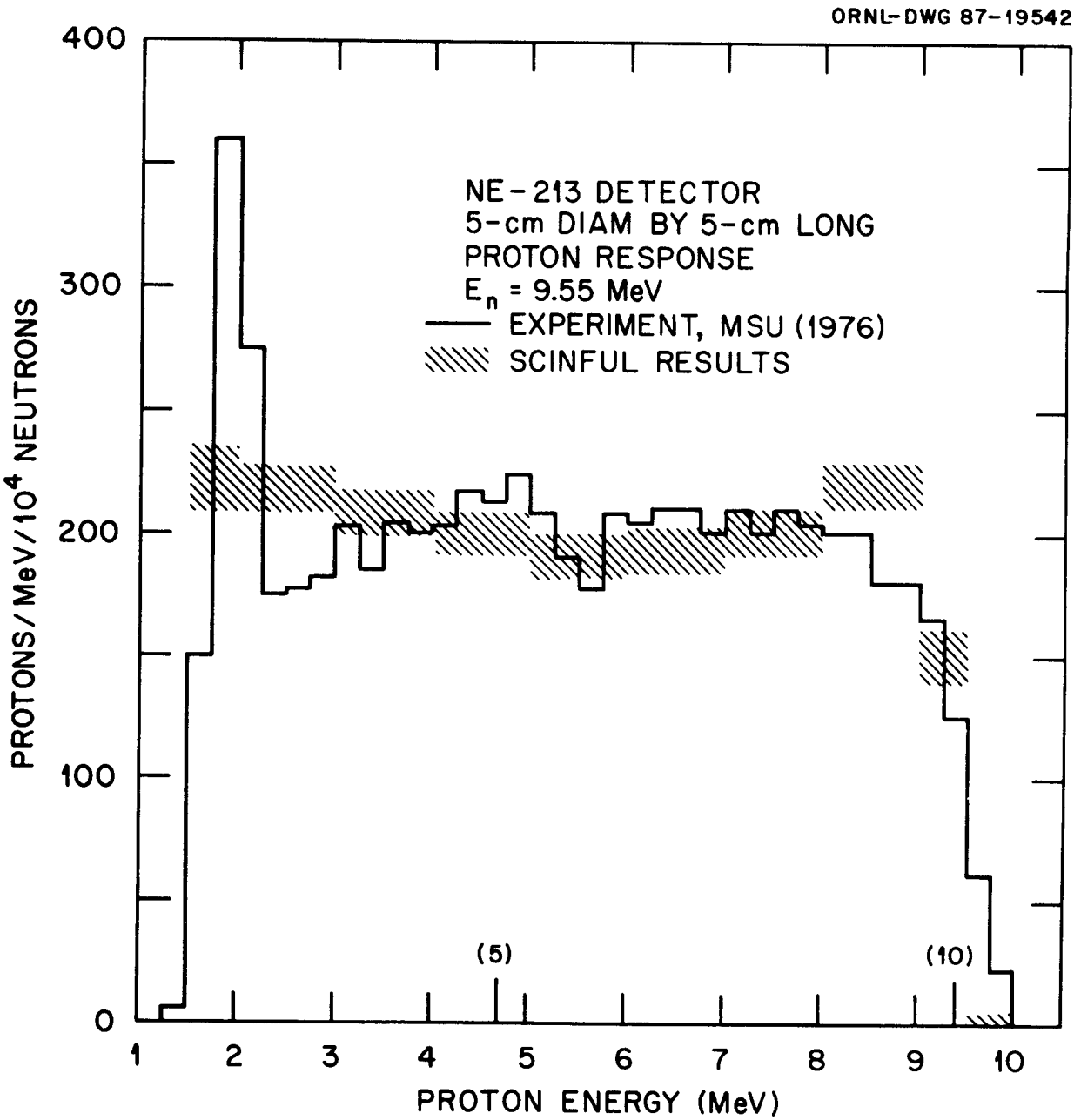

Fig. 52. Comparison of an experimental response measurement for $E_n = 9.55$ MeV by Lockwood et al. (ref. 25) and results of a SCINFUL calculation stripped of alpha contributions at the lowest equivalent proton energies. See caption to Figure 51 regarding pulse-height calibration.

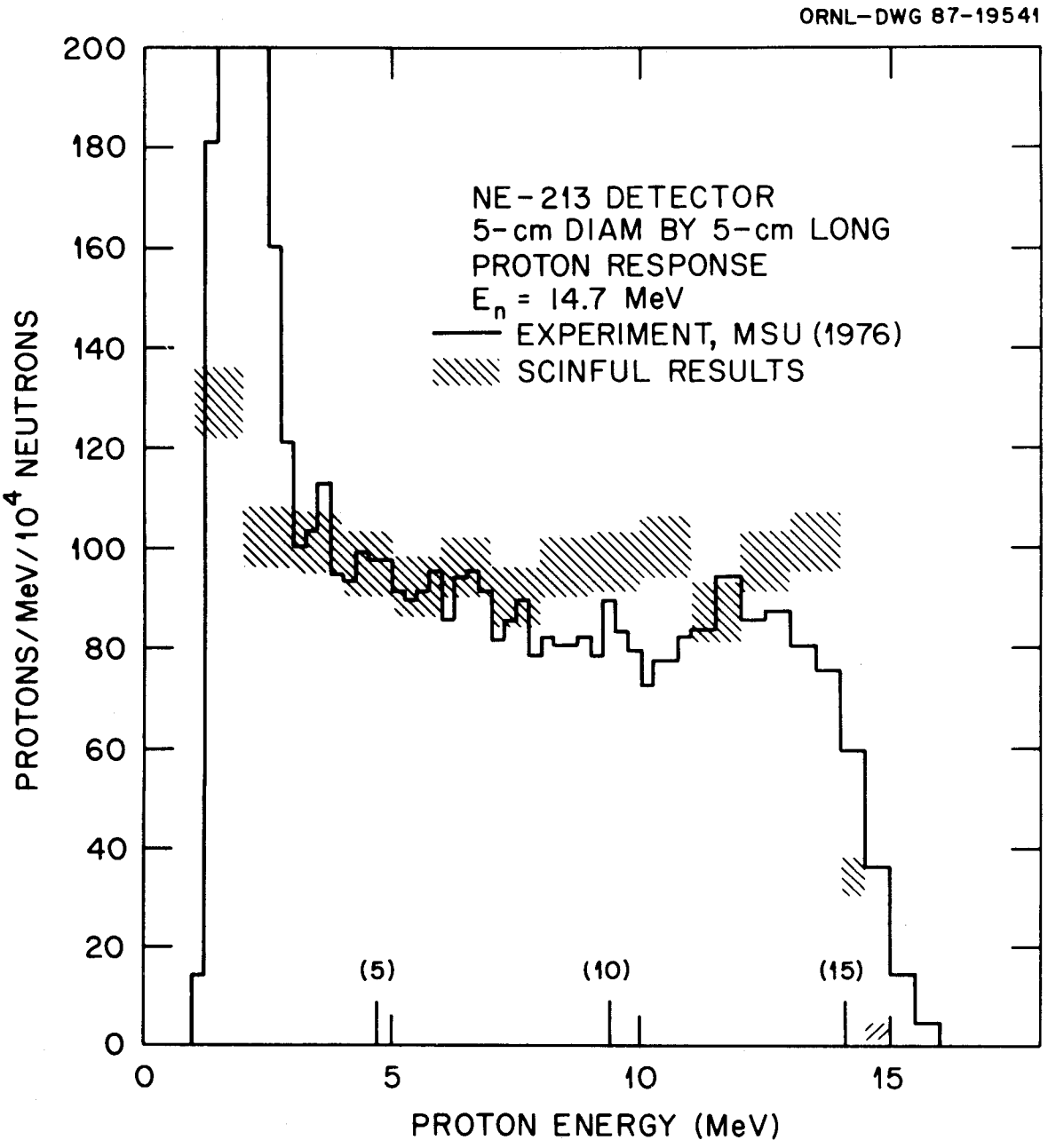

Fig. 53. Comparison of an experimental response measurement for $E_n = 14.7$ MeV by Lockwood et al. (ref. 25) and results of a SCINFUL calculation for only proton contributions similar to Figure 52.

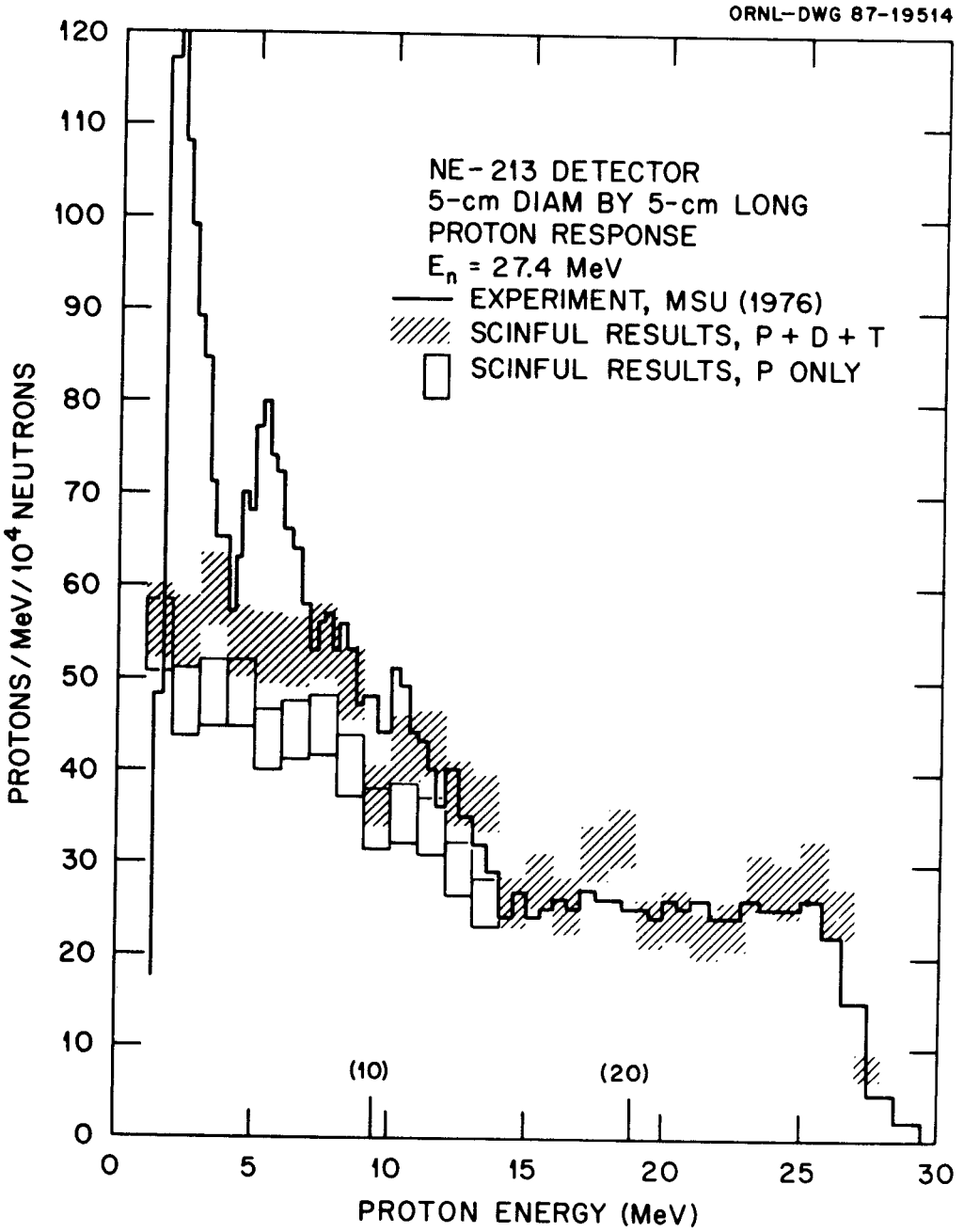

Fig. 54. Comparison of an experimental response measurement for $E_n = 27.4$ MeV by Lockwood et al. (ref. 25) and results of two SCINFUL calculations. The open rectangles represent proton contributions only, similar to Figure 52. The cross-hatched results represent proton-plus-deuteron-plus-triton results, and the better comparison with experiment suggests that the experimental discrimination was for $Z = 1$ and not just protons as suggested by the authors of ref. 25.

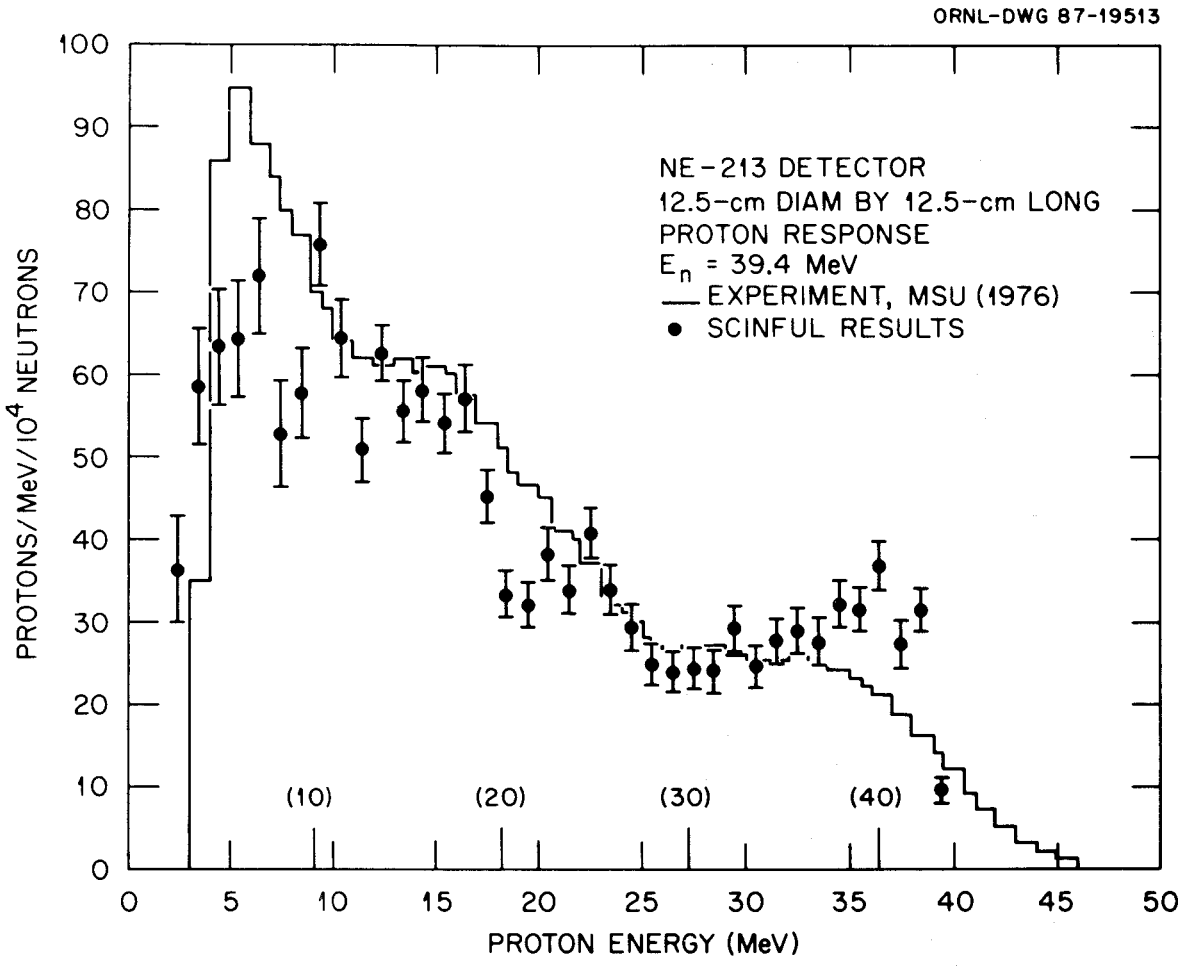

Fig. 55. Comparison of an experimental response measurement for $E_n = 39.4$ MeV by Lockwood et al. (ref. 25) and results of a SCINFUL calculation stripped of α and ^{3}He contributions. The agreement for $E_{p'} > 33$ MeV would be improved by folding in a resolution function to better approximate the detector response. The integral yields for $E_{p'} > 27$ MeV are equal.

is quite good. Indeed, the agreement is about what one might expect from the discussion of the Subramanian et al.[20] experiment above and the comparisons of SCINFUL results with their data at $E_n = 39.7$ MeV exhibited in Figures 14 through 16. SCINFUL results agree with the MSU experiment, at least for proton energies > 20 MeV, for $E_n = 48.5$ MeV as exhibited in Figure 56. For smaller pulse heights the calculated results somewhat underpredict the experiment, which may or may not be due (again) to mis-identified alpha pulses in the experimental response. The agreement between calculation and experiment is just as good for $E_n = 60.7$ MeV as shown in Figure 57. Again one may recall the discussion regarding the data of Subramanian et al.[20] as exhibited in Figures 19 through 21. The peak in vicinity of 30-MeV proton energy in Figure 57 is due to deuteron contributions, at least in the calculation. Moving to $E_n = 70.6$ MeV as shown in Figure 58, the agreement between experiment and calculations is not as good. However, the response at large pulse heights, namely > 55 MeV proton energy, is due only to $n + H$ interactions for which the cross section is well known, and one might assume that the calculations should have that portion of the response spectrum very nearly correct, if the $n + H$ cross section given by the Gammel formula[23] is correct. If so, perhaps one might construe a possible overall normalization error in the experiment; and continuing along this line of reasoning one might envision reducing the plotted histogram by about 15% which would result in a response spectrum in really quite good agreement with the SCINFUL calculation. Indeed, then mentally applying a resolution to the large value plotted for the SCINFUL results at a pulse height equivalent to about 36-MeV proton energy will yield a rounded peak very similar to that experimentally observed. A similar mental evaluation of the comparison shown in Figure 59 for $E_n = 74.3$ MeV may be about as valid, although the experimental results for pulse heights between 40 and 50 MeV may not be as well reproduced as may be desired.

Finally in this section we will show comparisons from SCINFUL calculations with calculations of responses from a recently released program named RESU by Uwamino et al.[12]. RESU has many similarities to O5S, the major improvements being in extending the light-unit tables and changes in cross sections for higher-energy neutron interactions with ^{12}C. There are several difficulties with RESU. In the first place, in RESU the $^{12}\mathrm{C}(n, n')3\alpha$ reaction is assumed to proceed only via excitation of energy levels in ^{12}C having E_x up to 12.7 MeV; hence contributions

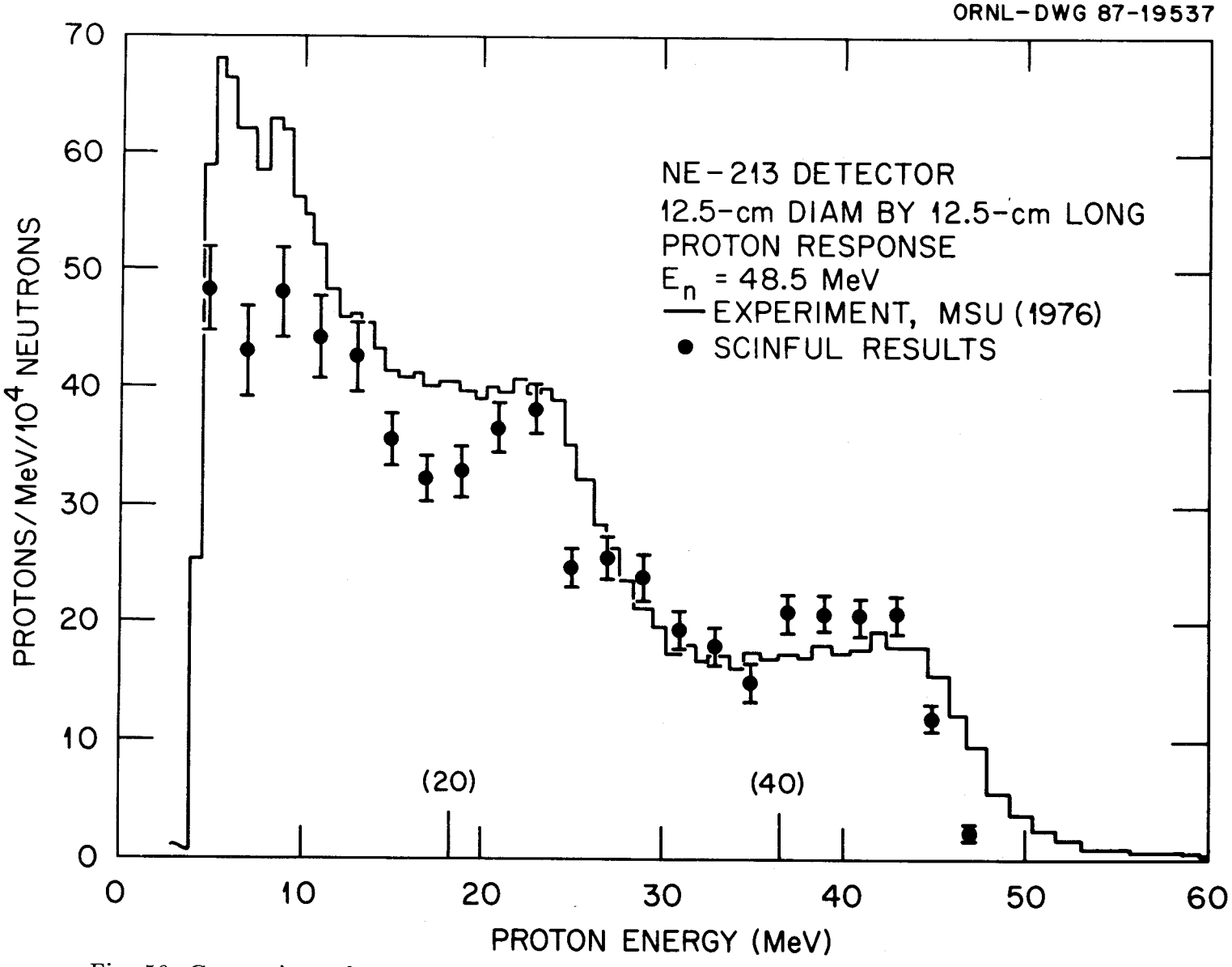

Fig. 56. Comparison of an experimental response measurement for $E_n = 48.5$ MeV by Lockwood et al. (ref. 25) and results of a SCINFUL calculation stripped of α and ^{3}He contributions. The integral yields for $E_{p'} > 35$ MeV are equal.

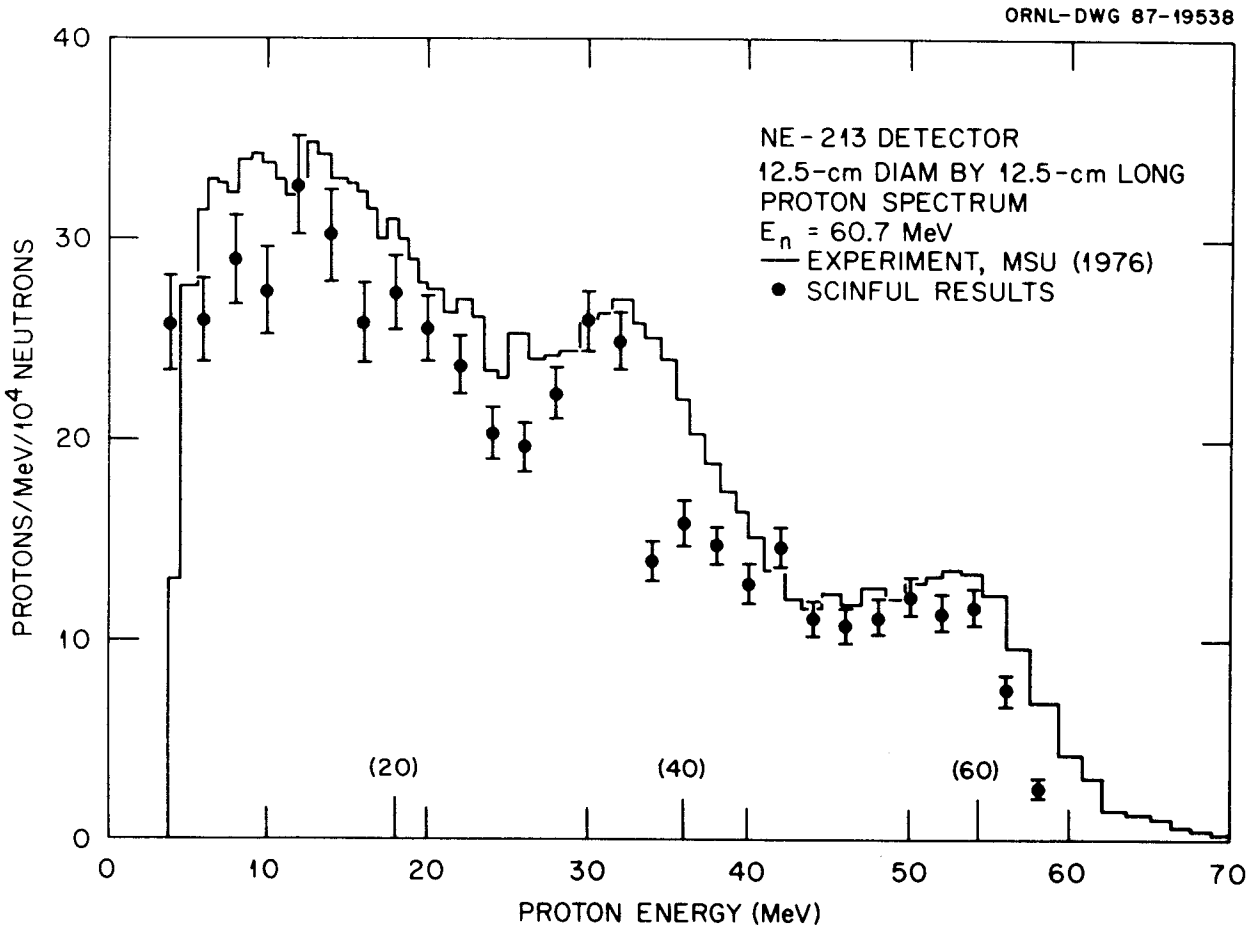

Fig. 57. Comparisons of an experimental response measurement at $E_n = 60.7$ MeV by Lockwood et al. (ref. 25) and results of a SCINFUL calculation stripped of α and ^{3}He contributions. The integral yields for $E_{p'} > 45$ MeV are ~8% different.

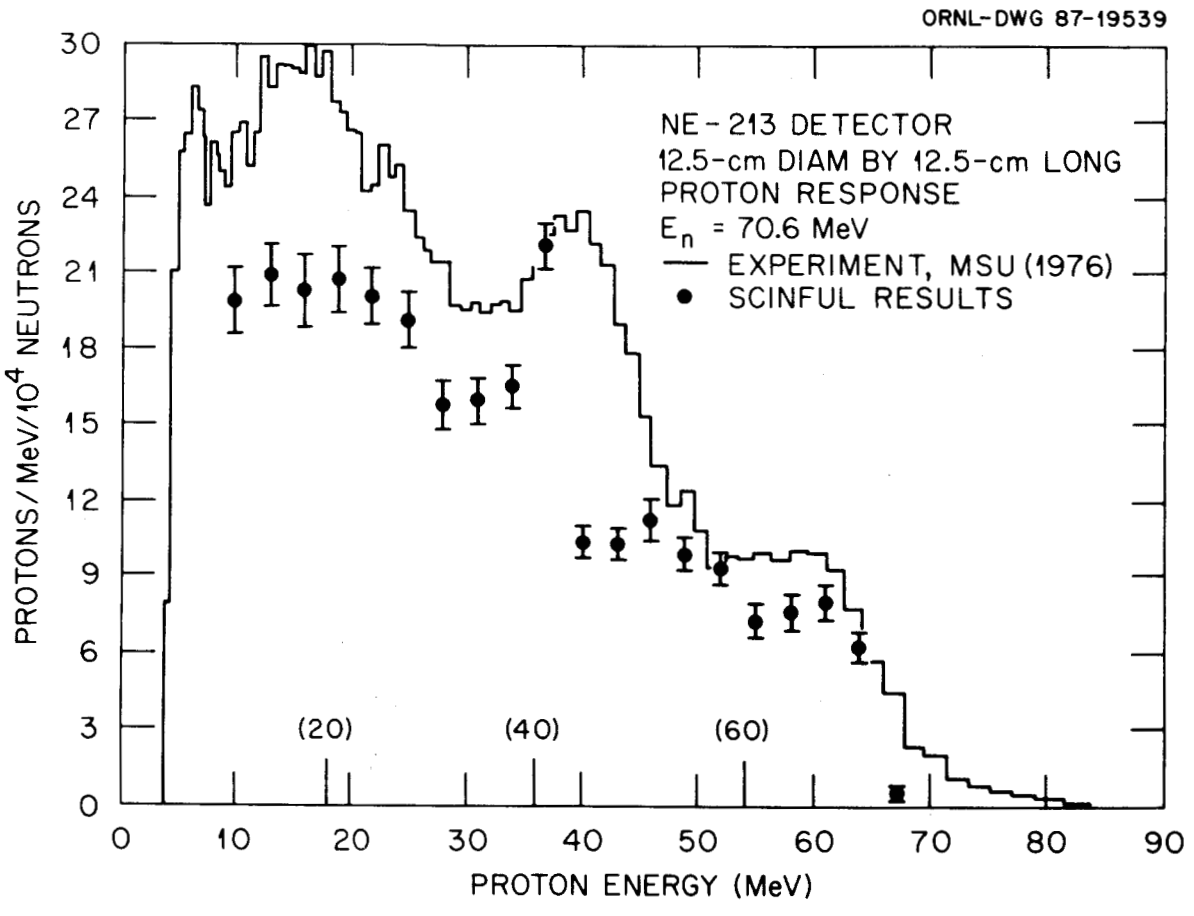

Fig. 58. Comparisons of an experimental response measurement at $E_n = 70.6$ MeV by Lockwood et al. (ref. 25) and results of a SCINFUL calculation stripped of α and ^{3}He contributions. The integral yields for $E_{p'} > 55$ MeV differ by ~15%. The calculational results for these large pulse heights are due to $n + H$ interactions for which the cross section is presumed to be known to better than ~3% (ref. 23).

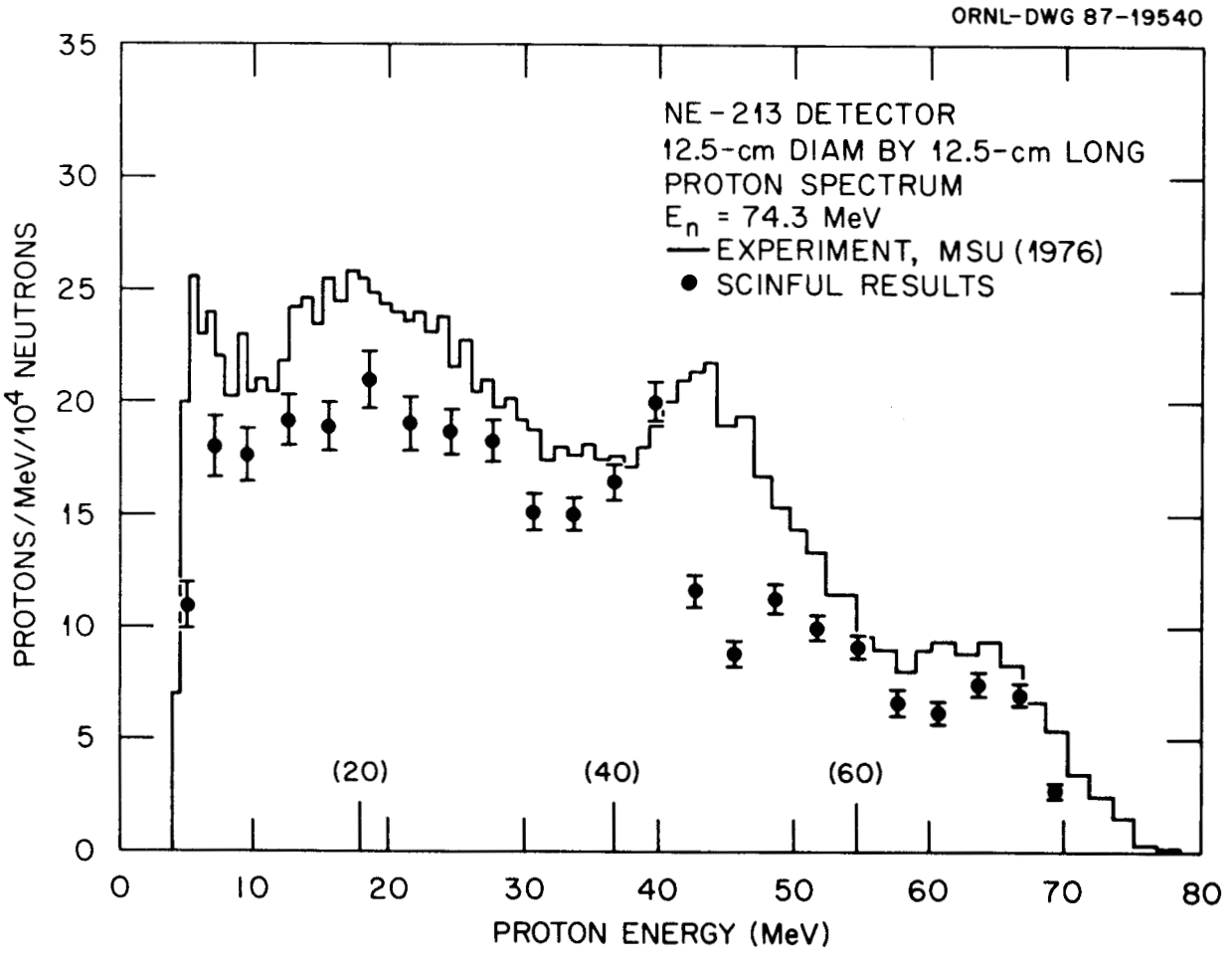

Fig. 59. Comparisons of an experimental response measurement at $E_n = 74.3$ MeV by Lockwood et al. (ref. 25) and results of a SCINFUL calculation stripped of α and ^{3}He contributions. The integral yields for $E_{p'} > 60$ MeV differ by ~20%.

to the response from the fluorescent light from the 3α breakup reaction can be only at small pulse heights, i.e., only for equivalent proton energies < 5 MeV. The 3α contribution is very evident in the RESU calculation for $E_n = 30.5$ MeV shown in Figure 60, being the peak centered about 2 MeV. Another problem is the treatment of the reaction particles from $n + {}^{12}\mathrm{C} \rightarrow p + \ldots$ reactions. In RESU for $E_n > 32$ MeV the reaction is treated solely as $\rightarrow p + n + {}^{11}\mathrm{B}$, with no further breakup of the ${}^{11}\mathrm{B}$ ion, but also no contribution from the $\rightarrow p + {}^{12}\mathrm{B}$ (bound state) reactions. However, for $E_n < 32$ MeV, the proton contribution from this reaction channel is solely from the two-body ${}^{12}\mathrm{B}$ bound state reaction. As a consequence for $E_n = 21.8$ MeV, as shown in Figure 48 where the RESU results are shown as the histogram, the RESU code predicts a substantial contribution for protons for the ${}^{12}\mathrm{C}(n,p){}^{12}\mathrm{B}$ (bound-state) reactions which are manifest in the calculated spectrum as a bulge between 2.5 and 4 light units (the SCINFUL results are the more accurate in this pulse-height region). On the other hand, for $E_n = 41$ MeV as exhibited in Figure 61, the RESU response exhibits a substantial contribution for pulse heights between 9 and 18 MeV, a "bulge" occurring at pulse heights about 50% larger than computed from the SCINFUL program. However, once again referring to Figure 14, the nuclear data of Subramanian et al.[20] do not support these higher energy protons from the three-body reaction. In addition, the little peak in the SCINFUL calculation at about 24 MeV equivalent proton energy in Figure 61 is due to the $n + {}^{12}\mathrm{C} \rightarrow p + {}^{12}\mathrm{B}$ (bound state) reactions, not reproduced in the RESU calculation, but supported by the data of Subramanian et al.[20] Similar disagreement is seen for $E_n = 51$ MeV in Figure 62, and for $E_n = 62$ MeV in Figure 63. The "peak" shown at about 33 MeV equivalent energy in Figure 63 for the SCINFUL results is due to deuterons from the $n + {}^{12}\mathrm{C} \rightarrow d + \ldots$ reactions and is supported by the peak at about 45 MeV outgoing deuteron energy shown in Figure 20. It is also the contribution to the response of Figure 57 at about 30-MeV proton energy. Indeed, it is not at all evident that the RESU results would reproduce the experimental response shown in Figure 57 as well as the SCINFUL results do. Finally, a comparison of RESU results and SCINFUL results for $E_n = 78$ MeV is shown in Figure 64. Here one may say that if a resolution function were folded into the results of the calculations, as surely would be the case with an experimental response, the two calculations would resemble each other quite a bit, with the difference being about 15 to 20%

up to about 40-MeV equivalent proton energy, not a substantial difference within the current state of the art.

Thus ends this long section on comparisons of SCINFUL calculations with experimental data. The comparisons in the first part of the section with the data of Subramanian et al.[20] tend to validate the nuclear physics concepts used to determine energies of outgoing charged ions. It should be pointed out that although the calculational nuclear physics concept is one of a sequentially decaying highly-excited "compound" nucleus, it is not here asserted that just because calculated results agree well with experimental data that the model concept is, indeed, the real nuclear physics of neutron interactions with ^{12}C in the region of incident neutron energies between 20 and 80 MeV. What is offered, however, is the conclusion that the calculational model works for the desired task, and that SCINFUL may be considered a reliable tool for obtaining scintillator full energy responses for incident neutrons up to 80 MeV.

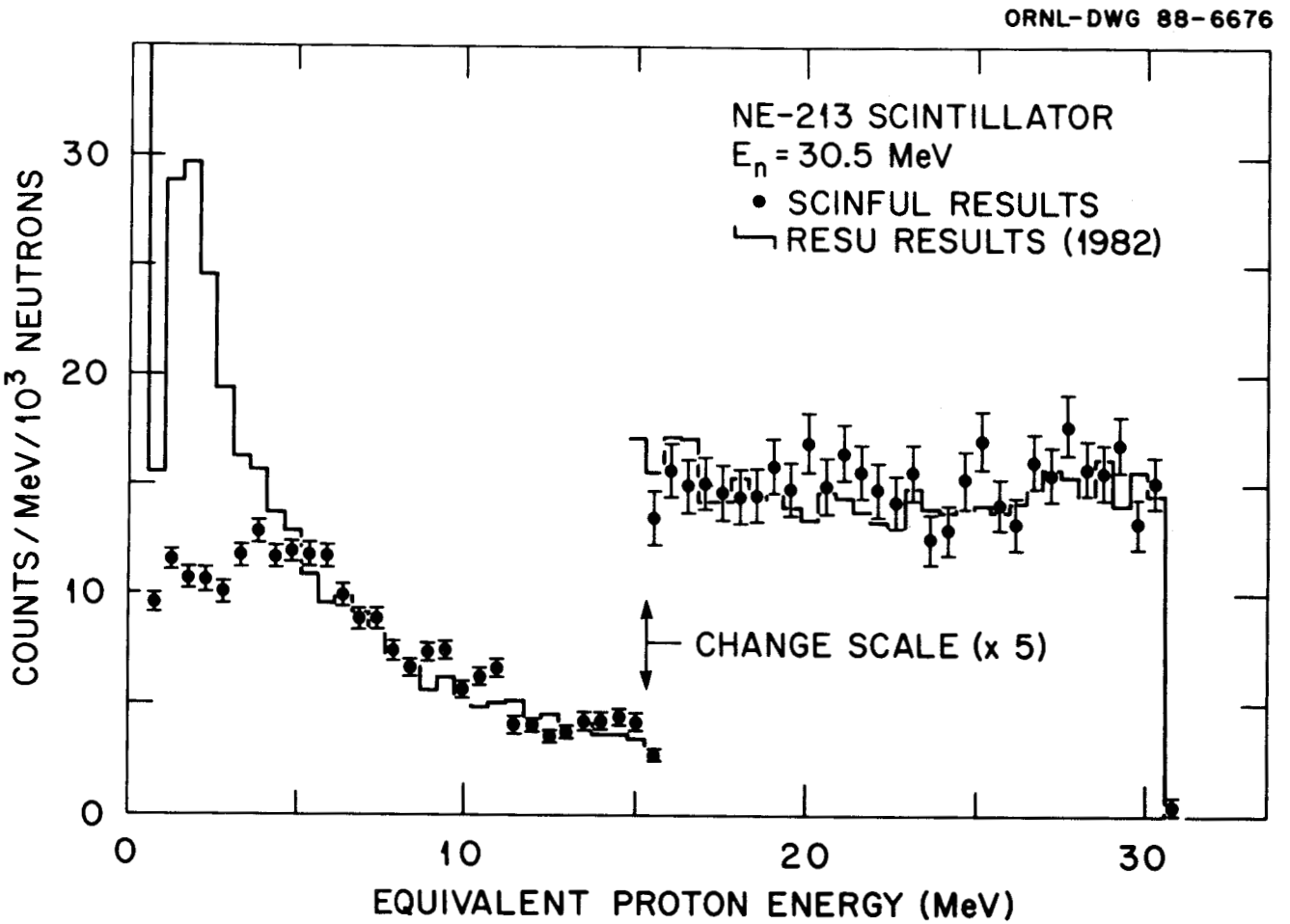

Fig. 60. Comparison of a calculated response at 30.5 MeV using the RESU code (ref. 12) with a calculated response using SCINFUL. The major difference, for $E_{p'}$ between 1 and 3 MeV, is due to the RESU code's different analysis of the 3α breakup reaction, as discussed in the text.

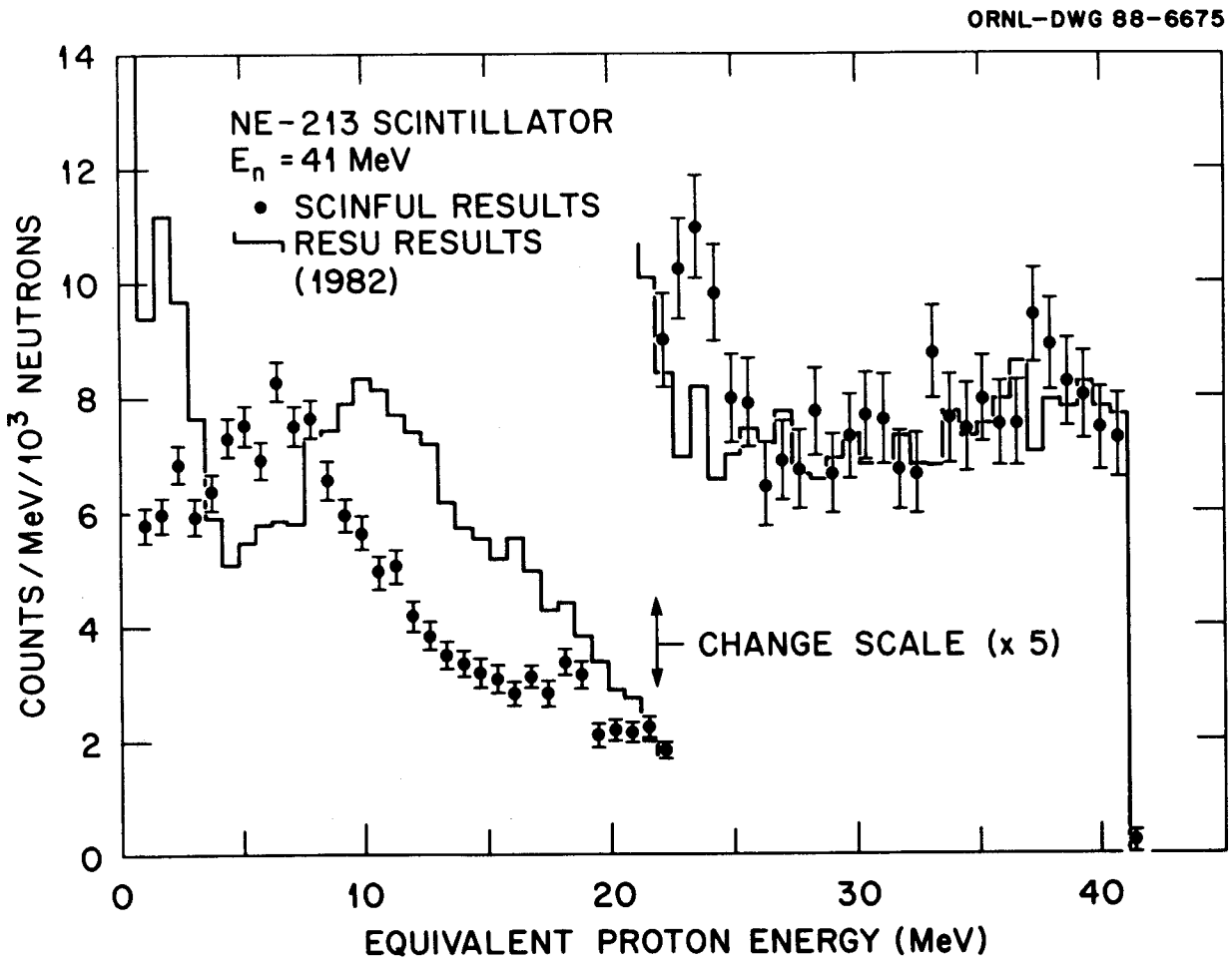

Fig. 61. Comparison of a calculated response at 41 MeV using the RESU code (ref. 12) with a calculated response using SCINFUL.

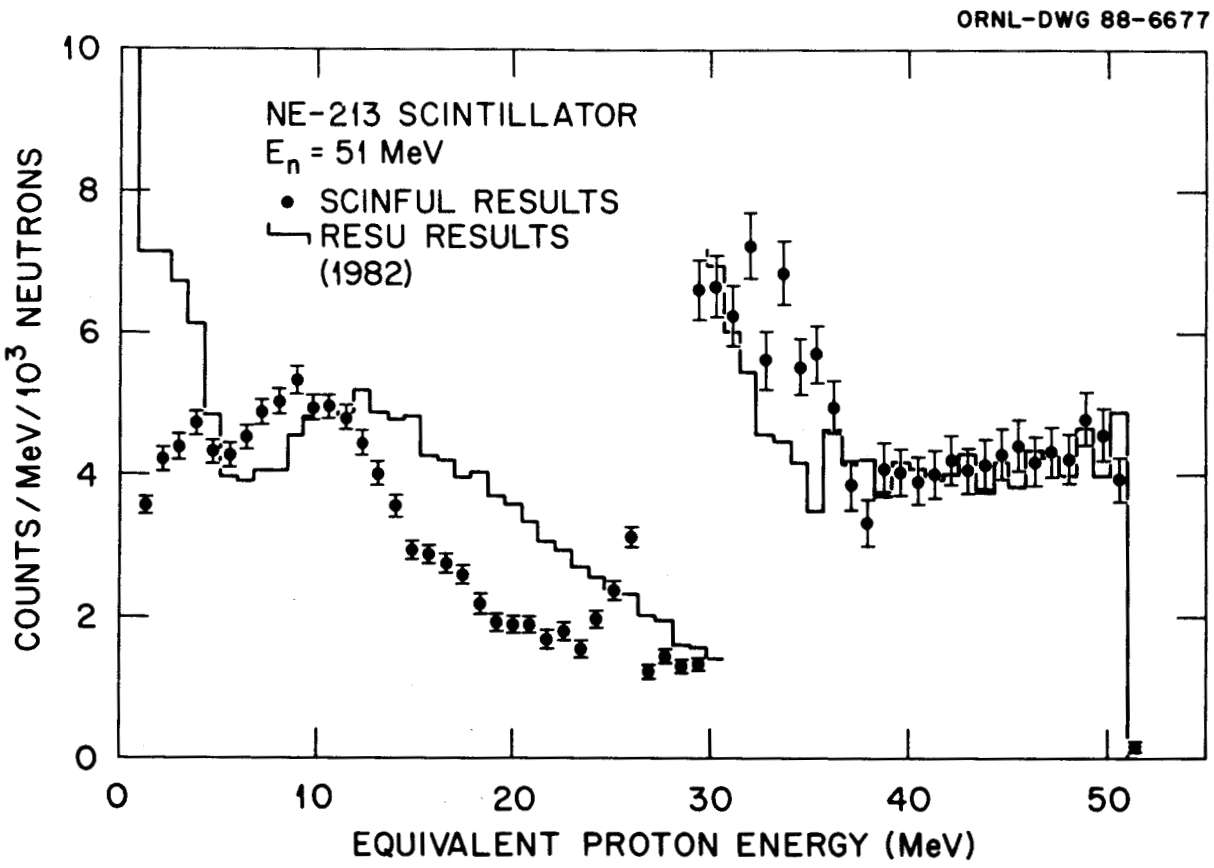

Fig. 62. Comparison of a calculated response at 51 MeV using the RESU code (ref. 12) with a calculated response using SCINFUL.

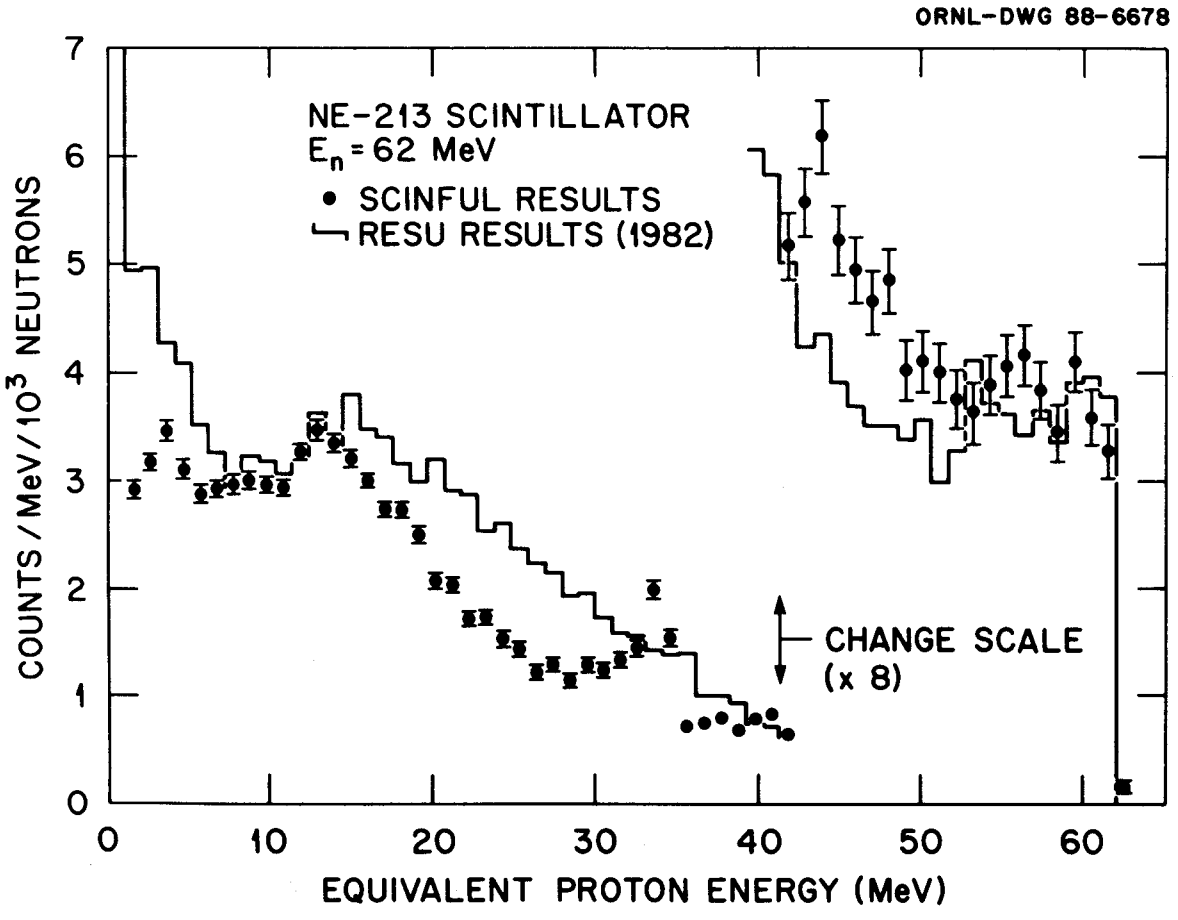

Fig. 63. Comparison of a calculated response at 62 MeV using the RESU code (ref. 12) with a calculated response using SCINFUL.

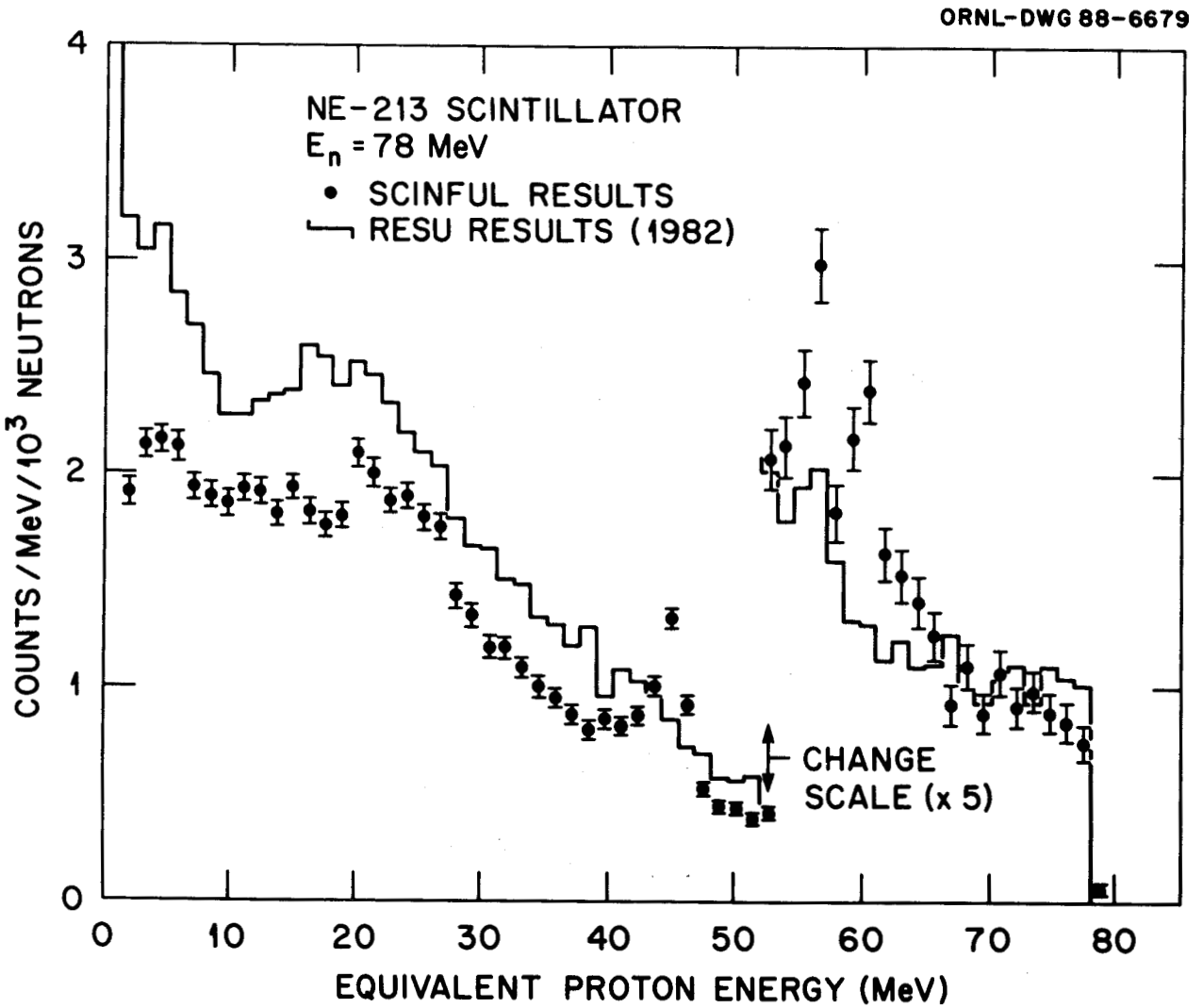

Fig. 64. Comparison of a calculated response at 78 MeV using the RESU code (ref. 12) with a calculated response using SCINFUL.

9. IMPROVEMENTS AND POTENTIAL EXTENSIONS

There are several extensions and improvements to SCINFUL that may be considered in addition to applications of techniques to speed up the execution. Some improvements to the cross sections for the major types coupled with improvements in the programming might be considered to improve the agreements with the data of Subramanian et al.[20] as exhibited in Figures 10 through 23, which, in turn, could result in moderate improvements in agreement with the MSU response data of Figures 56 through 59.

A second useful effort might involve modelling effects of materials in the near environment of the scintillator. In particular, since the liquid scintillator NE-213 must be contained, some estimates of the effects of the container could be added to the program. For the solid scintillator NE-110, effects due to a light pipe that might be coupled to the scintillator could be computed.

A third addition might be to consider programming for an extended source. In a typical experimental configuration the neutron "source" is not at a point but instead results from neutron scattering from a finite-sized sample. As discussed above, computed responses are somewhat sensitive to geometric considerations.

A fourth consideration might be to include the capability of folding a resolution into the output from parameters included as part of the input. After all, all real detectors have some less-than-perfect resolving capacity.

A fifth addition might be adding the capability of studying other scintillators, e.g. NE-218.[51,64] Besides a small effect on proton range-energy relationships,[65] the major task would be to determine light-unit values vs charged-particle energies for all of the residual charged particles for the added scintillator type relative to those values in SCINFUL for NE-213.

Extending SCINFUL to neutron energies greater than 80 MeV will require, at the least, (a) determining effective cross sections for the major types of reactions as currently programmed, (b) determining light-unit conversions for high-energy charged particles from protons to carbon ions, (c) programming of additional multi-body reactions including capacity to handle reactions involving more than two neutrons, more than two protons (with possible escape from the detector), etc. and (d) improving the charged-particle range-energy computations and extending the program to include escape of the heavier charged particles.

The present version (V. 1) of SCINFUL is being "frozen" for purpose of documentation and distribution since the program should be useful and reliable for providing scintillator responses for neutrons of substantially higher energies than here-to-fore available. Several of the above additions are being considered for implementation, however, in the future.

REFERENCES

1. R. E. Textor and V. V. Verbinski, *O5S: A Monte Carlo Code for Calculating Pulse Height Distributions due to Monoenergetic Neutrons Incident on Organic Scintillators*, ORNL-4160 (1968). See also M. A. Cleemput, *O5S – A Version Suitable for Use on the DEC System-10*, ORNL/CF-82/268/R1 (1982).

2. R. J. Schuttler, *Efficiency of Organic Scintillators for Fast Neutrons*, ORNL-3888 (1966).

3. R. J. Kurz, *A 709/7090 FORTRAN II Program to Compute the Neutron-Detection Efficiency of Plastic Scintillator for Neutron Energies from 1 to 300 MeV*, UCRL-1139 (1964). See also S. A. Elbakr, J. W. Watson, and C. A. Miller, *Nucl. Instrum. Meth.* **115**, 115 (1974) for a correction to the Kurz program.

4. S. T. Thornton and J. R. Smith, *Nucl. Instrum. Meth.* **96**, 551 (1971).

5. N. R. Stanton, *A Monte Carlo Program for Calculating Neutron Detection Efficiencies in Plastic Scintillator*, Ohio State University Report No. COO-1545-92 (1971).

6. R. M. Edelstein, J. S. Russ, R. C. Thatcher, M. Elfield, E. L. Miller, N. W. Reay, N. R. Stanton, M. A. Abolins, M. T. Lin, K. W. Edwards, and D. R. Gill, *Nucl. Instrum. Meth.* **100**, 355 (1972).

7. V. Fajer and L. Alvarez, *Organic Scintillator Efficiency Using a Monte Carlo Code*, Hungarian Academy of Sciences, KFKI-1979-60 (1979) (in English). Their program name is TAYRA.

8. R. R. Cecil, B. D. Anderson, and R. Madey, *Nucl. Instrum. Meth.* **161**, 439 (1979).

9. M. Anghinolfi, G. Ricco, P. Corvisiero, and F. Masulli, *Nucl. Instrum. Meth.* **165**, 217 (1979).

10. G. Dietze and H. Klein, *NRESP4 and NEFF4 Monte Carlo Codes for the Calculation of Neutron Response Functions and Detection Efficiencies for NE 213 Scintillation Detectors*, Physikalisch-Technische Bundesanstalt Report ND-22; ISSN 0572-7170 (1982).

11. E. DeKempeneer, H. Liskien, L. Mewissen, and F. Poortmans, *Nucl. Instrum. Meth.* **A256**, 489 (1987).

12. Y. Uwamino, K. Shin, M. Fujii, and T. Nakamura, *Nucl. Instrum. Meth.* **204**, 179 (1982).

13. D. C. Irving, R. M. Freestone, Jr., and F. B. K. Kam, *O5R, A General-Purpose Monte Carlo Neutron Transport Code*, ORNL-3622 (1965).

14. C. Renner, N. W. Hill, G. L. Morgan, K. Rush, and J. A. Harvey, *Nucl. Instrum. Meth.* **154**, 525 (1978).

15. J. K. Dickens, *SCINFUL: A Monte-Carlo-Based Computer Program to Determine a Scintillator Full Energy Response to Neutron Detection for E_n Between 0.1 and 80 MeV: User's Manual and FORTRAN Program Listing*, ORNL-6462 (1988).

16. F. Ajzenberg-Selove, *Nucl. Phys.* **A413**, 1 (1984).

17. B. Antolkovic, I. Slaus, D. Plenkovic, P. Macq and J. P. Meulders, *Nucl. Phys.* **A394**, 87 (1983).

18. C. Y. Fu, *Atomic Data and Nucl. Data Tables* **17**, 127 (1976); K. Shibata and C. Y. Fu, *Recent Improvements of the TNG Statistical Model Code*, ORNL/TM-10093 (1986).

19. M. W. McNaughton, N. S. P. King, F. P. Brady and J. L. Ullmann, *Nucl. Instrum. Meth.* **129**, 241 (1975).

20. T. S. Subramanian, J. L. Romero, F. P. Brady, J. W. Watson, D. H. Fitzgerald, R. Garrett, G. A. Needham, J. L. Ullmann, and C. I. Zanelli, *Phys. Rev. C* **28**, 521 (1983).

21. F. Ajzenberg-Selove and C. L. Busch, *Nucl. Phys.* **A336**, 1 (1980).

22. D. A. Kellogg, *Phys. Rev.* **90**, 224 (1953).

23. J. L. Gammel, see J. R. Stehn, M. D. Goldberg, B. A. Magurno and R. Wiener-Chasman, *Neutron Cross Sections*, Vol. 1, $Z = 1$ to 20, BNL-325, Second Edition, Supplement No. 2 (May 1964), p. 1-0-5.

24. W. Dodder and J. Hale, Los Alamos National Laboratory (unpublished, 1987).

25. J. A. Lockwood, C. Chen, L. A. Friling, D. Swartz, R. N. St. Onge, A. Galonsky and R. R. Doering, *Nucl. Instrum. Meth.* **138**, 353 (1976).

26. C. Y. Fu, *Summary of ENDF/B-V Evaluations for Carbon, Calcium, Iron, Copper, and Lead and ENDF/B-V Revision 2 for Calcium and Iron*, ORNL/TM-8283 (1982).

27. A. del Guerra, *Nucl. Instrum. Meth.* **135**, 337 (1976).

28. D. J. Brenner, M. Zaider, J. J. Coyne, H. G. Menzel, and R. E. Prael, *Nucl. Sci. and Eng.* **95**, 311 (1987).

29. E. J. Axton, private communication, 1987.

30. B. Anders, P. Herges and W. Scobel, *Z. Phys. A* **301**, 353 (1981).

31. J. E. Brolley, Jr., J. L. Fowler, and L. K. Schlacks, *Phys. Rev.* **88**, 618 (1952); see also J. R. Stehn et al. *op. cit.* p. 6-12-4.

32. F. D. Beechetti, C. E. Thorn and M. J. Levine, *Nucl. Instrum. Meth.* **138**, 93 (1976); see also T. J. Gooding and H. G. Pugh, *Nucl. Instrum. Meth.* **7**, 189 (1960).

33. N. Olsson and B. Trostell, *Nucl. Instrum. Meth. Phys. Res.* **A245**, 415 (1986).

34. F. P. Brady, G. A. Needham, J. L. Ullmann, C. M. Castaneda, T. D. Ford, N. S. P. King, J. L. Romero, M. L. Webb, V. R. Brown, and C. H. Poppe, *J. Phys. G: Nucl. Phys.* **10**, 363 (1984).

35. A. S. Meigooni, J. S. Petler and R. W. Finlay, *Phys. Med. Biol.* **29**, 643 (1984); see also R. W. Finlay, A. S. Meigooni, J. S. Petler and J. P. Delaroche, *Nucl. Instrum. Meth. Phys. Res.* **B10/11**, 396 (1985).

36. D. W. Glasgow, F. O. Purser, H. Hogue, J. C. Clement, K. Stelzer, G. Mack, J. R. Boyce, D. H. Epperson, S. G. Buccino, P. W. Lisowski, S. G. Glendinning, E. G. Bilpuch, H. W. Newson, and C. R. Gould, *Nucl. Sci. Eng.* **61**, 521 (1976).

37. G. Dietze, H. J. Brede, H. Klein and H. Schölermann, in *Nuclear Data for Science and Technology, Proc. of Int. Conf. 6-10 Sept. 1982, Antwerp*, K. H. Böckhoff, ed. (D. Reidle Publ. Co., Dordrecht/Boston/London, 1983), p. 930.

38. M. Brendle, M. Morike, G. Staudt, and G. Steidle, *Z. Naturforsch* **23a**, 1229 (1968).

39. R. C. Haight, S. M. Grimes, R. G. Johnson and H. H. Barschall, *Nucl. Sci. Eng.* **17**, 41 (1984).

40. W. E. Mott and R. B. Sutton, in *Handbook of Physics*, S. Flügge, ed. (Springer-Verlag, Berlin-Gottingen-Heidelberg, 1958), pp. 144-154.

41. J. K. Dickens, N. W. Hill, F. S. Hou, J. W. McConnell, R. R. Spencer, and F. Y. Tsang, *An NE-213-Scintillator-Based Neutron Detection System for Diagnostic Measurements of Energy Spectra for Neutrons Having Energies $\geq$ 0.8 MeV Created During Plasma Operations at the Princeton Tokamak Fusion Test Reactor*, ORNL/TM-9561 (1985), in particular section 3.2 of this reference.

42. P. Kuijper, C. J. Tiesinga and C. C. Jonker, *Nucl. Instrum. Meth.* **42**, 56 (1966).

43. R. de Leo, G. D'erasmo, A. Pantaleo and G. Russo, *Nucl. Instrum. Meth.* **119**, 559 (1974).

44. H. Schölermann and H. Klein, *Nucl. Instrum. Meth.* **169**, 25 (1980).

45. V. V. Filchenkov, A. D. Konin and V. G. Zinov, *Nucl. Instrum. Meth. Phys. Res.* **A245**, 490 (1986).

46. M. Buenerd, D. L. Hendrie, U. Jahnke, J. Mahoney, A. Menchaca-Rocha, C. Olmer and D. K. Scott, *Nucl. Instrum. Meth.* **136**, 173 (1976).

47. D. L. Smith, R. G. Polk and T. G. Miller, *Nucl. Instrum. Meth.* **64**, 157 (1968); see also R. L. Craun and D. L. Smith, *Nucl. Instrum. Meth.* **80**, 239 (1970) and references cited in this paper.

48. G. Dietze and H. Klein, *Nucl. Instrum. Meth.* **193**, 549 (1982).

49. A. G. DaSilva, L. T. Auler, J. C. Suita, L. J. Antunes and A. A. DaSilva, *Nucl. Instrum. Meth. Phys. Res.* **A264**, 381 (1988).

50. J. B. Czirr, D. R. Nygren and C. D. Zafiratos, *Nucl. Instrum. Meth.* **31**, 226 (1964).

51. R. Madey, F. M. Waterman, A. R. Baldwin, J. N. Knudson, J. D. Carlson, and J. Rapaport, *Nucl. Instrum. Meth.* **151**, 445 (1978).

52. V. V. Verbinski, W. R. Burrus, T. A. Love, W. Zobel and N. W. Hill, *Nucl. Instrum. Meth.* **65**, 8 (1968).

53. J. L. Romero, private communication, 1987.

54. H. J. Brede, G. Dietze, K. Kudo, and D. Schlegel-Bickmann, *Rad. Effects* **94**, 129 (1986).

55. J. L. Fowler, J. A. Cookson, M. Hussain, R. B. Schwartz, M. T. Swinhoe, C. Wise, and C. A. Uttley, *Nucl. Instrum. Meth.* **175**, 449 (1980).

56. J. B. Hunt, C. A. Baker, C. J. Batty, P. Ford, E. Friedman, and L. E. Williams, *Nucl. Instrum. Meth.* **85**, 269 (1970).

57. M. W. McNaughton, F. P. Brady, W. B. Broste, A. L. Sagle, and S. W. Johnsen, *Nucl. Instrum. Meth.* **116**, 25 (1974).

58. R. A. J. Riddle, G. H. Harrison, P. G. Roos and M. J. Saltmarsh, *Nucl. Instrum. Meth.* **121**, 445 (1974).

59. S. Cierjacks, M. T. Swinhoe, L. Buth, S. D. Howe, F. Raupp, H. Schmitt and L. Lehmann, *Nucl. Instrum. Meth.* **192**, 407 (1982).

60. C. E. Wiegand, T. Elioff, W. B. Johnson, L. B. Averbach, J. Lach and T. Ypsilantis, *Rev. Sci. Instrum.* **33**, 526 (1962).

61. P. Leleux, P. C. Macq, J. P. Meulders, and C. Pirart, *Nucl. Instr. Meth.* **116**, 41 (1974).

62. F. P. Brady, J. A. Jungerman, J. C. Young, J. L. Romero, and P. J. Symonds, *Nucl. Instr. Meth.* **58**, 57 (1986); *Errata*, *Nucl. Instr. Meth.* **63**, 358 (1968); J. C. Young, J. L. Romero, F. P. Brady, and J. R. Morales, *Nucl. Instr. Meth.* **68**, 333 (1969).

63. T. A. Love, R. T. Santoro, R. W. Peelle, and N. W. Hill, *Rev. Sci. Instrum.* **39**, 541 (1968).

64. T. G. Masterson, *Nucl. Instr. Meth.* **88**, 61 (1970).

65. R. M. Sternheimer, *Phys. Rev.* **115**, 137 (1959).

APPENDIX A

KINETICS AND ENERGETICS OF THE $^{12}C(n,n')3\alpha$ REACTION

For $E_n < 25$ MeV the most important of the multibody breakup reactions for neutron interactions with ^{12}C is the breakup into 3 alphas plus neutron. In O5S[1] this reaction is treated as a multistep reaction in which the first step is inelastic neutron scattering leading to excitation of one of the known excited states in ^{12}C between $E_x = 7.65$ and 12.7 MeV followed by alpha decay of the chosen excited state to ^{8}Be, and that followed by fission of the ^{8}Be ion into two alpha particles. The calculations in O5S are complicated because they are all carried out in the laboratory frame of reference. The probability for excitation of any particular excited state is, for $E_n < 14$ MeV, of course determined by whether or not the state is energetically available to the inelastic scattering reaction. For $E_n \sim 14$ MeV, the programming of O5S uses ratios suggested by experiment at $E_n \sim 14$ MeV; however, for $E_n > 14$ MeV the O5S programming is essentially unchanged except for the cross section for the reaction. The program RESU[12] has adopted the O5S programming to handle the nuclear physics of this reaction.

The major effect of this programming is to restrict to ~5.3 MeV as the total energy to distribute in the center of mass among the 3 alphas, i.e., the energy between the highest energy excited state at 12.7 MeV and the Q value for the reaction of about 7.4 MeV. For $E_n = 14$ MeV this total energy is about that expected, but as $E_n \rightarrow 20$ MeV and higher, one might expect that a sensible equipartition of available energy among the four outgoing particles would result in the total energy of the 3 alphas to increase beyond ~5.3 MeV. Indeed, the alpha spectrum of Subramanian et al.[20] for $E_n = 27.4$ MeV shown in Figure 13, which must be due to alphas from the 3α breakup reaction plus a few high-energy alphas from the ground-state $^{12}C(n,\alpha)^{9}Be$ reaction, does exhibit alphas having energies between 5 and 20 MeV.

The programming in SCINFUL is, therefore, considerably more extensive in handling the energetics and kinetics of this reaction. Indeed, in the chronology of the development of SCINFUL, the subroutine governing the handling of this reaction was written first and served as a model of method for the writing of subroutines handling other multibody breakup reactions.

The calculation follows one of several reaction schemes:

1.	(a)	$n + {}^{12}C$	$\rightarrow$	$n' + {}^{12}C$ (excited)
	(b)	${}^{12}C$ (excited	$\rightarrow$	$\alpha + {}^{8}Be$ (ground state)
	(c)	${}^{8}Be$ (ground state)	$\rightarrow$	2α
2.	(a)	Same as 1. (a)		
	(b)	${}^{12}C$ (excited)	$\rightarrow$	$\alpha + {}^{8}Be$ (excited state at 3.0 MeV)
	(c)	${}^{8}Be$ (excited)	$\rightarrow$	$2\ \alpha$.
3.	(a)	Same as 1. (a)		
	(b)	${}^{12}C$ (excited)	$\rightarrow$	3α via 3-body breakup.
4.	(a)	$n + {}^{12}C$	$\rightarrow$	$\alpha + {}^{9}Be$ (excited)
	(b)	${}^{9}Be$ (excited)	$\rightarrow$	$n + {}^{8}Be$ (ground state)
	(c)	Same as 1. (c)		
5.	(a)	Same as 4. (a)		
	(b)	${}^{9}Be$ (excited)	$\rightarrow$	$n + {}^{8}Be$ (excited state at 3.0 MeV)
	(c)	Same as 2. (c)		
6.	(a)	Same as 4. (a)		
	(b)	${}^{9}Be$ (excited)	$\rightarrow$	$\alpha + {}^{5}He$
	(c)	${}^{5}He$	$\rightarrow$	$n + \alpha$.

The program does not consider an initial 4-body breakup reaction since the experimental results of Antolkovic et al.[17] indicate that this phase-space reaction was not detected and so is weak to nonexistent, at least for E_n up to 35 MeV.

For neutron inelastic scattering, reaction 1. (a), SCINFUL has seven choices of level population. These are (1) $E_x = 7.65$ MeV, (2) 9.64 MeV, (3) 10.84 MeV, (4) 11.8 + 12.7 + 13.3 MeV, i.e., combining levels at 11.8 and 13.3 MeV (see ref. 21 for the evaluated ${}^{12}C$ level structure) into the level at 12.7 MeV, (5) 14.08 MeV, (6) 16.1 - 18.0 MeV, skipping the 15.1-MeV level as a known gamma emitter,[21] and (7) a "continuum" state at even higher excitation. For this last case, the outgoing neutron energy is chosen from the function given in equation (3). The two lowest-energy excited states can decay only to the ${}^{8}Be$ ground state, but the higher energy states can decay to the excited state of ${}^{8}Be$, and the probability of this decay in SCINFUL is adopted from the evaluation.[21] For a "continuum" state, however,

SCINFUL chooses either a 3-body breakup reaction or decay to the ^{8}Be ground state.

For an initial alpha reaction, reaction 2. (a), SCINFUL again has seven choices of level population chosen from the recent evaluation.[16] These are E_x = (1) 2.43 MeV, (2) 2.8 + 3.05 MeV together, (3) 4.70 MeV, (4) 6.76 MeV, (5) 11.5-MeV group, (6) 14.0-MeV group, and (7) a "continuum" state at even higher excitation in ^{9}Be. For this last case the outgoing energy of the initial alpha is chosen from the proton distribution function given in equation (1) by setting the variable $Temp = 4$. The rationalizations for using equation (1) to determine this alpha energy are: (1) probability of this branch is small, a few percent of the total 3α breakup reaction for any E_n; and (2) the calculated alpha "continuum" using TNG[18] is very similar in shape to that calculated for the proton "continuum."

The probability of choosing any one of these 14 reaction channels is governed by a table of probabilities in SCINFUL. This table, in turn, was derived by merging such experimental cross-section data as are available with excitation functions calculated from the TNG code.[18] As might be expected for $E_n > 40$ MeV most of the 3α reaction in SCINFUL proceeds via an initial "continuum" level in ^{12}C.

The decay[16,A1] of the E_x = 2.43 MeV state in ^{9}Be proceeds 7% by neutron emission to ^{8}Be (ground state) and 93% by alpha emission to ^{5}He. This latter is clearly an unusual decay mode, since the Q-value for decay of ^{9}Be into α + ^{5}He is 2.46 MeV, or some 30 keV larger than E_x. However, both the level in ^{9}Be in the ground state of ^{5}He are quite broad, and the decay mechanism must take these widths into account. Programming this interesting bit of nuclear physics into SCINFUL seems a bit much and isn't done. Instead the program simply observes that (on the average) there is no residual kinetic energy in the ^{9}Be center of mass to be shared by the alpha and the ^{5}He ion after the decay.

For the other higher-lying excited states in ^{9}Be the program chooses which of the decay modes 4. (b), 5. (b) or 6. (b) will be followed with probabilities estimated from the evaluation.[16] For excitation of a "continuum" state in ^{9}Be there is one added feature and that is the possibility of decay of the highly excited ^{9}Be into a proton + ^{8}Li. The probability for this reaction path was estimated from TNG[18] calculations and is on the order of 10% of the ^{9}Be "continuum" level decay.

As mentioned above the program allows computation of the phase-space reaction $^{12}\mathrm{C} \rightarrow 3\alpha$ following inelastic excitation into a "continuum" level. For this calcula-

tion the program chooses an energy for one alpha in the center-of-mass system from the simple formulation,

$$\Phi(E) = E^2 * (E_{\max} - E)^2 \tag{8}$$

where $E_{\max}$ is the total energy in the center of mass to be shared by the 3 alphas. Having chosen an energy for one of the alphas, the other two share the remaining energy; and having chosen a polar direction for the first alpha, the kinematics in the center of mass may be computed for all 3 alphas.

REFERENCE TO APPENDIX A

A1. There is some indication from early work by R. R. Spencer, G. C. Phillips and T. E. Young, *Nucl. Phys.* **21**, 310 (1960) that the 2.43-MeV state in ^{9}Be decays by neutron emission to the first-excited state in ^{8}Be in preference to the ground state in ^{8}Be.

APPENDIX B

MULTIBODY BREAKUP REACTIONS IN SCINFUL

In this appendix are listed the $n + {}^{12}\mathrm{C} \rightarrow \ldots$ reactions currently programmed in SCINFUL. Some of these are listed separately even though the final reaction products are the same [e.g., $(n, 2np)$ and $(n, p2n)$] because the intermediate steps are different. Reaction Q values are determined in the program on a step-by-step basis, for example, how much energy is needed for ${}^{11}\mathrm{C} \rightarrow p + {}^{10}\mathrm{B}$ after having formed ${}^{11}\mathrm{C}$ will enter into the computation, and not the Q value for the $(n, 2np)$ reaction. Reactions currently programmed are:

$$
\begin{aligned}
n + {}^{12}\mathrm{C} \quad &\rightarrow \quad \alpha + {}^{9}\mathrm{Be} \\
&\rightarrow \quad n' + 3\alpha \\
&\rightarrow \quad \alpha + p + {}^{8}\mathrm{Li} \\
&\rightarrow \quad \alpha + p + n + {}^{7}\mathrm{Li} \\
&\rightarrow \quad \alpha + p + 2n + {}^{6}\mathrm{Li} \\
&\rightarrow \quad 2\alpha + p + n + t \\
&\rightarrow \quad 2\alpha + p + 2n + d \\
&\rightarrow \quad p + {}^{12}\mathrm{B} \\
&\rightarrow \quad p + \alpha + {}^{8}\mathrm{Li} \\
&\rightarrow \quad p + n + {}^{11}\mathrm{B} \\
&\rightarrow \quad p + n + \alpha + {}^{7}\mathrm{Li} \\
&\rightarrow \quad p + 2n + {}^{10}\mathrm{B} \\
&\rightarrow \quad p + 2n + \alpha + {}^{6}\mathrm{Li} \\
&\rightarrow \quad p + 2n + d + 2\alpha \\
&\rightarrow \quad p + n + t + 2\alpha \\
&\rightarrow \quad 2p + {}^{11}\mathrm{Be} \\
&\rightarrow \quad 2p + n + {}^{10}\mathrm{Be} \\
&\rightarrow \quad 2p + 2n + {}^{9}\mathrm{Be} \\
&\rightarrow \quad d + {}^{11}\mathrm{B} \\
&\rightarrow \quad d + \alpha + {}^{7}\mathrm{Li} \\
&\rightarrow \quad d + n + {}^{10}\mathrm{B} \\
&\rightarrow \quad d + n + p + {}^{9}\mathrm{Be} \\
&\rightarrow \quad d + n + \alpha + {}^{6}\mathrm{Li}
\end{aligned}
$$

$$\rightarrow \quad 2d + n + 2\alpha$$
$$\rightarrow \quad 2n + {}^{11}\mathrm{C}$$
$$\rightarrow \quad 2n + p + {}^{10}\mathrm{B}$$
$$\rightarrow \quad t + {}^{10}\mathrm{B}$$
$$\rightarrow \quad t + p + {}^{9}\mathrm{Be}$$
$$\rightarrow \quad t + d + 2\alpha$$
$$\rightarrow \quad t + \alpha + {}^{6}\mathrm{Li}$$
$$\rightarrow \quad t + p + n + 2\alpha$$
$$\rightarrow \quad t + p + d + {}^{7}\mathrm{Li}$$
$$\rightarrow \quad {}^{3}\mathrm{He} + {}^{10}\mathrm{Be}$$
$$\rightarrow \quad {}^{3}\mathrm{He} + n + {}^{9}\mathrm{Be}$$
$$\rightarrow \quad {}^{3}\mathrm{He} + 2n + 2\alpha$$
$$\rightarrow \quad {}^{3}\mathrm{He} + n + p + {}^{8}\mathrm{Li}$$
$$\rightarrow \quad {}^{3}\mathrm{He} + 2n + p + {}^{7}\mathrm{Li}$$
$$\rightarrow \quad {}^{3}\mathrm{He} + 2n + p + t + \alpha$$

These reactions represent a fairly complete set of reactions within the limitations initially set for the programming effort, in particular, limiting the number of outgoing neutrons to two and limiting the number of outgoing charged particles to four including checking possible escape from the detector for up to two protons or two deuterons or one of each. Indeed, in the actual running of the program, many of the possible 4-body reactions are scarcely populated even though energetically available simply because the energy partitioning takes place sequentially, and so after the second such determination of energy from either equation (1) or (3), the excitation of the residual intermediate ion (^{10}B to ^{6}Li) is often too small to support further decay. These 4-body reactions begin to exhibit yields in the calculations as E_n becomes >60 MeV, however, and very likely if SCINFUL were to be extended for $E_n > 80$ MeV, the above-mentioned limitations would have to be relaxed and additional multibody breakup reactions entered into the program. Such might be an interesting task for the future.

APPENDIX C

COMPARISONS OF $n + H$ CROSS SECTIONS AND ANGULAR DISTRIBUTIONS

Very recently (September 1987) W. Dodder and J. Hale[24] completed a new evaluation of cross sections for, and angular distributions of the scattered neutron following, $n + H$ interactions for E_n up to 20 MeV, and as a private communication from Dr. J. Hale, of cross sections for E_n up to 30 MeV. The Gammel formula[23] used for the cross section for this reaction in SCINFUL was developed some three decades ago. It is important to compare cross section computed for SCINFUL with those in the new evaluation,[24] and this comparison is exhibited in Table C1. From this table one may observe that ratios of cross sections for E_n between 1 keV (a lower useful limit for SCINFUL calculations) and 30 MeV vary between 0.993 and 1.006. Cross sections for $n + {}^{12}C$ reactions used in SCINFUL are not as precisely known as the $n + H$ scattering cross sections, and, at least for $E_n \geq 40$ MeV, the corresponding reactions contribute substantially to the overall computed detector response. For the accuracy required, then, either representation for the $n + H$ cross section should be satisfactory. What has not yet been done, and ought to be done, is a test to determine which method (formula vs interpolation of tabular data) is faster.

The new evaluation provides tabulated coefficients for Legendre polynomials up to P_6 for $E_n \geq 1$ keV, whereas the O5S[1] programming adopted into SCINFUL assumes isotropy of scattering for $E_n \leq 13.7$ MeV and provides coefficients only for powers of $\cos\theta$ up to three. For $E_n = 13.5$ MeV, the evaluation[24] gives the coefficients as follows:

$a_0 = 1.000000$; $a_1 = -0.016145$; $a_2 = 0.004480$;
$a_3 = -0.000842$; $a_4 = 0.000210$; $a_5 = -0.000003$; and
$a_6 = 0.000002$.

The maximum anisotropy will be ~3% compared to isotropy at $E_n = 13.5$ MeV computed at SCINFUL.

Table C1. Comparisons of cross sections for the $n + H$ reaction

Neutron Energy (MeV)	Cross section (b)		Ratio S/E
	SCINFUL	Evaluation	
0.001	20.21	20.34	0.993
0.005	19.71	19.83	0.994
0.01	19.12	19.22	0.995
0.04	16.30	16.33	0.998
0.07	14.29	14.28	1.001
0.1	12.79	12.77	1.002
0.16	10.69	10.65	1.004
0.28	8.279	8.243	1.004
0.40	6.919	6.891	1.004
0.55	5.860	5.841	2.003
0.70	5.156	5.145	1.002
0.85	4.648	4.642	1.001
1.0	2.459	2.459	1.000
1.3	3.693	3.699	0.998
1.6	3.293	3.302	0.997
1.9	2.989	3.000	0.996
2.2	2.747	2.759	0.996
2.5	2.547	2.559	0.995
2.8	2.378	2.390	0.995
3.2	2.188	2.200	0.995
3.8	1.959	1.969	0.995
4.4	1.775	1.783	0.995
5.0	1.623	1.629	0.996
6.5	1.337	1.340	0.998
8.0	1.135	1.135	1.000
9.5	0.983	0.981	1.002
11.0	0.865	0.862	1.004
12.5	0.771	0.767	1.005
14.0	0.693	0.689	1.006
16.0	0.609	0.605	1.006
18.0	0.541	0.538	1.006
20.0	0.485	0.482	1.006
22.0	0.438	0.436	1.005
24.0	0.399	0.397	1.005
26.0	0.365	0.365	1.000
28.0	0.3351	0.3349	1.000
30.0	0.3095	0.3104	0.997

For higher values of E_n comparisons between SCINFUL and the evaluation[24] started out by generating angular distributions at E_n given in the evaluation using the prescription in SCINFUL. These angular distributions were then subjected to a standard Legendre polynomial fitting procedure. Because of the structure of the calculation in SCINFUL, only Legendre polynomial coefficients up to a_2 are meaningful in this latter stage of analysis. The extracted coefficients are compared with the coefficients given in the Dodder and Hale evaluation[24] in Table C2, where, because of the very small values given in the evaluation[24] for a_5 and a_6 for $E_n \leq 20$ MeV) they have not been included in this table. In the middle two columns of Table C2 are listed the coefficients in numerical order, a_1 through a_4 (top to bottom for a given E_n); the final column lists the ratios of either a_1 (SCINFUL):$a_1 + a_3$ (Evaluation) or a_2 (SCINFUL):$a_2 + a_4$ (Evaluation), ratios which will give some indication of the variations in yields for $\theta = 0$ and $\theta = 180$ deg.

The major conclusion that may be drawn from this study is that angular distributions computed using the SCINFUL prescription as taken from O5S[1] are sufficiently similar to those which would be computed using coefficients tabulated in the evaluation[24] for E_n between 14 and 20 MeV such that detector responses calculated by both methods would be essentially indistinguishable. The SCINFUL prescription has the advantage of extending up to $E_n = 100$ MeV. However, this prescription was deduced more than two decades ago, and (particularly if the new evaluation is extended beyond $E_n = 20$ MeV) it should be tested with respect to newer data or evaluation results.

Table C2. Comparisons of Legendre polynomial coefficients

Neutron Energy (Mev)	Coefficients[a] SCINFUL	Evaluation	$S(a^i)/E(a_i + a_{i+2})$
14.0	−0.01670	−0.01641	0.964
	0.00371	0.00459	0.768
		−0.00094	
		0.00024	
15.0	−0.02385	−0.01684	1.325
	0.00494	0.00481	0.969
		−0.00116	
		0.00029	
16.0	−0.02540	−0.01713	1.371
	0.00484	0.00502	0.900
		−0.00140	
		0.00036	
18.0	−0.02854	−0.01730	1.487
	0.00474	0.00551	0.787
		−0.00189	
		0.00051	
20.0	−0.01776	−0.01697	0.920
	0.00796	0.00626	1.149
		−0.00234	
		0.00067	

[a]Based on $a_0 = 1.0$ exactly; the coefficients are listed in descending order for each E_n, namely a_1 on line with the energy value, a_2 on the next line, etc.

INTERNAL DISTRIBUTION

1. B. R. Appleton
2–6. J. K. Dickens
7. C. Y. Fu
8. T. A. Gabriel
9. R. Gwin
10. D. M. Hetrick
11. N. W. Hill
12. D. T. Ingersoll
13. R. W. Ingle
14–18. D. C. Larson
19. F. C. Maienschein
20. J. W. McConnell
21–25. R. W. Peelle
26–30. F. G. Perey
31. B. D. Rooney
32. R. W. Roussin
33. R. T. Santoro
34. R. R. Spencer
35. J. J. Dorning (consultant)
36. G. H. Golub (consultant)
37. R. M. Haralick (consultant)
38. D. Steiner (consultant)
39–40. Laboratory Records Department
41. Laboratory Records, ORNL–RC
42. Document Reference Section
43. Central Research Library
44. ORNL Patent Section

EXTERNAL DISTRIBUTION

45. Office of the Assistant Manager for Energy Research and Development, Department of Energy, Oak Ridge Operations, P. O. Box E, Oak Ridge, TN 37831
46. E. J. Axton, National Bureau of Standards, Building 245, Room C308, Gaithersburg, MD 20899
47. G. F. Auchampaugh, Los Alamos National Laboratory, P. O. Box 1663, MS D449-P3, Los Alamos, NM 87545
48. F. E. Cecil, Colorado School of Mines, Department of Physics, Golden, CO 80401
49. Roger W. Finlay, Department of Physics and Astronomy, Ohio University, Athens, OH 45701
50. S. M. Grimes, Department of Physics and Astronomy, Ohio University, Athens, OH 45701
51. R. R. Keziah, Department of Physics, Air Force Academy, Colorado Springs, CO 80840
52. R. Madey, Department of Physics, Kent State University, Kent, OH 44242
53. G. L. Morgan, Los Alamos National Laboratory, P. O. Box 1663, Group P-15, MS D406, Los Alamos, NM 87545
54. J. L. Romero, Crocker Nuclear Laboratory, University of California at Davis, Davis, CA 95616
55. D. L. Smith, Argonne National Laboratory, Applied Physics Division, Building 314, 9700 South Cass Avenue, Argonne, IL 60439
56. F. Y. Tsang, Idaho National Engineering Laboratory, EG&G Idaho Inc., TRA652, P. O. Box 1652, Idaho Falls, ID 83415
57. S. Wender, Los Alamos National Laboratory, P. O. Box 1663, Group P-3, MS D449, Los Alamos, NM 87545
58. S. L. Whetstone, Department of Energy, ER-23/GTN, 19901 Germantown Rd., Germantown, MD 20874

59. Warren Wilson, AFWL/AWYW, Building 416, Kirtland Air Force Base, New Mexico 87117-5008

60–69. Office of Scientific and Technical Information, P. O. Box 62, Oak Ridge, TN 37831